AD NUMBER

AD801912

NEW LIMITATION CHANGE

TO

Approved for public release, distribution unlimited

FROM

Distribution authorized to U.S. Gov't. agencies and their contractors; Critical Technology; OCT 1966. Other requests shall be referred to Air Force Weapons Laboratory, Attn: WLDC, Kirtland AFB, NM 87117.

AUTHORITY

AFWL ltr, 30 Nov 1971

AFWL-TR-66-56

AFWL-TR
66-56

STRESS WAVE PROPAGATION IN CONFINED SOILS

Dolon Hampton
R. A. Watzel

IIT Research Institute Technology Center
Chicago, Illinois 60616

Contract AF 29(601)-6717

TECHNICAL REPORT NO. AFWL-TR-66-56

October 1966

AIR FORCE WEAPONS LABORATORY
Research and Technology Division
Air Force Systems Command
Kirtland Air Force Base
New Mexico

STRESS WAVE PROPAGATION IN CONFINED SOILS

Delon Hampton
R. A. Wetzel

IIT Research Institute Technology Center
Chicago, Illinois 60616
Contract AF 29(601)-6717

TECHNICAL REPORT NO. AFWL-TR-66-56

FOREWORD

This report was prepared by the IIT Research Institute, Chicago, Illinois, under Contract AF 29(601)-6717. The research was performed under Program Element 7.60.06.01.D, Project 5720, Subtask 13.144, and was funded by the Defense Atomic Support Agency (DASA).

Inclusive Dates of research were 15 January 1965 to 15 August 1966. The report was submitted 19 September 1966 by the Air Force Weapons Laboratory Project Officer, Lt Jimmie L. Bratton (WLDC).

This technical report has been reviewed and is approved.

Jimmie L. Bratton

JIMMIE L. BRATTON
Lt, USAF
Project Officer

ALLEN F. DILL
CDR, CEC, USNR
Chief, Civil Engineering Branch

George C Darby, Jr

GEORGE C. DARBY, JR.
Colonel, USAF
Chief, Development Division

ABSTRACT

Phenomena involved with the propagation of air-induced stress waves in soil were investigated in experiments on Edgar Plastic Kaolin (EPK) clay and Ottawa sand. The principal soil variables were moisture content and density in the case of clay, and density in the case of sand. The soil specimens were loaded with overpressures in the range of from approximately 50 to 300 psi. Two overpressure wave shapes were used, one where peak overpressure had a dwell time of approximately 1 msec and the other having essentially a zero dwell time of peak pressure. Stress-time and strain-time relationships were measured at various points along the length of the specimens. Peak stress attenuation, strain and strain-rate relationships, propagation velocity, changes in wave shape, and stress-strain relationships are discussed in the light of the data obtained. Experimental data are compared with theoretical predictions of a linear hysteretic model in the case of Ottawa sand, and a constant tan δ viscoelastic model, in the case of the EPK clay. It was found that in both cases the theories could be used to predict the experimental results with proper evaluation of critical attenuation parameters to be input with the theories.

This page intentionally left blank.

CONTENTS

CONTENTS, Contd.

ILLUSTRATIONS

ILLUSTRATIONS, Contd.

ILLUSTRATIONS, Contd.

TABLES

Section I

INTRODUCTION

Much research effort has been devoted to the development of a better understanding of the dynamic properties of soils. To date (1966) most of this work has been initiated to aid in the design of underground structures capable of resisting nuclear weapon effects. However, research designed to satisfy the need has provided basic information and stimulated research in related areas such as earthquake stability of dams, foundation vibrations, excavation by explosion, etc.

This report covers an experimental investigation of the propagation of air shock-induced stress waves in confined columns of soil with attention being given to the study of the attenuation and change in shape of these waves as they travel through soil. The majority of stress wave propagation research in the past has been theoretical in nature which has led to the development of a large number of theoretical approaches to the problem of stress wave propagation in soils, with essentially no experimental data to evaluate these theories.

Within the past few years, there has been published significant amounts of experimental data on stress wave propagation in soil. Examples of the type of research performed are given in References 1 through 8. The available data includes tests conducted on both sand and clay with a variety of confining conditions ranging from no lateral restraint to one-dimensional compression.

This research study is a contribution to the experimental data on one-dimensional stress wave propagation in sand and clay. Data were obtained for improving the basic understanding of the phenomena and for evaluating wave propagation theories. Peak stress attenuation and change in wave shape with distance of

propagation are among the parameters investigated. In addition, the stress-strain characteristics of the soils as a function of stress level and distance of propagation were investigated. Other parameters considered were wave propagation velocity and peak strain attenuation.

Unfortunately, it was not possible to fully evaluate the wave propagation theories considered using the experimental data obtained in this study because one-dimensional stress-strain data for the soils utilized was not conclusive. Nevertheless, useful information to aid in evaluation of the feasibility of theoretical models was obtained.

Section II

EQUIPMENT AND INSTRUMENTATION

Equipment used in the wave propagation experiments consisted basically of 1) a gas driven shock tube used to load the soil specimen, 2) a confining chamber to restrict the soil specimen to one-dimensional movement, and 3) necessary transducers, conditioning and recording instrumentation to measure the wave propagation characteristics. A schematic diagram of this equipment is shown in Figure 1.

1. Shock Tube

The shock tube used in the experiments (Figure 1) consisted of a cylindrical tube with an inside diameter of 2-31/64 in. and an overall length of 31 ft. The tube was made up of two sections; an 11-ft driver section containing helium and a 20-ft driven section containing air at atmospheric pressure. Wood cylinders with a diameter of 2-3/4 in. were provided for insertion in the driver section to vary the driver gas volume. The length of the driven or downstream section was sufficient to allow generation of a clean wave front. To minimize friction losses the inside surface of the tube was honed over the entire length.

In operation, an acetate diaphragm was clamped between the driver and the driven section, then the driver was filled with helium to the desired pressure. A plunger with a sharp-pointed tip was actuated to puncture the acetate diaphragm, allowing the shock wave to develop and travel down the tube.

A schematic diagram of the downstream end of the shock tube and the mounting system to receive the soil specimen is shown in Figure 2. A pressure transducer was located 3 ft from the downstream end for triggering the instrumentation as the wave passed that position. Another pressure transducer was positioned 11/64 in. from the end of the soil specimen to measure the shock wave impinging on the soil. Both of these

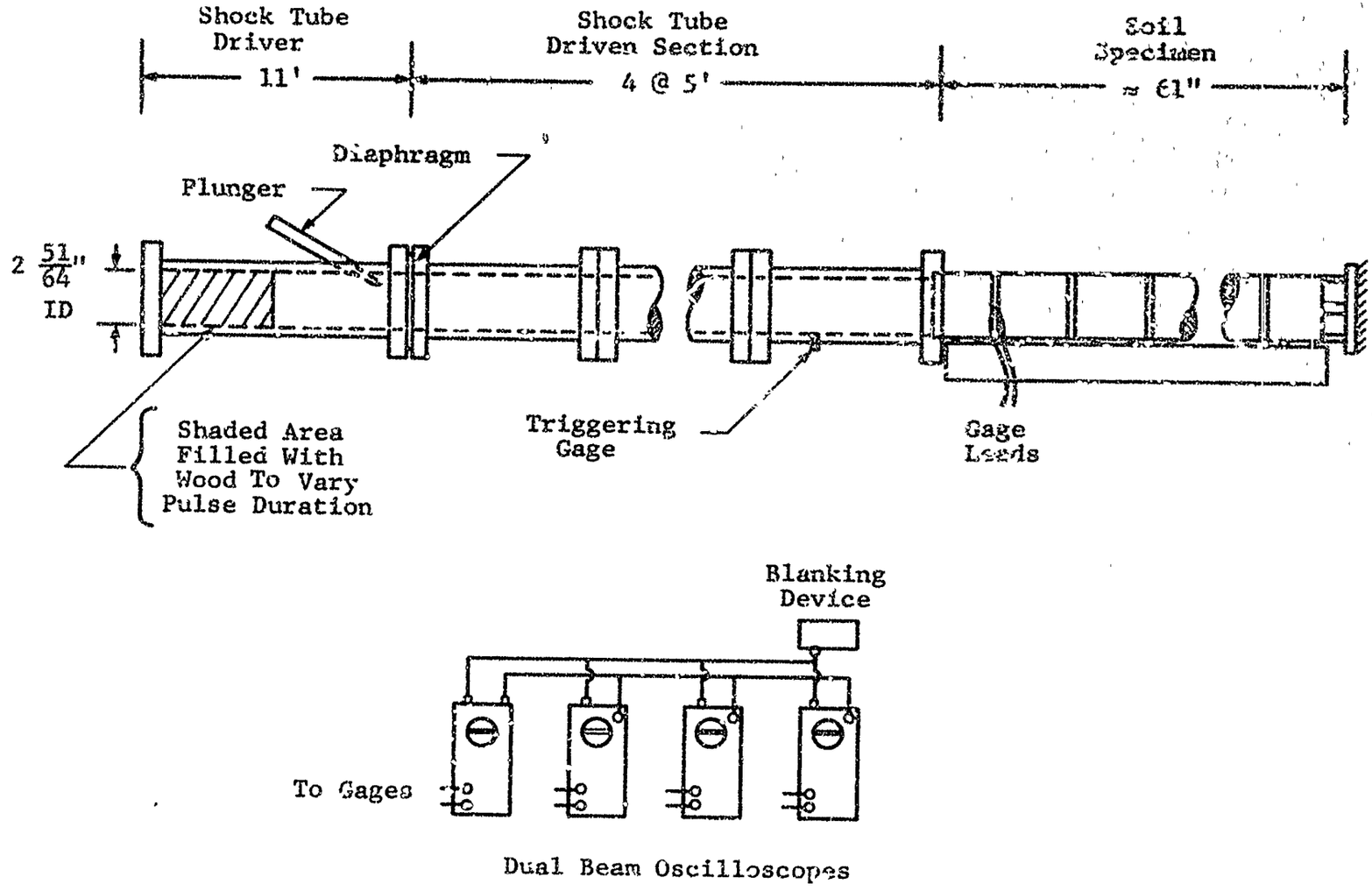

Figure 1 Schematic Diagram of Apparatus for Stress Wave Propagation

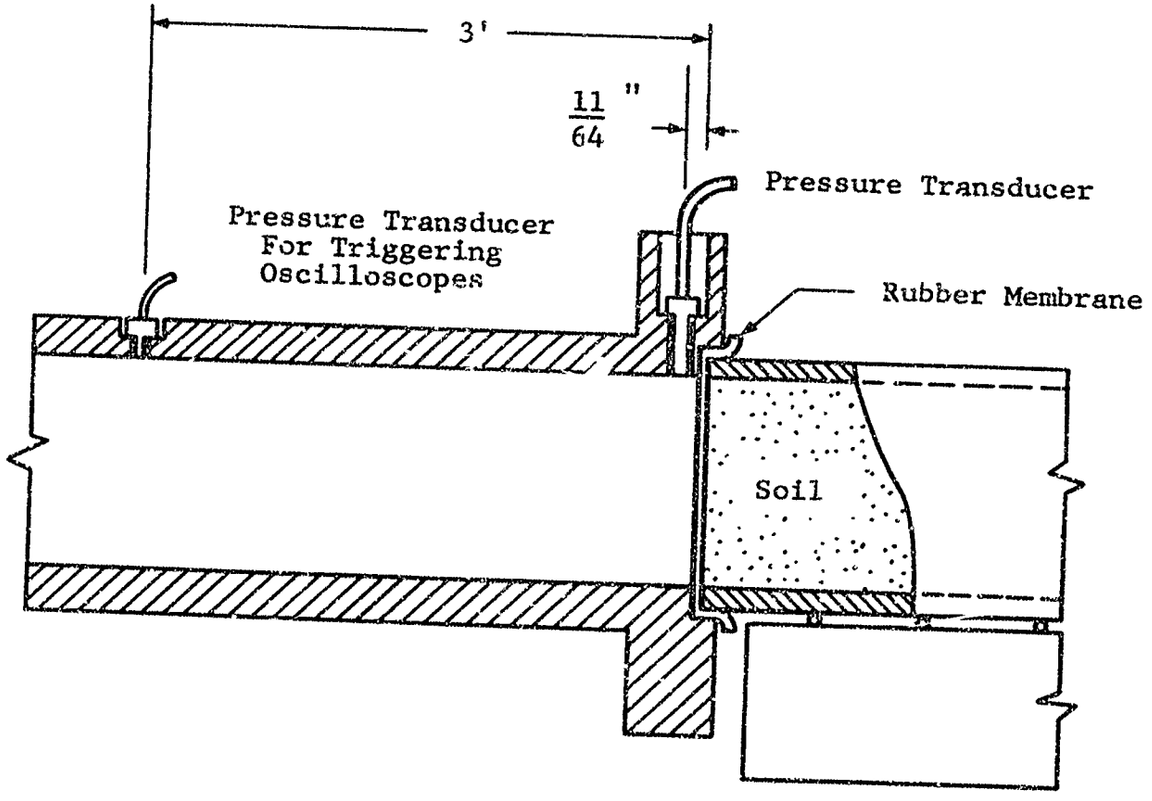

Figure 2 Schematic Diagram of Soil Specimen Mounting in Shock Tube

transducers were mounted perpendicular to the direction of flow (side-on) and flush with the inside surface. A recess 1/4 in. deep and with a 3-1/4 in. diameter was machined in the end of the shock tube to receive the soil specimen. As the inside diameter of the tube was identical to the inside diameter of the chamber confining the soil, the shock wave loading was applied (at least initially) over the soil area only.

It should be noted that as the specimen and confining chamber compressed under the applied load a gap was created between the specimen and the shock tube which permitted air to escape. This escape of air produced a load on the walls of the confining chamber which could possibly have an effect on stress wave propagation through the soil since any load applied to the end of the confining chamber would be transmitted to the soil at the location of the first compressible spacer. The area of the confining chamber was approximately 36 percent of the soil specimen.

It is difficult to assess the significance of this type of loading; however, it is intuitively felt that, for the conditions of test considered herein, it is not significant. The upstream end of the confining chamber is inserted in a groove in the downstream end of the shock tube and wedged tightly against it (see Figure 2). Initially, only the soil is loaded and as it compresses it produces a shortening of the confining chamber which creates a gap between its upstream end and the walls of the shock tube into which air from the shock wave flows.

It is felt that the time necessary for the creation of this gap after the onset of the shock wave onto the soil is significant in terms of 1) the rate at which the stress wave is propagating through the soil, and 2) the length of the rigid segments of the confining chamber (2-1/8 in.). Consequently, the load which may travel through the walls of the confining chamber would produce a stress in the soil which would lag, by a significant amount, the stress produced by the initial loading of the soil specimen. It is therefore reasoned that measured values of peak stress are independent of the motion of the upstream end of the confining chamber. This motion may have an effect on stresses measured after the peak.

No evidence of the presence of a confining chamber induced soil stress could be pinpointed. One reason may be that the volume increase resulting from the creation of the gap would cause a large drop in pressure resulting in a much smaller load on the end of the confining chamber than on the soil specimen. Another reason may be that by the time the gap is created the peak pressure in the shock wave has reflected and traveled a significant distance away from the soil surface leaving a much smaller pressure in this area. Since no evidence of a significant effect of the production of the air gap on the stress in the soil was discerned, it will be assumed that none exists. Concise clarification of this question requires additional research.

2. Confining Chamber

A requirement of the wave propagation experiments was that the soil be constrained to one-dimensional motion. To accomplish this, the chamber confining the soil must be rigid in the radial direction (perpendicular to the direction of wave propagation) and yet not impede axial soil motion (parallel to the direction of wave propagation). A composite ring-type of confining system was used to meet these requirements. The development of this system and an evaluation of its efficiency are presented in Appendix I.

A diagram of the confining chamber used in the experiments is shown in Figure 3. The chamber was composed of 23 individual composite sections positioned in series plus a special section placed at the reaction end. Each individual section consisted of a hollow aluminum cylinder 2-1/8 in. long with a compressible foam rubber ring 1/4 in. in length on both ends. The composite section had an outside diameter of 3-1/4 in., an inside diameter of 2-51/64 in. and an overall length of 2-5/8 in. Each section was lined with a lubricated rubber membrane to reduce the wall friction. The compressible rings also served as a convenient location to bring gage leads out of the soil. Strain gages were mounted on four of these sections to measure the circumferential strain in the section.

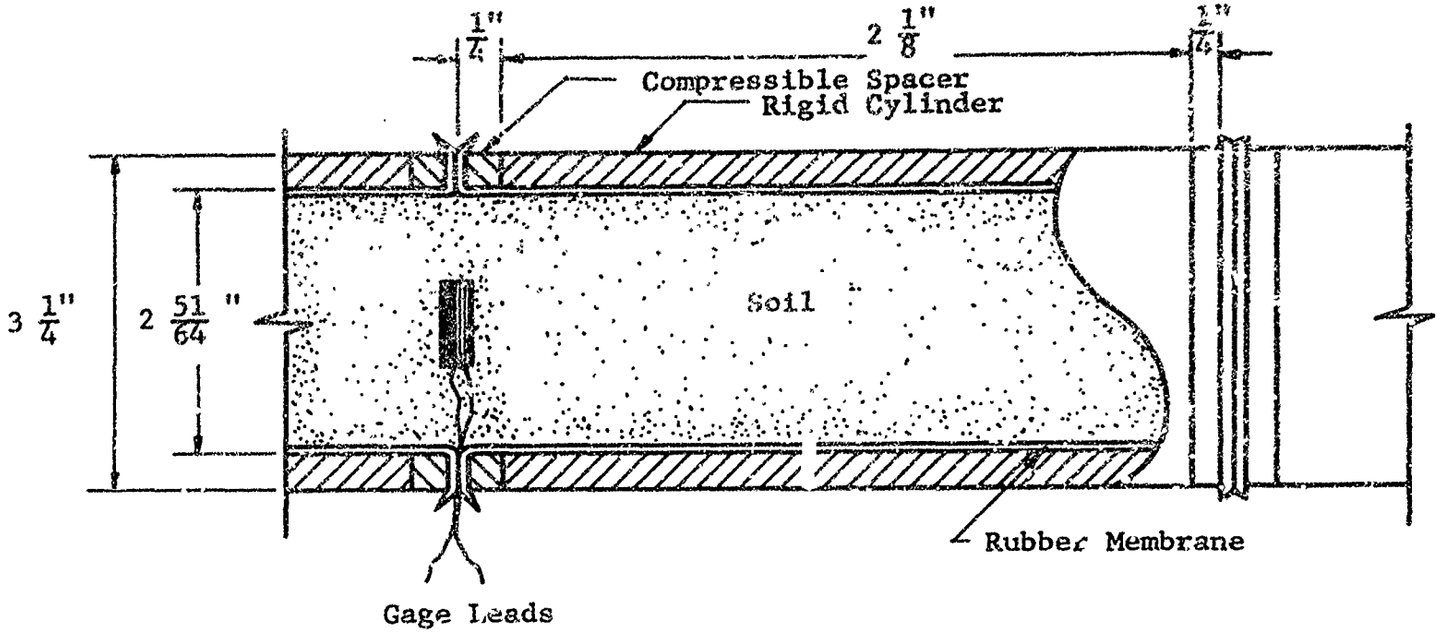

Figure 3 Schematic Diagram Composite Ring Confining Chamber

The special chamber section used for the reaction end of the specimen consisted of a regular section such as described with one end modified as shown in Figure 4. The chamber section was rigidly attached to an end block through two load cells such that the load in the chamber walls could be measured. The soil was supported by a circular plate attached to the same end block through a load cell in such a way that the load in the soil could be measured.

For the conduct of the experiments, the chamber was positioned horizontally and rested on steel ball bearings as shown in Figures 5 and 6. The ball bearings were 1/4 in. in diameter and ran in V-grooves machined in an aluminum bar. Supports for the top of the chamber were provided approximately every 10 in. along the length to prevent buckling of the specimen. The contact of these buckling supports with the chamber was also through ball bearings, which provided relatively free axial motion of the chamber in the support system.

3. Instrumentation

Measurements taken during the wave-propagation experiments included: 1) stress-time history in the soil at several locations, 2) soil strain-time history at several locations, 3) the pressure-time history of the shock wave impinging on the soil specimen, 4) the circumferential strain in the confining chamber, and 5) the arrival time of the wave at the different gage positions. This section describes the instrumentation used in making these measurements.

a. Soil Stress Gage

The embedded gages employed for soil stress measurement were developed at IITRI especially for laboratory measurements (Reference 9). The gage consists basically of a piezoelectric ceramic disk (lead titanate zirconate), positioned inside an aluminum case. It is disk-shaped with overall dimensions of 1 in. diameter by 1/10 in. thick. An exploded view showing details of the gage components and the ceramic is shown in Figure 7.

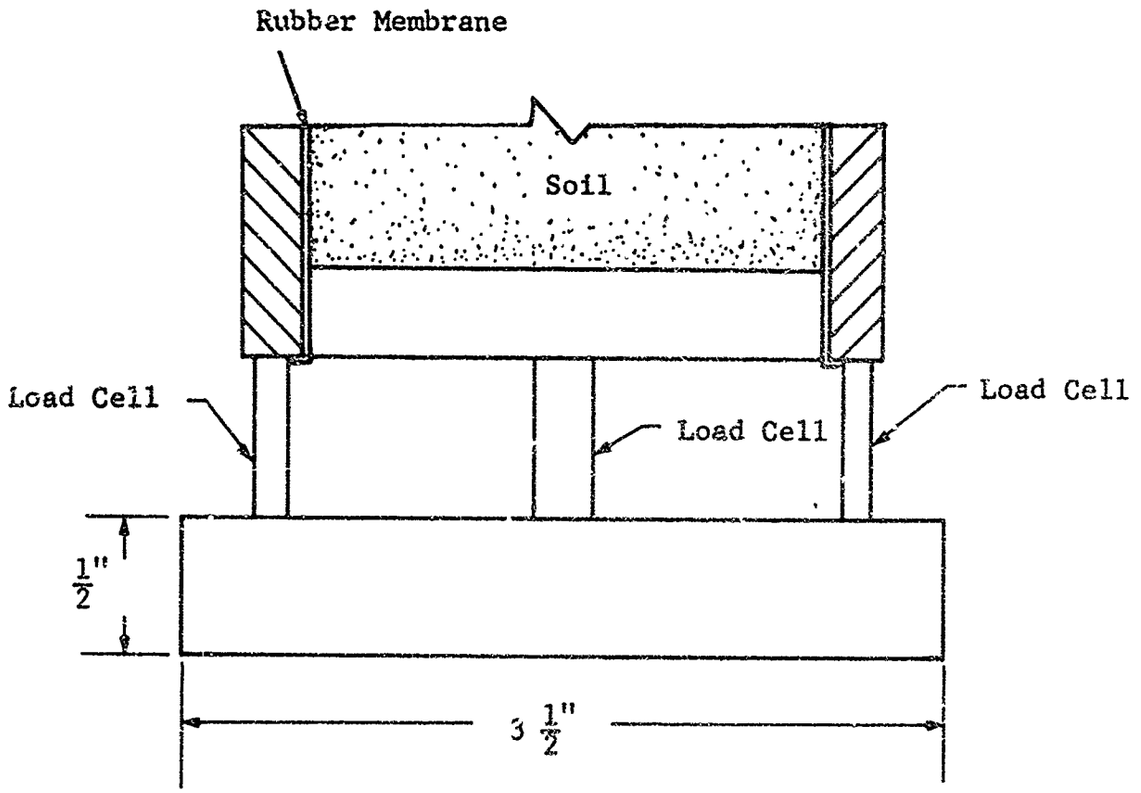

Figure 4 Reaction End Load Measuring Device

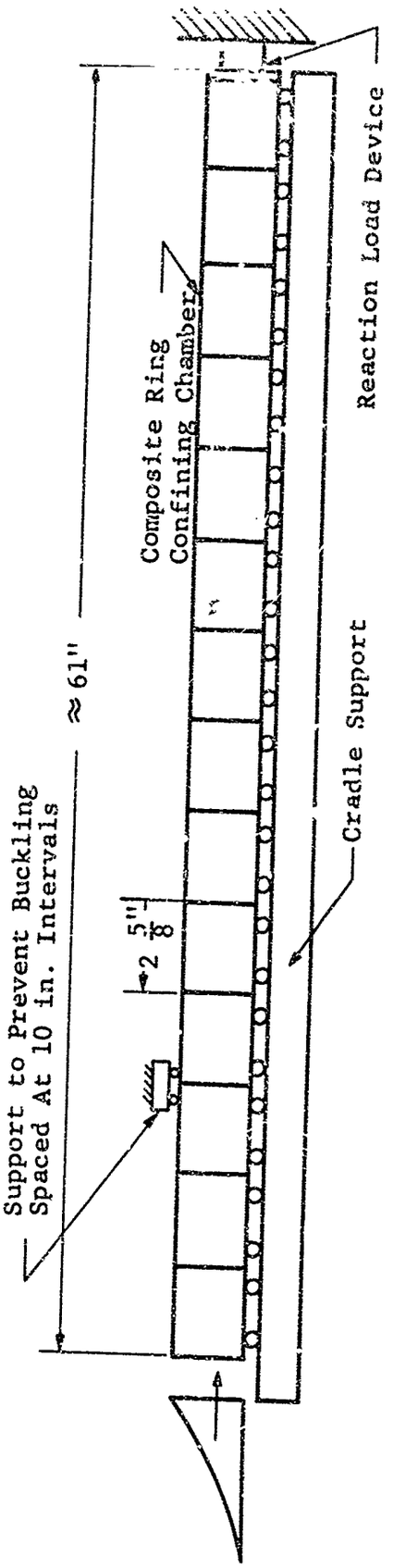

Figure 5 Schematic Side View of Chamber Support System

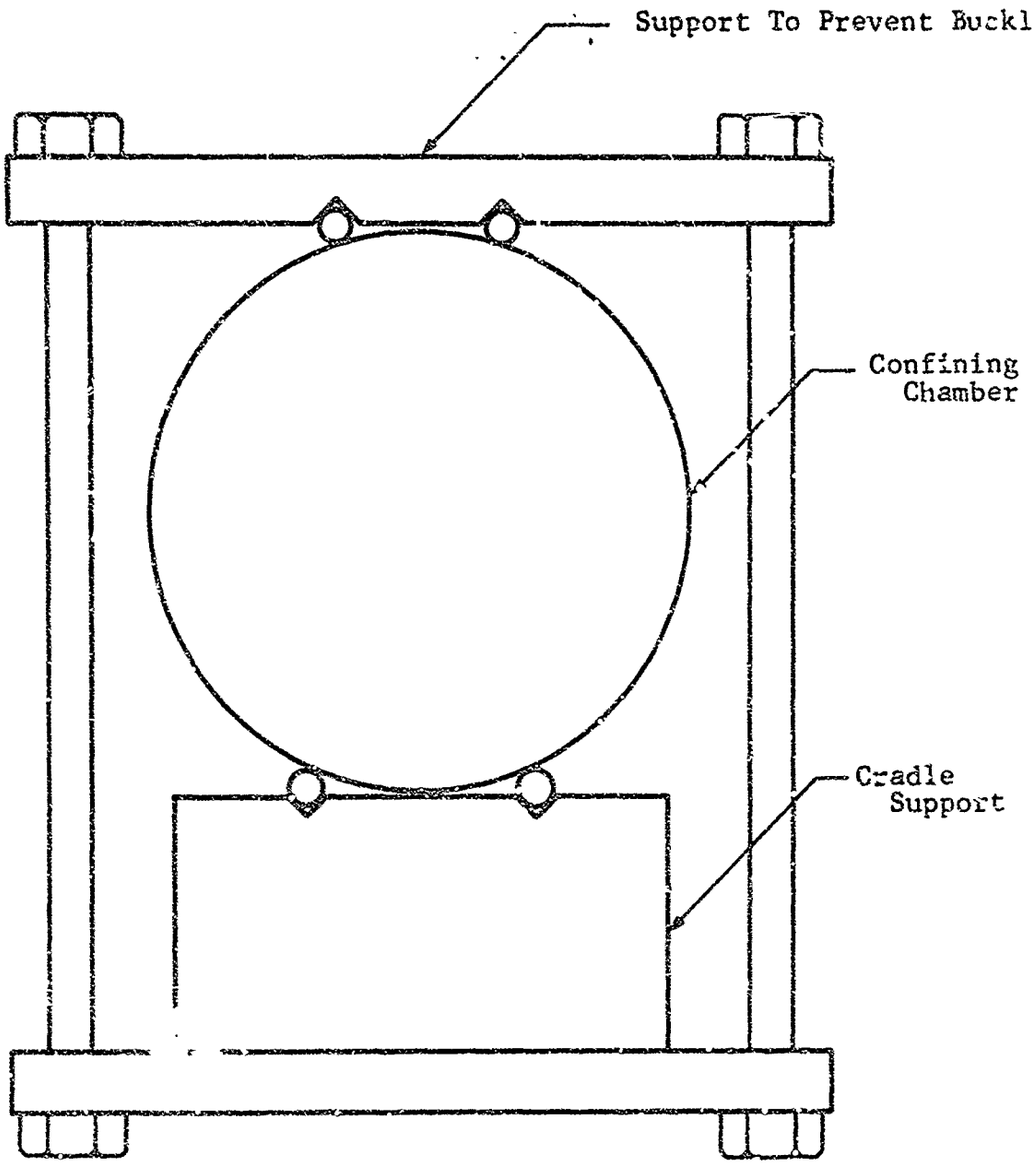

Figure 6 Schematic Front View of Chamber Support System

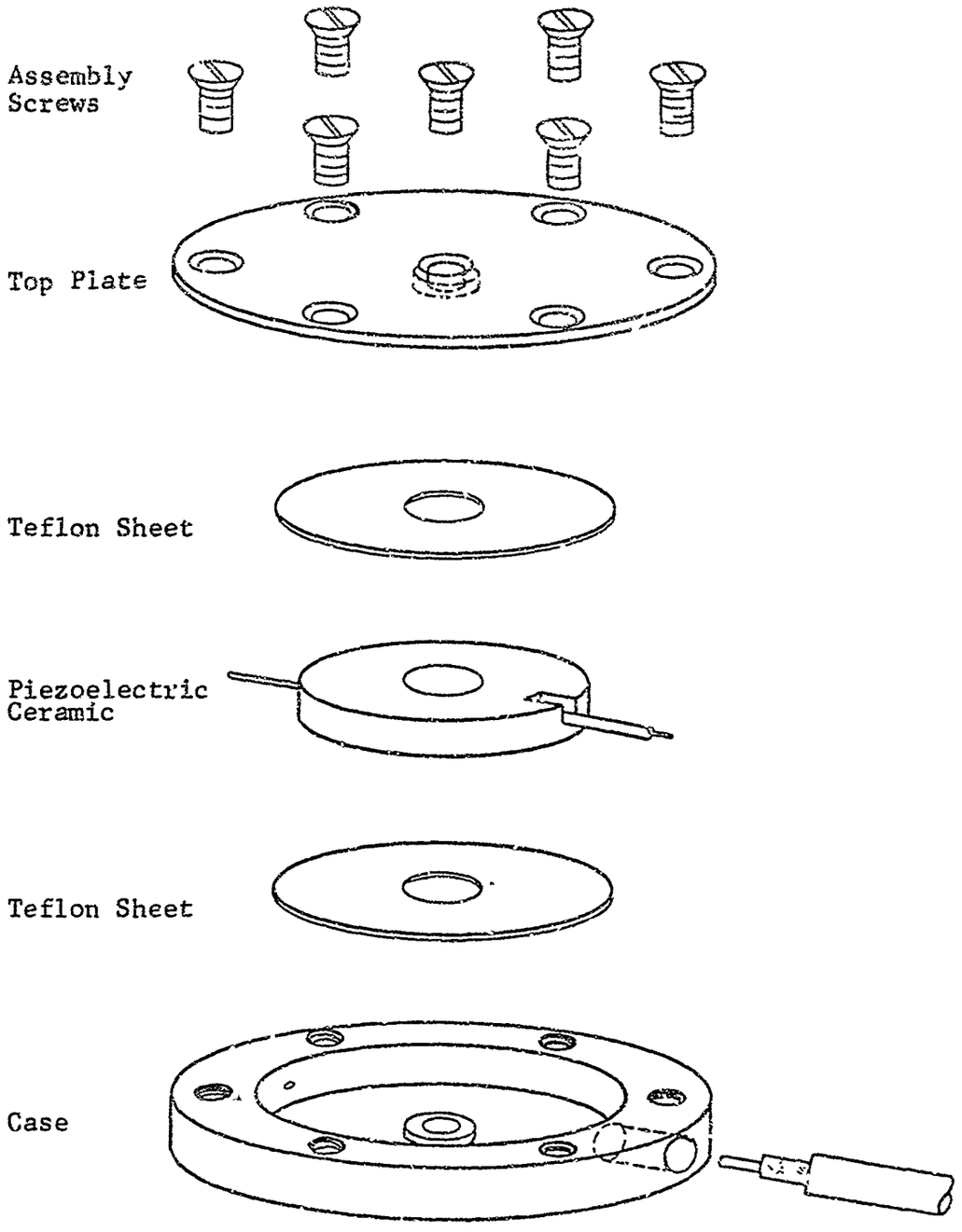

Figure 7 Exploded View of Soil Stress Gage

The gage was designed to respond primarily to the component of soil stress which is normal to the face of the gage with the effect of the other stress components, e.g., shear stresses on the face of the gage and normal stresses on the edge of the gage, being minimized. The gage is capable of both static and dynamic response (in the range of from microseconds to minutes).

The gage circuit is shown schematically in Figure 8. For the circuit used, the equivalent circuit resistance was 1×10^{7} ohms and the equivalent circuit capacitance was 1×10^{-7} farads. This gives a circuit time constant (resistance x capacitance) of 1 second, which was adequate for the experiments. The output voltage of the circuit was converted to charge input (i.e., charge generated by the piezoelectric gage) by using a standard charge generator to determine the transfer function of the circuit.

Static embedded calibrations were obtained for each gage in both sand and clay under test boundary conditions similar to those of the wave propagation experiments. A typical calibration curve for a gage embedded in sand is presented in Figure 9. The curve is approximately linear on loading with a nominal sensitivity of 425 picocoulombs/psi and exhibits some hysteresis on unloading. The list on the following page summarizes the calibration results and provides information on the effect of the soils on the gage response. These embedded calibrations were employed in data reduction for the wave propagation experiments. Based on previous experience (Reference 9) the expected variation in sensitivity of the gage is approximately $\pm$ 20 percent of the nominal value.

b. Soil Strain Gage

The soil strain gages used in the experimental program were those developed under contract with AFWL (Reference 10, 11, 12). The gage, shown in Figure 10, consists of two sets of two mechanically uncoupled 1/16 in. thick by 3/4 in. diameter coil disks and associated electronic driving, amplifying, and recording circuitry.

Gage No.	Fluid Pressure Sensitivity (pcb/psi)	Embedded Sensitivity (pcb/psi)	
		Sand	Clay
1	290	390	400
2	310	410	375
3	290	480	305
4	270	325	395
5	240	275	-
6	260	345	400
CS-2	315	510	-
11	260	415	440

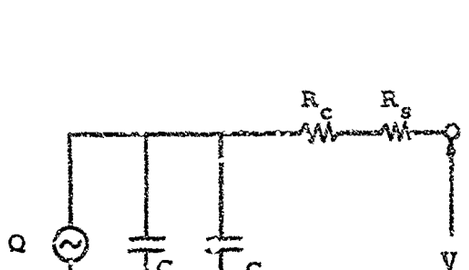

V = Induced Voltage
C_g = Capacitance of Gage
C_c = Circuit Capacitance
R_c = Circuit Resistance
R_s = Oscilloscope Resistance
Q = Piezoelectric Charge Generator (Gage)

Figure 8 Schematic of Piezoelectric Circuit

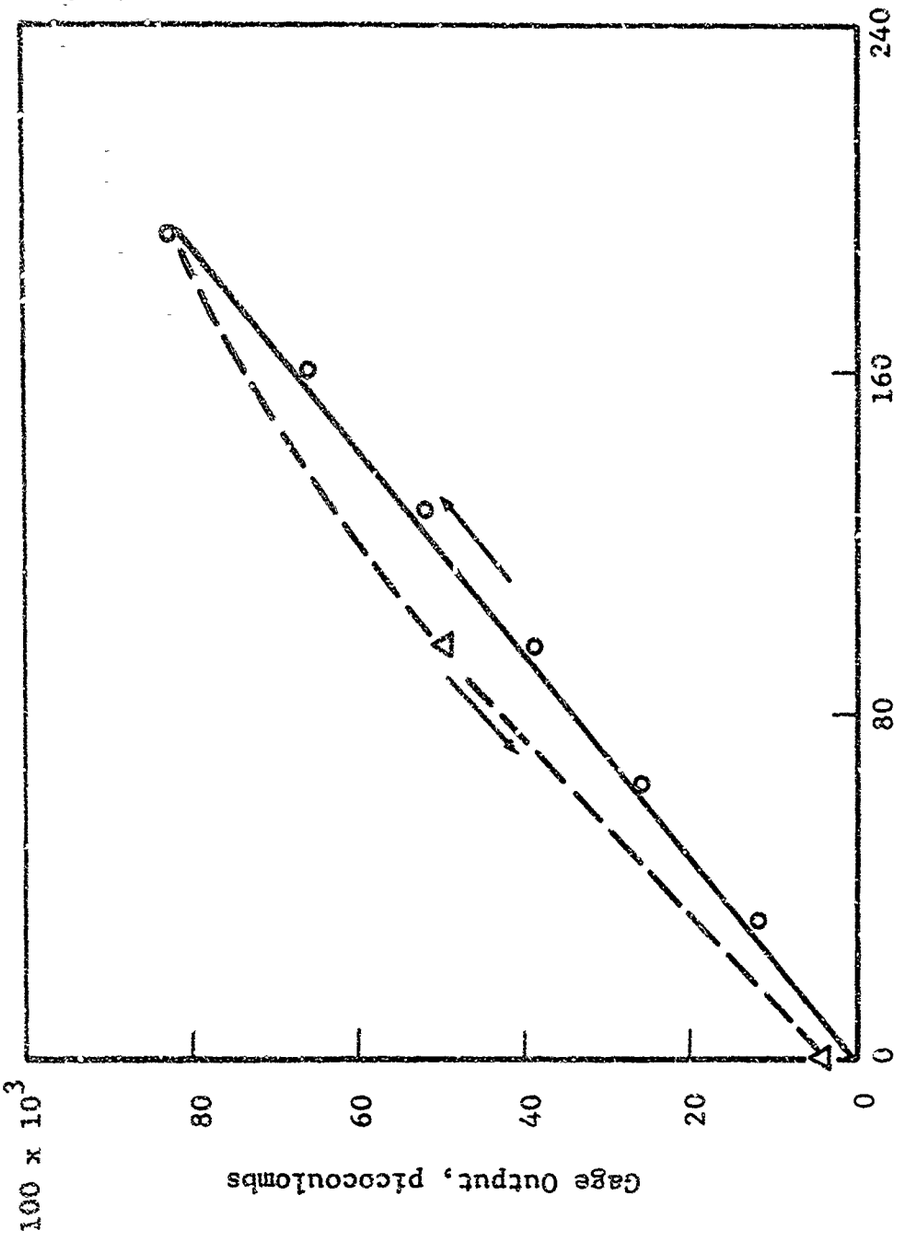

Figure 9 Typical Soil Stress Gage Calibration Curve, Gage Embedded in Sand

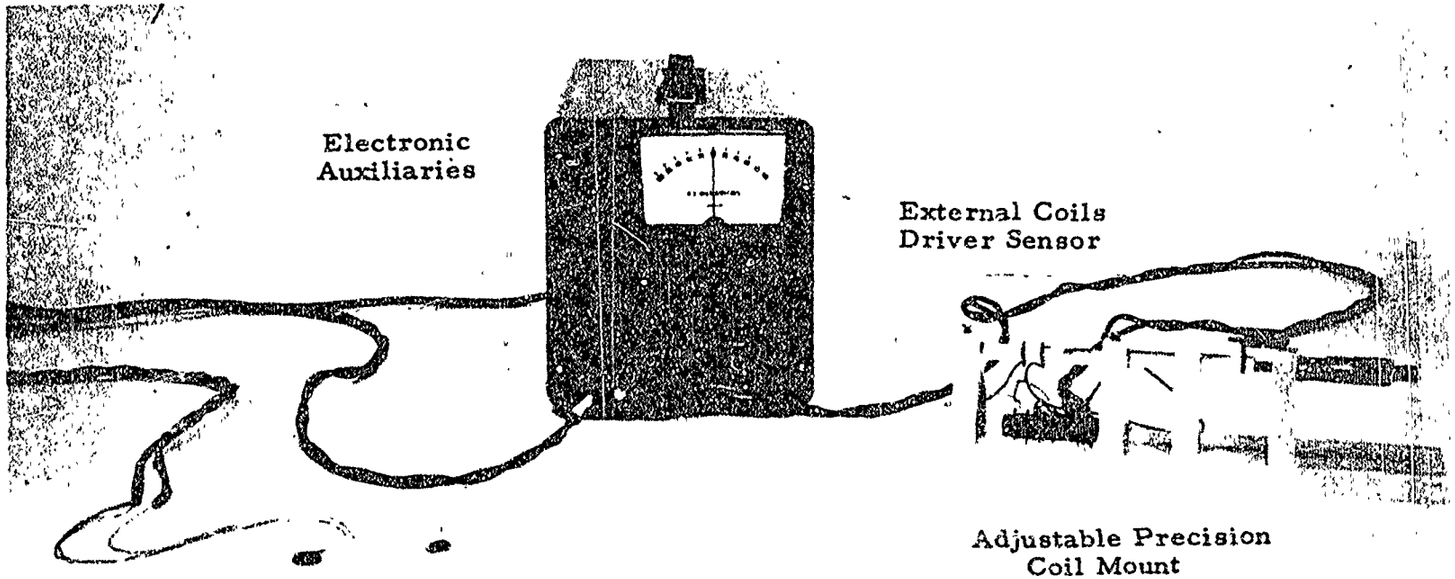

Figure 10 Soil Strain Gage

The principle of operation is that of a null balance differential transformer, i.e., each set of coils represents transformer primary and secondary windings and are so arranged in the circuitry that the resulting signal is the difference of the individual coil outputs. When the coils in each set are equally spaced, the resulting differential output is zero or nulled.

In operation, one set of coils is embedded in the soil in near parallel and concentric orientation as the strain sensing element, the other set is positioned on an adjustable micrometer mount to serve as a reference. Initial spacing of the embedded coils is determined by adjusting the reference coils, until a null is obtained. Soil deformations are measured by the resulting changes in the spacing of the embedded coils which are sensed as changes in the mutual inductance of the soils.

Four gages were used in the experimental studies. Three gages were used with electronics developed for laboratory investigation as described in Reference 10 while the fourth was with a field gage instrument of the type described in Reference 12. The laboratory gage instruments were modified slightly in that the 10-kc output filter was replaced with a 2-kc filter to improve the S/N (signal to noise) ratio. This modification resulted in a gage rise time, defined as time from 10 percent to 90 percent full scale output, of 0.30 msec. This was about the same as the rise time of the field gage instrument and was considered as satisfactory for the purposes of the program.

c. Other Transducers

A quartz pressure transducer* was used to measure the shock wave impinging on the end of the soil specimen. The transducer was mounted side-on and located 11/64 in. from the end of the specimen (Figure 2). Another pressure transducer of the same type, located 3 ft from the specimen end, was used to trigger the recording

* Quartz Pressure Transducer, Model 601A, Kistler Instrument Corp.

instrumentation as the wave passed that location. The output charge of the transducer was converted to a voltage signal by a charge amplifier*.

Three quartz load cells** were located at the reaction end of the soil specimen as shown in Figure 4, to measure independently the soil load and the chamber load at that position. A charge amplifier such as previously mentioned was used to convert the charge output to voltage.

Circumferential strain in the confining chamber was measured by a metalfilm strain gage*** which was bonded to the aluminum chamber. The gage was connected as the active arm in a two-arm resistance bridge. A strain gage plug-in unit**** was used to provide the excitation voltage and amplify the signal.

d. Recording Instrumentation

A bank of six oscilloscopes***** was used to measure the response of the gages with the traces being recorded on polaroid film. Normally, 11 instrumentation channels were recorded for each test. The first oscilloscope in the bank was triggered by the signal from a pressure transducer located 3 ft from the end of the soil specimen. The remaining oscilloscopes were triggered simultaneously by the gate out signal from the first oscilloscope.

A time reference signal was recorded on each scope by applying a square wave signal to the Z axis of the oscilloscopes. The square wave blanked the beam initially and at some predetermined later time caused a momentary increase in the trace intensity. This technique produced two time reference markers at selectable intervals accurate to within 3 percent of the total sweep time.

The time reference signals were generated by using a pulse generator****** and a wave form generator*******. The wave form

---

* Charge Amplifier, Model 566, Kistler Instrument Corp.
** Load Cell, Model No. 912, Kistler Instrument Corp.
*** Strain Gage, Model No. C12-121, Budd Co.
****Strain Gage Plug-In Unit, Type Q, Textronix, Inc.
***** Oscilloscopes, Type 502, Textronix, Inc.
****** Pulse Generator, Type 161, Textronix, Inc.
******* Wave Form Generator, Type 162, Textronix, Inc.

generator produced a negative sawtooth wave form, which in turn was used to trigger the pulse generator. The pulse generator produced a square wave with a predetermined duty cycle. This square wave was fed to the Z axis input to each oscilloscope. The Z axis input is capacitive coupled to the cathode of the CRT such that the square wave is differentiated, producing a positive pulse at the leading edge of the square wave and a negative pulse at the trailing edge. The pulse produced by the leading edge of the square wave blanked the beam and the pulse at the trailing edge increased the beam intensity.

Section III

EXPERIMENTAL PROCEDURES

1. Specimen Preparation

The soil specimens were prepared in the following manner. A 6-ft channel section with a base plate attached at one end was placed in an upright position. The special confining chamber section for the reaction end (Figure 4) was then attached to the channel directly on top of the base plate as shown in Figure 11. A portion of the specimen was then prepared by placing soil in the chamber section until it was full. A regular section of the confining chamber (Figure 3) was then clamped to the channel directly on top of the first section and filled with soil. This procedure was repeated until the entire specimen was prepared. During the soil placement a vacuum was drawn on the void between the chamber walls and the rubber membrane liner to hold the rubber tight against the chamber wall.

Sand specimens were prepared at three different densities. The low density specimen was prepared by pouring the sand through a funnel and tube arrangement with a thin slot at the lower end. The bottom of the tube was held 1/4 in. above the sand surface. The resulting average sand density was 96.6 pcf.

Four medium density specimens were prepared by pouring the sand through the same funnel arrangement with the bottom of the tube held 6 in. above the sand surface. The resulting average densities of these specimens were 101.9, 101.9, 102.4 and 103.8 pcf.

One high density sand specimen was prepared. For this test the funnel and pouring tube were taped to a vibro-tool with the plate of the vibro-tool extending about 1-1/4 in. below the end of the pouring tube (Figure 12). During operation the pouring device was slowly rotated and raised as the sand filled the

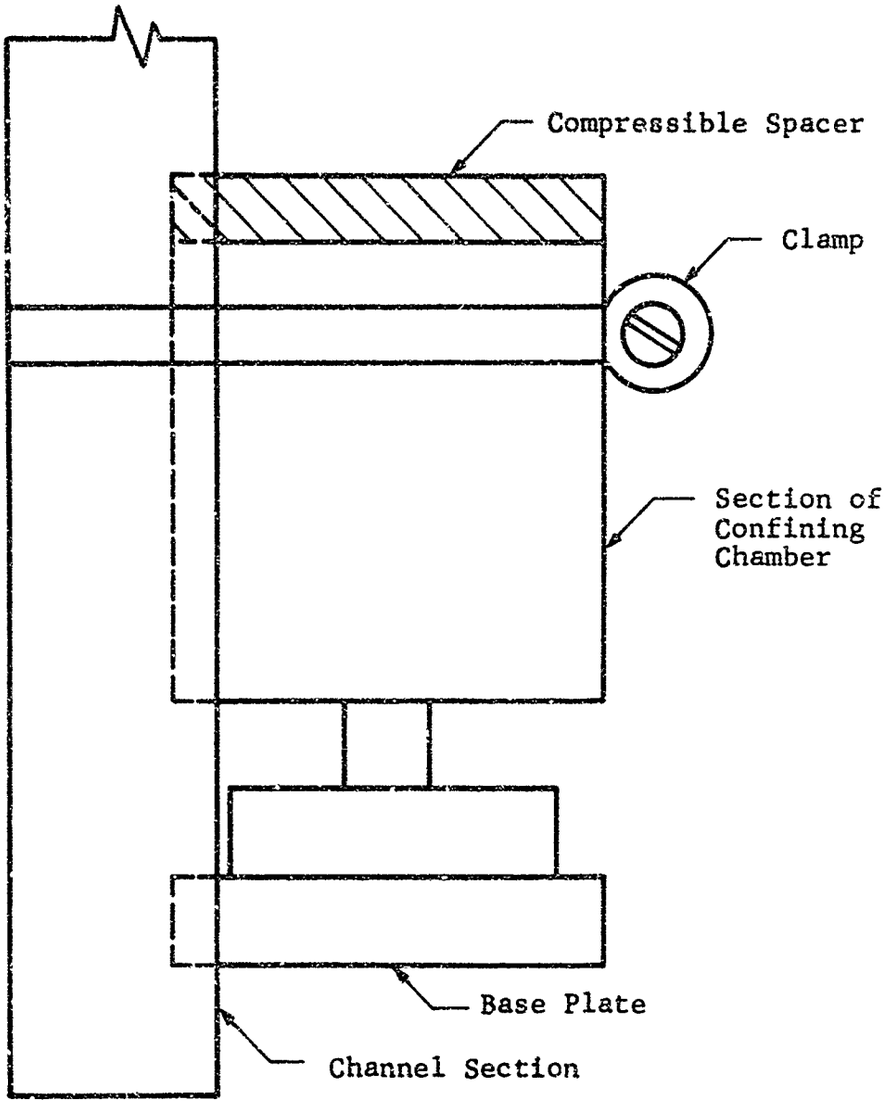

Figure 11 Specimen During Preparation

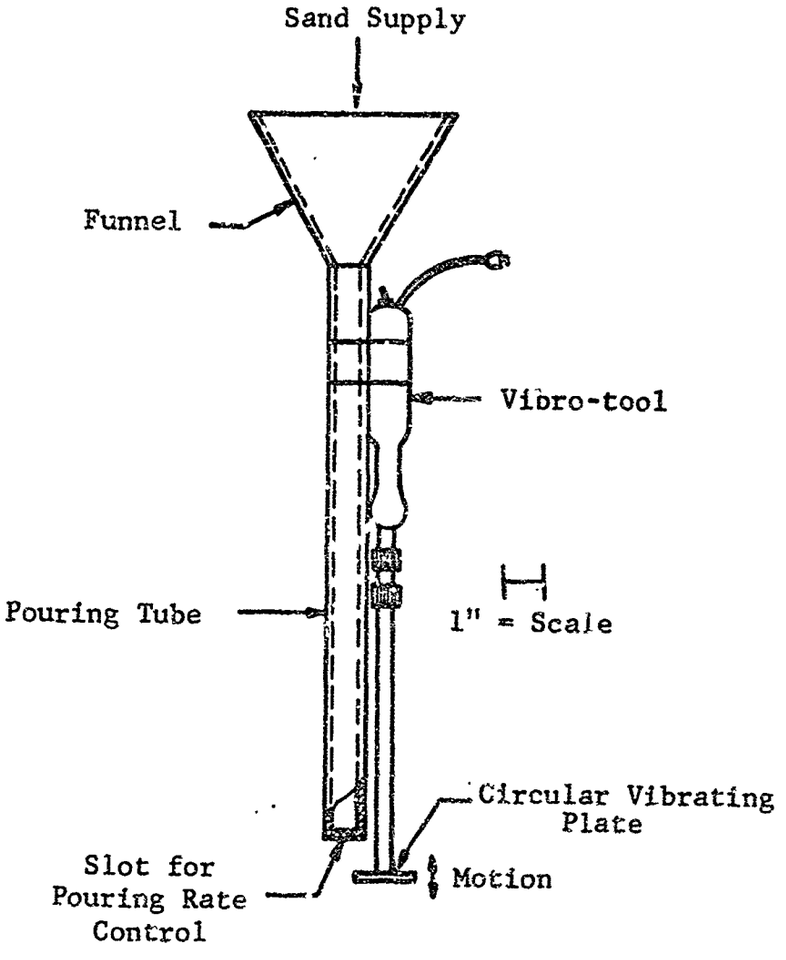

Figure 12 Equipment for Pouring and Vibrating Sand

sections such that the vibrating plate was always about 1/4 in. below the sand surface. The density of this specimen was 108.0 pcf.

The clay specimens were prepared by kneading compaction with the Harvard miniature tamper, in 1/2 in. layers using 90 blows per layer and a 20-lb spring. At the joint between the confining chamber sections, the clay had a tendency to push out the soft foam rubber spacers. To resist this bulging, masking tape was placed across the compressible rings. Six clay specimens were prepared at moisture contents ranging from 27.0 to 33.2 percent and wet densities ranging from 101.9 to 113.9 pcf.

Stress gages were positioned at the section joints along the specimens and were placed in the following manner. Soil was placed in the chamber section to the top of the section and then leveled. The stress gage was then positioned in the center of the specimen cross section and pushed gently to seat it. Another section of confining chamber was put in position with the gage leads being brought out between the compressible rings. Soil was then placed in the new chamber section being careful not to disturb the gage placement.

The soil strain gages were positioned 1 in. down from the section joint so that the soil strain would be measured at a point where the soil was rigidly constrained. The gages were placed in the following manner. The chamber section was filled with soil to a point 1 in. below the top of the section. An alignment rod was placed through the center of the coil to keep the coil in position while soil was being placed above it. A layer of soil approximately 4/10 in. thick was then placed on top of the first coil and the second coil in the set was placed on top of this soil layer. The alignment rod aided in aligning the first and second coils. Soil was then added to fill the chamber section and the alignment rod was removed. The spacing of the two coils was measured by adjusting the reference coils to null the meter.

After preparation was completed, the specimen was positioned horizontally on the ball-bearing support system (Figure 5) and the channel section and clamps were removed. A vacuum was applied to the pores of the sand specimens to minimize any disturbance to the specimen during handling.

2. Test Procedures

Twelve series of wave propagation tests were conducted with four tests being run in each series. The test sequence in each series consisted of 50, 100, 200, and 300 psi peak pressure shock loadings applied to the soil specimen in that order.

For the conduct of a test, the shock tube was assembled with the acetate diaphragm in position and the driver section filled with helium. The length of the specimen and the spacing of the soil strain gages were then recorded. After the trigger for the instrumentation was set the plunger was actuated and the shock wave traveled down the tube triggering the instrumentation and loading the end of the soil specimen. After completion of the test, the specimen was removed from the end of the shock tube and the tube cleaned out. The specimen was then repositioned for the next test. One difficulty encountered during the tests at the higher pressures (200 and 300 psi) was that, as the specimen was loaded, it compressed, which allowed the gas to escape around the end of the confining chamber. At the completion of a test series, the specimen was dismantled and the weight of the soil determined. For the tests on clay, three moisture content samples were taken.

Section IV

EXPERIMENTAL STUDY

Twelve series of tests were conducted in this study with each series consisting of tests on a given specimen at nominal overpressures of 50, 100, 200, and 300 psi. Six of the test series were conducted on Ottawa sand and the other six on the Edgar Plastic Kaolin (EPK) clay.

Of the six test series, for a given soil type, five were with an overpressure-time curve that had approximately a 1 msec dwell time of peak pressure and one with an essentially zero dwell time of peak pressure (see Figure 13 for typical input load functions). It should be noted that one of the tests at a dwell time of peak pressure of 1 msec was for the principal purpose of studying wave front development and propagation velocity. Detailed information on the soil properties for each series can be found in Appendix II and the procedure for conduct of the tests is contained in Section III.

The experimental results will be presented in six parts; peak stress attenuation, wave front development, wave shape changes, soil strain, propagation velocity, and stress-strain relationships. This section will be principally devoted to presentation of experimental data. The experimental results will be compared with theoretical predictions in Section V.

The soil stress gages were calibrated in both sand and clay under imposed boundary conditions similar to those in the wave propagation experiments. However, as presented in Section II, a variation in the gage sensitivity of $\pm$ 20 percent could be expected due to different gage placements. Most of the scatter in the data presented is most probably a result of the gage placement problem. A technique based on conservation of momentum could be used to give an in-place calibration, e.g., the gage placement effect would be included in the gage calibration. This technique essentially consists of determining the

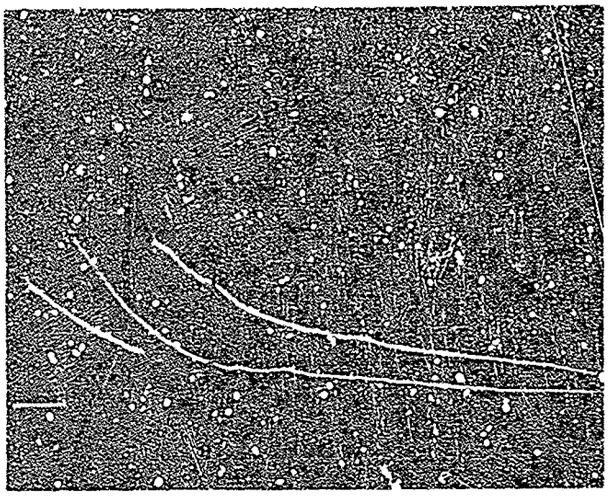

Upper
Trigger Gage

Lower
Overpressure Gage
Peak Overpressure: 55.3 psi

Sweep Speed: 2 msec/cm

a) Spiked Wave

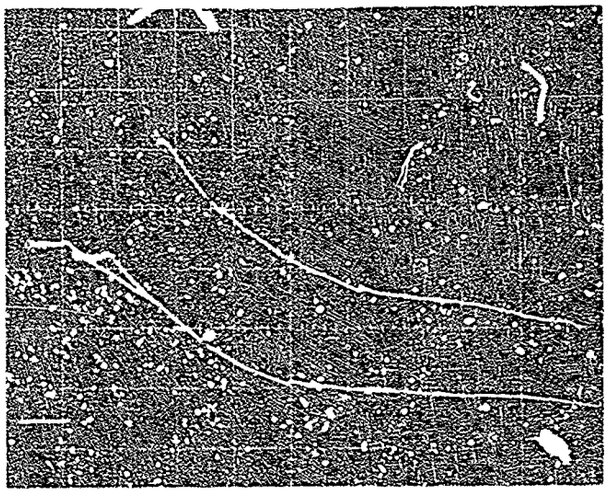

Upper
Trigger Gage

Lower
Overpressure Gage
Peak Overpressure: 50.7 psi

Sweep Speed: 2 msec/cm

b) Flat-Top Wave

Figure 13 Typical Overpressure Load-Time Relationships

total impulse of the applied shock loading and then adjusting the sensitivity of each soil stress gage such that the total impulse of the gage response equals the impulse of the applied loading. This technique would reduce the scatter of the data, however, lack of time prevented its use in this program.

1. Peak Stress Attenuation

a. Ottawa Sand

Figures 14, 15, and 16 are plots of data from three of the tests on Ottawa sand. The data show the results obtained from specimens with initial dry densities of 96.6, 103.8, and 108.0 pcf as plots of nondimensional peak stress versus distance of propagation. Peak stress was nondimensionalized by dividing the measured peak stress by the peak overpressure. In addition, it should be noted that the overpressure-time curve used in obtaining these data had a peak stress duration of approximately 1 msec for an overpressure of approximately 50 psi but this duration decreased slightly with an increase in overpressure. The curves shown in the aforementioned figures represent approximate upper and lower bounds to the experimental data.

The data indicate a general trend toward a decrease in nondimensional stress with distance of propagation. Considering the plots of σ_m/p_o versus distance of propagation, it is apparent that stress level is a significant factor in determining the rate of attenuation. Although there is some scatter in the test data at the high and low densities, (Figures 14 and 16), attenuation appears to be greater the smaller the peak stress. This relationship between stress level and rate of attenuation does not appear as valid for the tests at intermediate values of dry density, e.g., approximately 104 pcf (Figure 15).

Figures 14, 15, and 16 tend to show essentially no peak stress attenuation to a penetration of approximately 5 to 10 in. or more. This is due to the fact that the overpressure-time curve had a dwell time of peak pressure of approximately 1 msec.

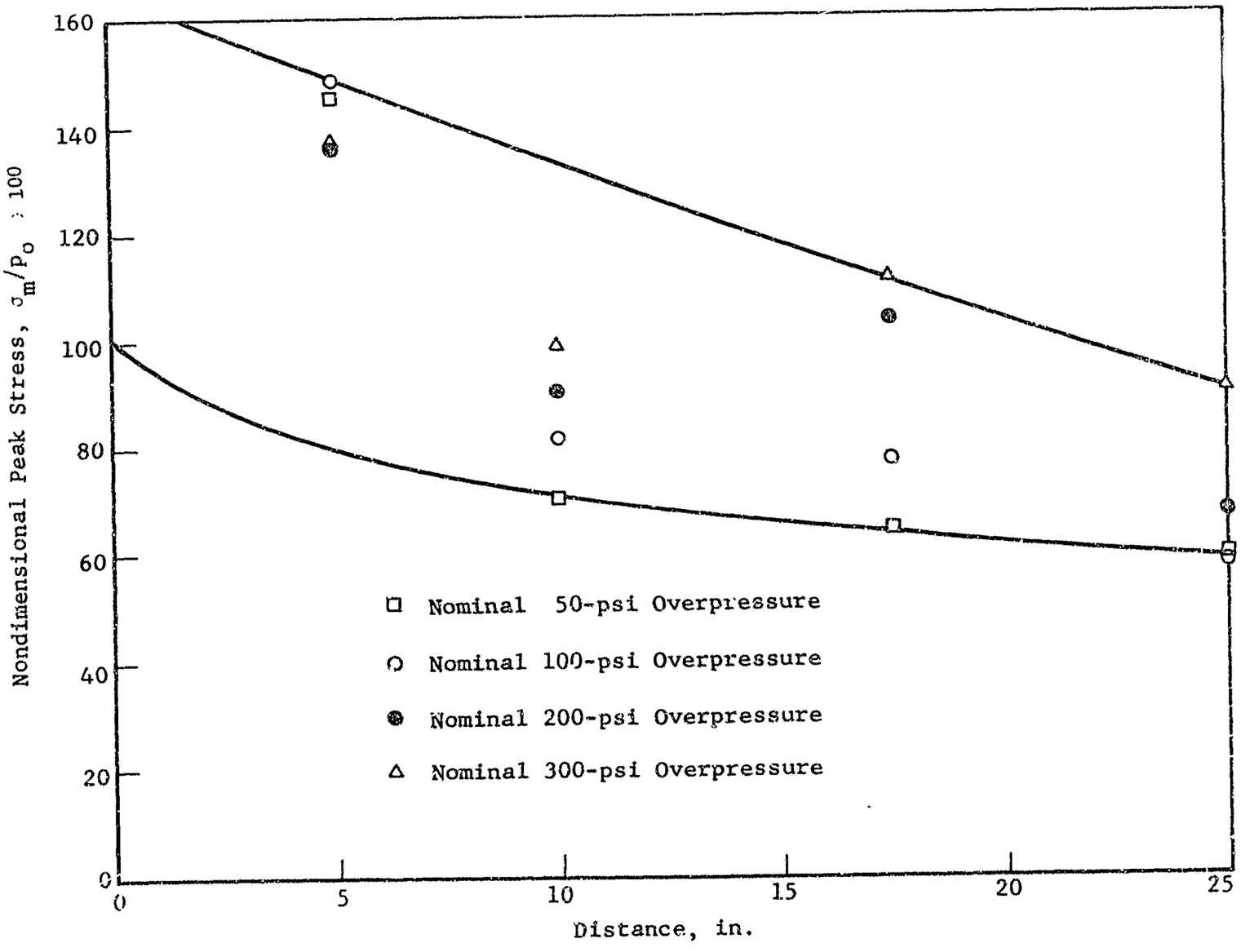

Figure 14 Nondimensional Peak Stress vs Distance of Propagation, Ottawa Sand, γ_m = 96.6 pcf

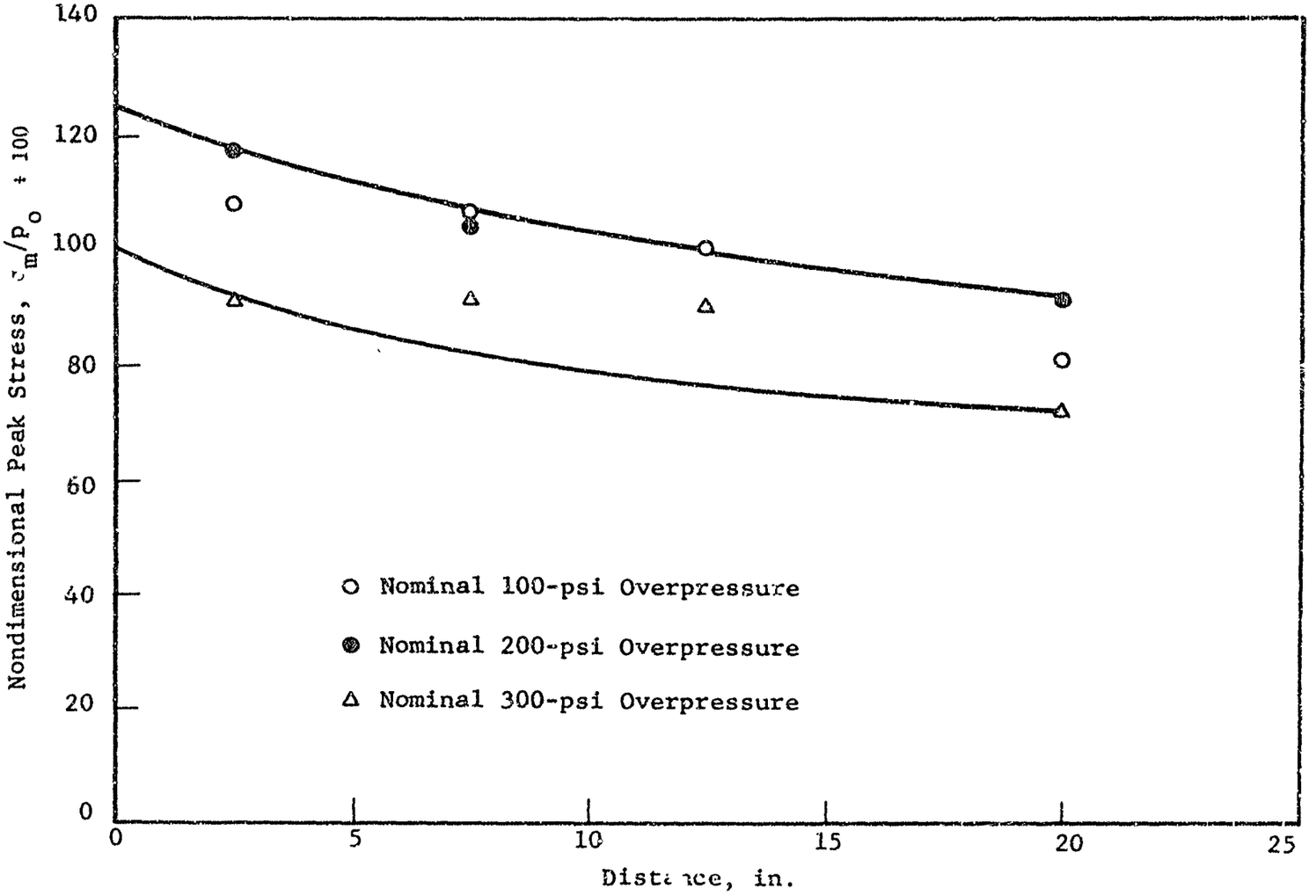

Figure 15 Nondimensional Peak Stress vs Distance of Propagation, Ottawa Sand, γ_m = 103.8 pcf

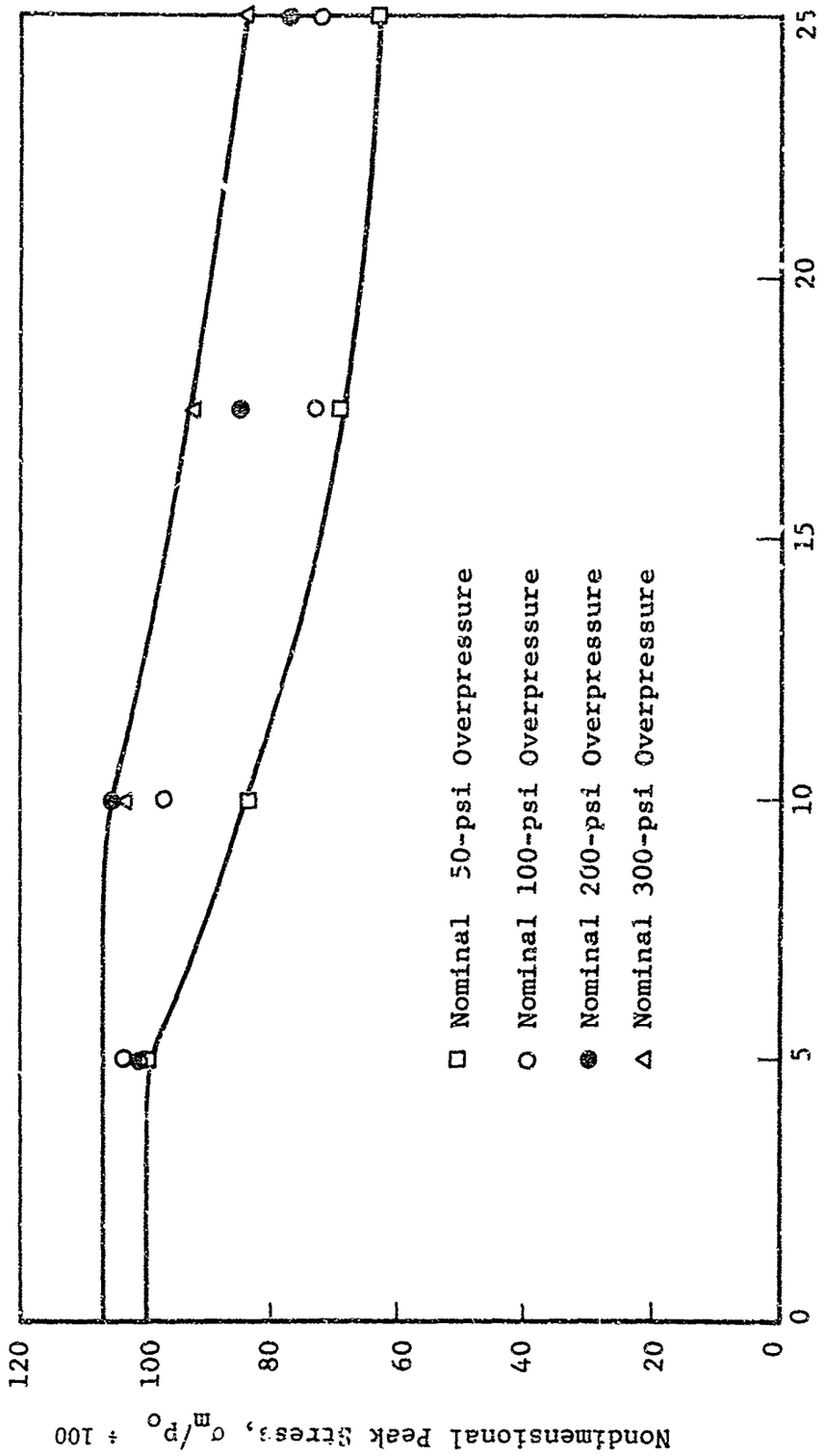

Figure 16 Nondimensional Peak Stress vs Distance of Propagation, Ottawa Sand, γ_m = 108.0 pcf

Therefore, it is to be expected that essentially no attenuation would occur over the distance the stress wave would travel during this interval. In this respect, the dissipative nature of the soil is an important factor that must be considered.

It is apparent from the figures previously discussed that measured stresses greater than the peak overpressures were recorded. This overregistration is considered to be principally the result of soil-gage interaction. Soil-gage interaction can take the form of active or passive arching, which may decrease or increase, respectively, the load coming onto the gage. The response of the gage is also affected by gage placement techniques. The difference between the measured and true free-field stress becomes more critical with greater differences between the stiffness of the soil and the gage. Therefore, it is to be expected that the lower the density of the soil the greater the significance of soil gage interaction phenomena on the measured stresses. The data collected, in general, support this conclusion.

It is also possible that the method of load application to the soil specimen accounts for a portion of the over-registration. As the shock wave impinges on the specimen it is applied initially only across the soil area; however, as the column is compressed, gas escapes around the end of the specimen and pressure is applied to the confining chamber as well as the soil area. This situation is fully discussed in Section II.1 and it is concluded that its effect on measured peak stress is probably negligible. The magnitude of over-registration due to soil-gage interaction is known to be a maximum of 20 percent based on past experience (References 1, 2 and 9).

Figure 17 shows data obtained by testing a specimen of Ottawa sand by subjecting it to a shock wave with a zero dwell time of peak pressure. The curves shown represent approximate upper and lower bounds for the data. In comparing the data for this series with those for the test series presented in Figure 15, their densities are comparable. It is apparent that the rate of attenuation for the zero dwell time overpressure tended to be greater.

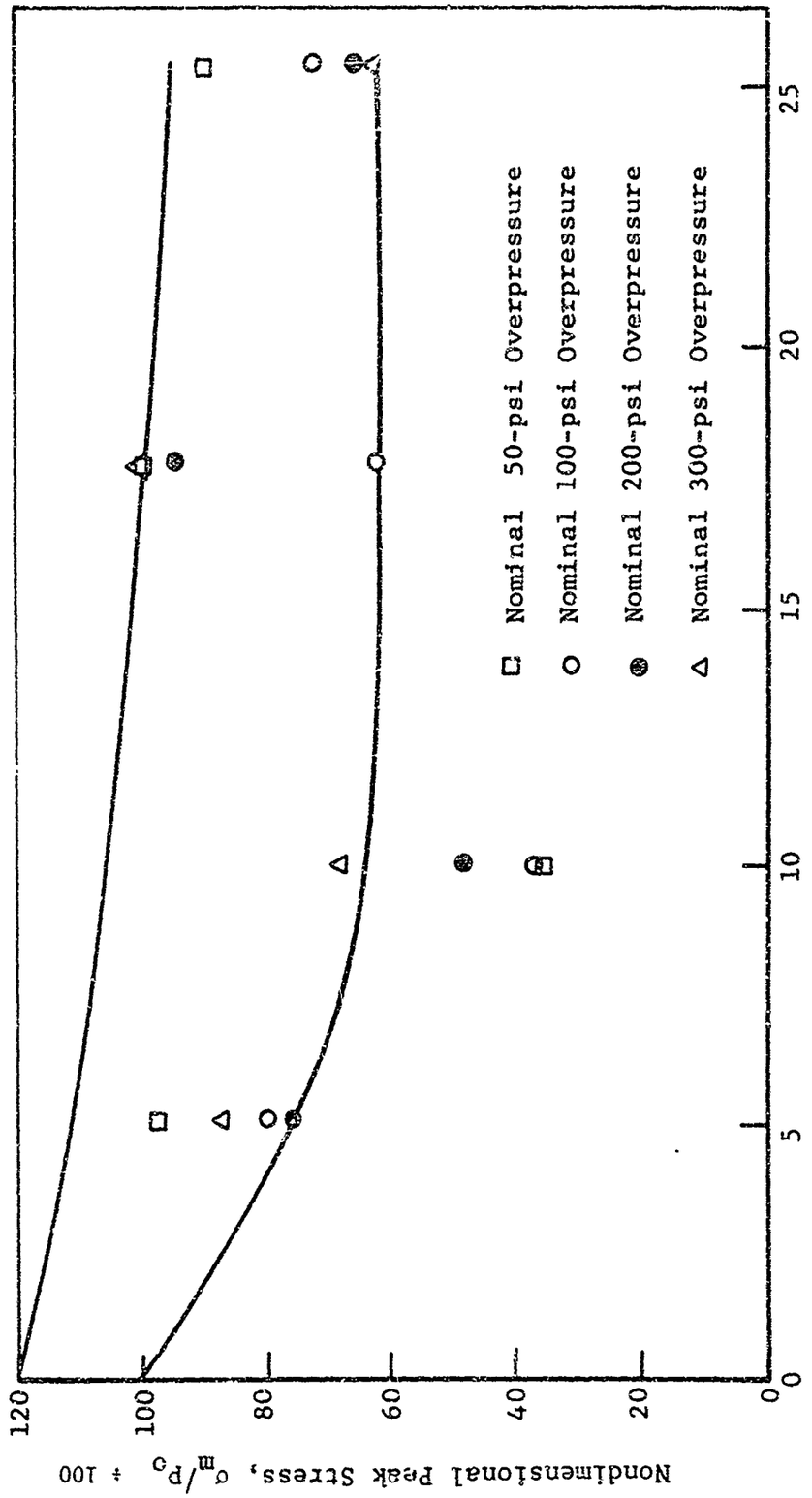

Figure 17 Nondimensional Peak Stress Vs Distance of Propagation, Ottawa Sand, γ_m = 102.4 pcf

This is most probably due to the greater rate of attenuation of peak overpressure in that case. Note that the gage at 10 in. read consistently low with respect to the other gages, which indicates a malfunction.

Based on the previous discussion, it can be said that attenuation increased with distance of propagation of the stress wave and, for a given overpressure level, the rate of attenuation increased with a decrease in dwell time of peak pressure. Also, rate of attenuation appeared to be dependent on stress level. In general, as stress level increased rate of attenuation tended to decrease; however, this is most probably the result of densification of the specimens under repeated loading.

It is evident that the shape of the loading pulse has a significant effect on stress attenuation with distance of propagation. Data tends to support the conclusion that the longer the dwell time of peak pressure the slower the rate of attenuation of peak stress. Correspondingly, for a given overpressure and duration, the more uniformly the impulse of the loading pulse is distributed over the time of loading the less the rate of attenuation with distance of propagation.

Maximum peak stress attenuation at a penetration of 25 in. was approximately 40 percent. The scatter in the data is such that it is not feasible to attempt to estimate the minimum attenuation.

b. EPK Clay

Figures 18, 19, 20, and 21 respresent plots of nondimensional peak stress versus distance of propagation for wave propagation tests on the EPK clay. These plots show the results of tests at essentially three different moisture contents and densities. The data in Figures 20 and 21 were obtained from tests on specimens whose moisture contents and densities were approximately the same. The principal difference was that the membrane which normally surrounded the specimens was omitted for the test data shown in Figure 20. However, in both cases a thin film of silicon grease was placed on the wall of the confining chamber to act as a lubricant.

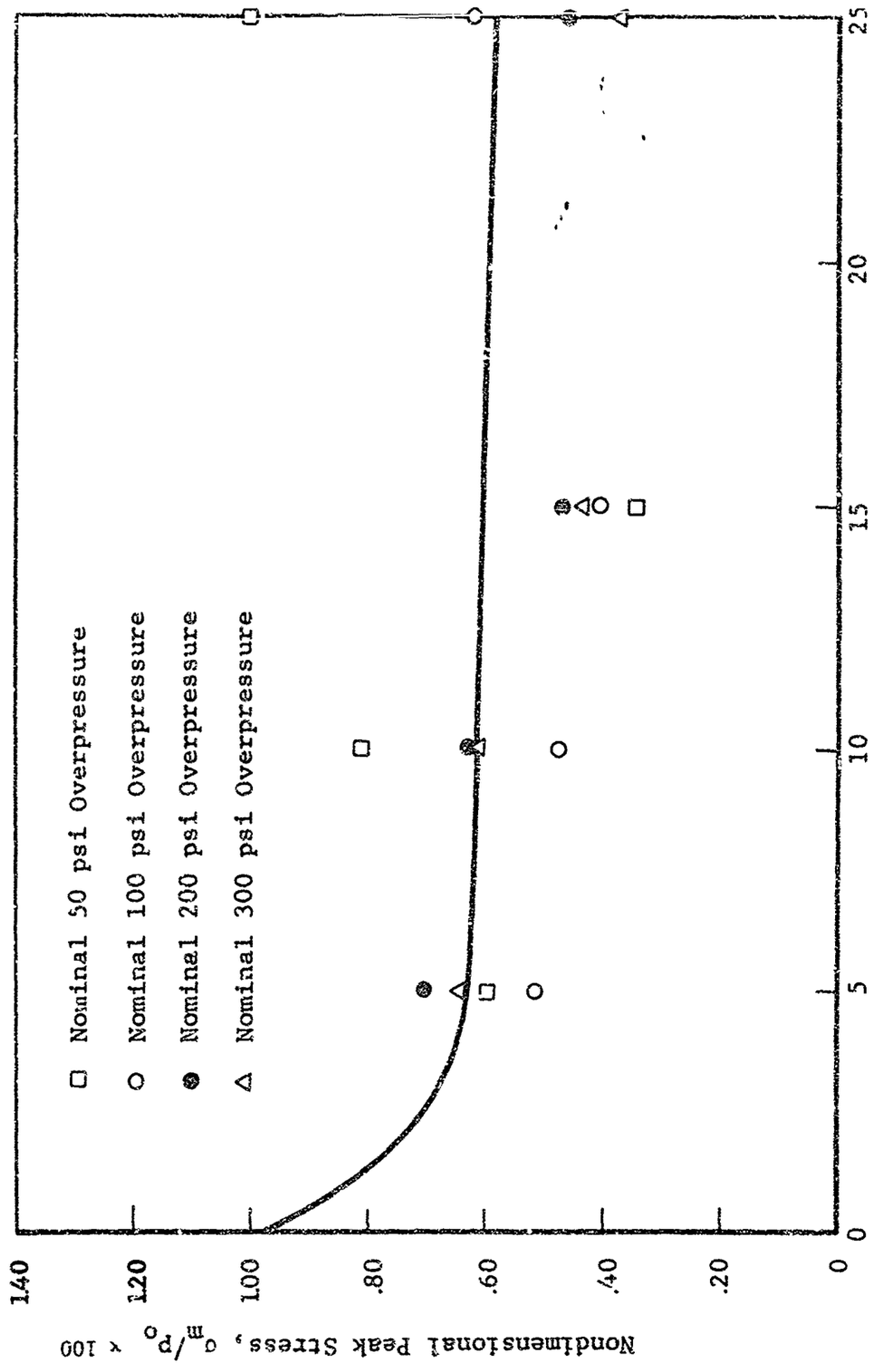

Figure 18 Nondimensional Peak Stress vs Distance of Propagation, EFK Clay, γ_m = 101.9 pcf, w = 27.0 Percent

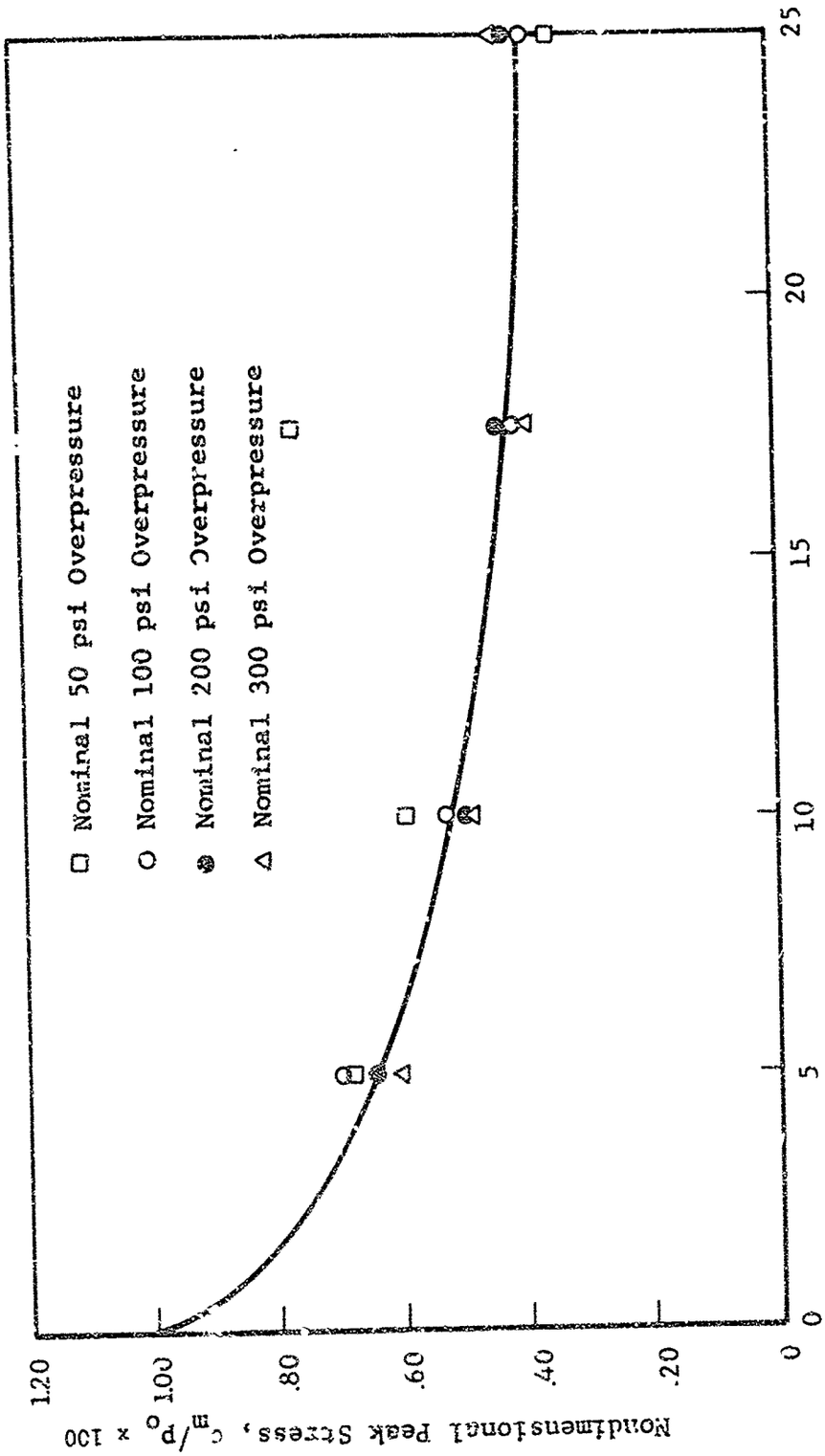

Figure 19 Nondimensional Peak Stress vs Distance of Propagation, EPK Clay, γ_m = 103.8, w = 29.7 Percent

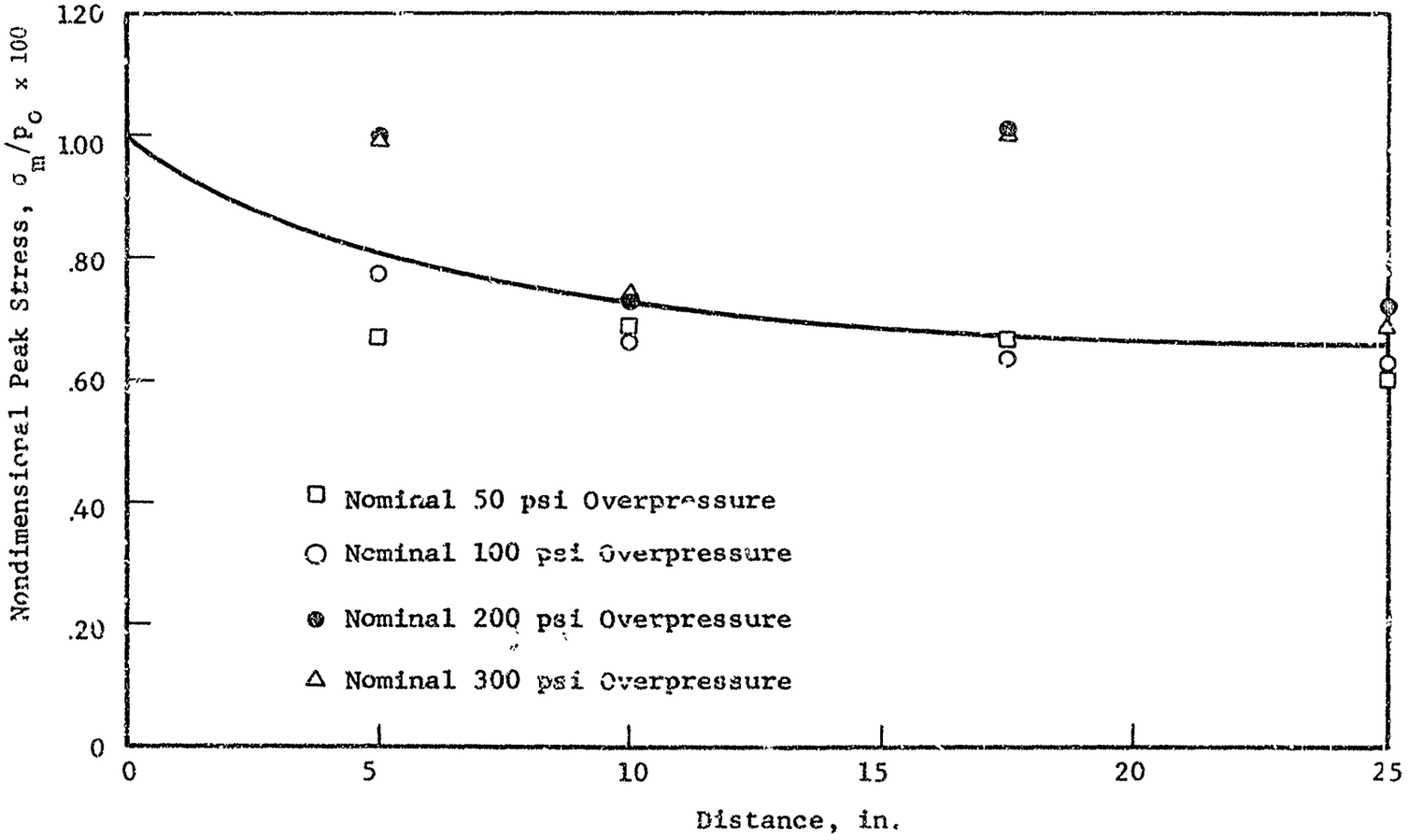

Figure 20 Nondimensional Peak Stress vs Distance of Propagation, EPK Clay, γ_m = 113.7 pcf, w = 33.1 Percent

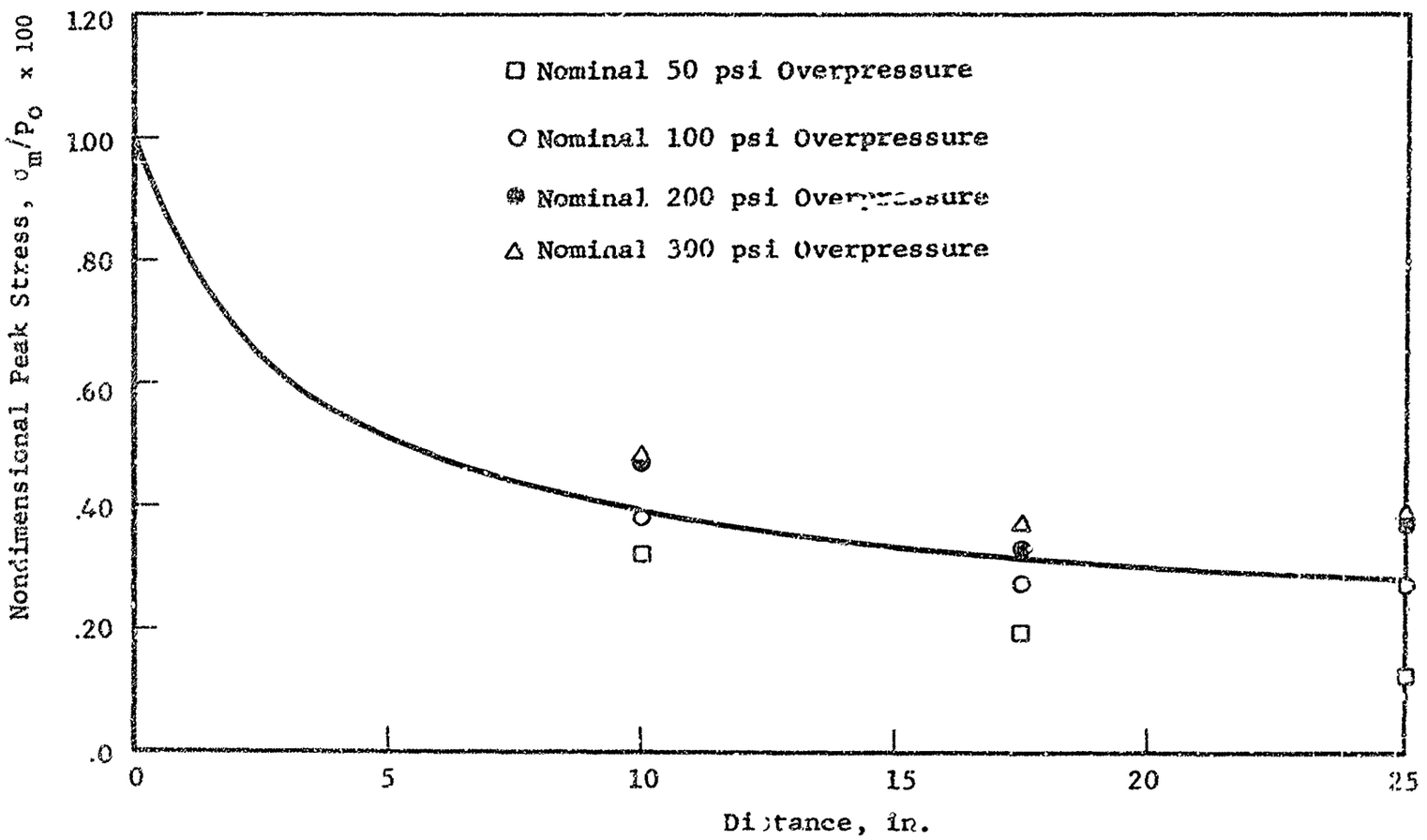

Figure 21 Nondimensional Peak Stress vs Distance of Propagation EPK Clay, γ_m = 113.2 pcf, w = 33.2 Percent

The data indicate that a relatively large amount of attenuation occurs in the first 5 in. of penetration. By the time the stress wave reaches the first gage (5 in. from the loaded surface) the peak stress has attenuated a minimum of approximately 25 percent. By the time the stress has propagated a distance of 25 in. a minimum of approximately 60 percent attenuation has occurred. Thus, the attenuation occurring in the first 5 in. is a large portion of that occurring in the next 20 in.

Included in Figures 18, 19, 20, and 21 are curves representing average trends in the data. Due to the scatter in the data a high degree of confidence cannot be placed in these curves. Nevertheless, the trend in the data is well documented with respect to an initial rapid rate of attenuation followed by a slower rate of attenuation with distance of propagation.

The two principal soil variables for the clay specimens were moisture content and density. The interrelationship between these two parameters in regard to their effect on stress wave propagation phenomena is complex and not readily discernable in the data collected. Based on data in Figures 18, 19, and 21, it appears that as moisture content and density increase attenuation also increases. However, when one considers the data in Figure 20 the trend is not as clear.

A direct comparison of the data of Figure 20 with that of the other tests may not be proper, recalling that in this case the membrane was omitted, and that only a thin layer of silicon grease separated the specimen from the wall of the confining chamber. This change in boundary condition may have increased the stiffness of the soil and thereby decreased the rate of attenuation of peak stress as it propagated through the soil.

In general, the scatter in the data appears to be reasonable. Outside of a few bad points, the data show a decrease in peak stress with distance of propagation. In addition, the effect of overpressure stress level does not manifest itself

strongly or consistently throughout all four test series. This may imply that rate of attenuation is independent of stress level, but at present, data are inadequate to arrive at this conclusion.

It should be noted that the rate of attenuation for the EPK clay is higher that for the Ottawa sand. This results from the more viscous nature of the clay and that the clay is softer with a greater hysteretic energy loss. Another reason for a higher attenuation in clay than sand is the lower wave velocity in clay. Attenuation occurs as more a function of travel time than distance. Hence, if the wave takes longer to travel through the clay column, more attenuation will probably occur.

Figure 22 represents data from a specimen of EPK clay subjected to an overpressure time curve having essentially a zero dwell time of peak pressure. The data appear to be no[t] consistent as those obtained in the previously mentioned [t]s on clay, e.g., the data obtained at depths of 10.1 and 23 in. appear to be much too high. Evidently, some form of soil gage interaction phenomena caused these gages to overregister.

The general trend is for an increase in attenuation with an increase in distance of propagation. In comparing the data of Figure 22 with those of Figure 19, their densities and moisture contents are approximately the same, one finds that a significant difference between the data is not readily apparent. This is principally due to the large scatter in the data of Figure 22. However, data of Figure 22 suggest that if more data were available, it would show a greater attenuation for the sample of clay subjected to an overpressure-time curve having a zero dwell time of peak pressure rather than one with a 1 msec dwell time.

The curves shown in Figures 18 through 22 represent the trends in the data. However, the quantitative validity of these curves is open to question due to the scatter in the data. A portion of Section V will be devoted to the establishment of attenuation curves of greater significance.

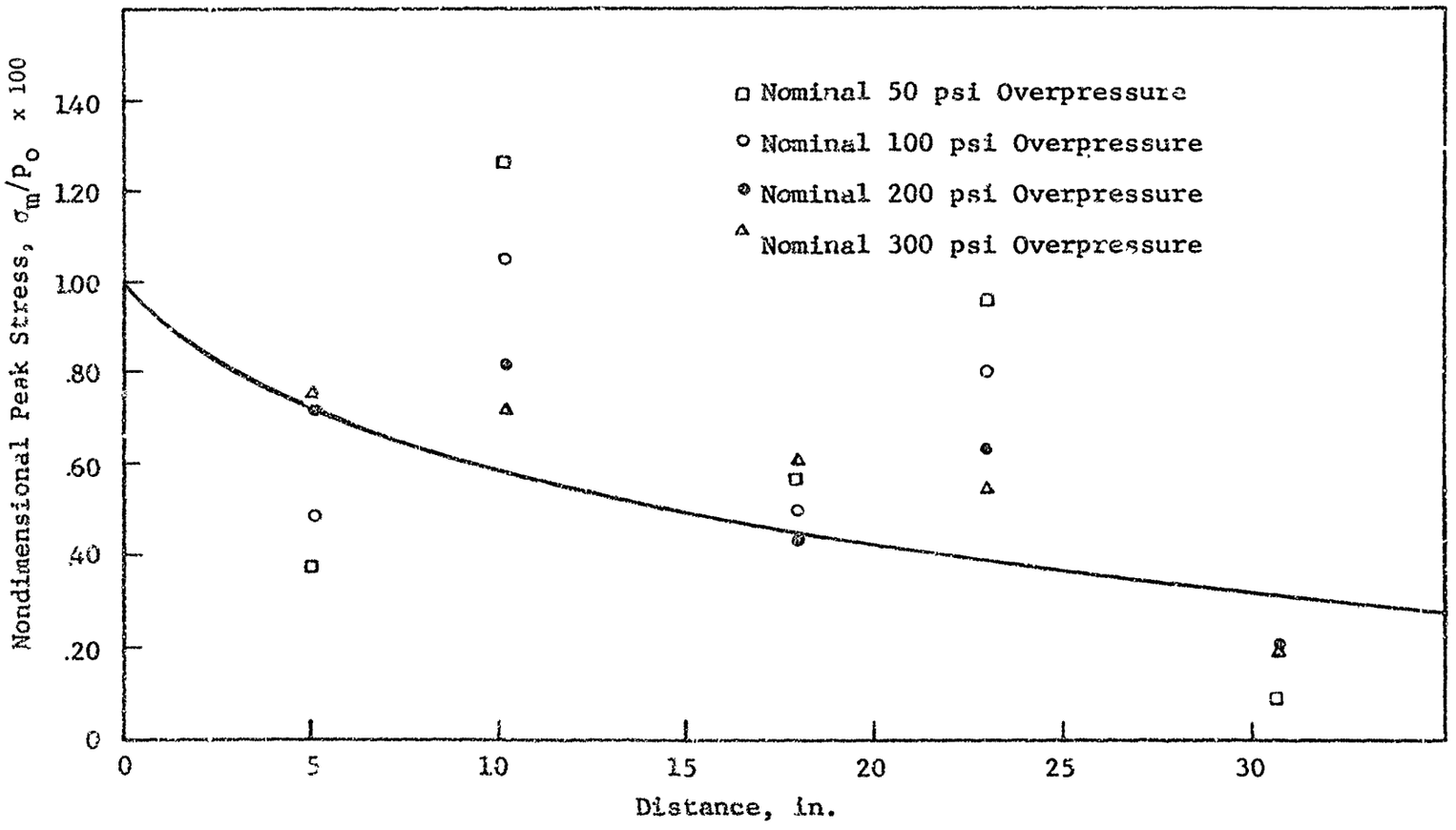

Figure 22 Nondimensional Peak Stress vs Distance of Propagation, EPK Clay, γ_m = 105.8 pcf, w = 29.3 Percent

2. Strain and Strain Rate

Measurements of strain as a function of time were made at various points along the length of the sample. The output from these gages was principally used 1) in conjunction with the data from the stress gages to establish stress-strain curves at various cross sections along the length of the specimen, 2) to determine peak strain and the change in peak strain with distance of propagation, and 3) to determine rate of strain and changes in rate of strain with distance of propagation. Items 2 and 3 will be considered in this subsection while item 1 will be discussed in a latter portion of Section IV.

Figures 23 and 24 show typical records of strain versus time obtained from the strain gages for both Ottawa sand and EPK clay. For both soils, the principal changes in the strain versus time relationship due to a change in the principal soil parameters, e.g., moisture content, density, or both were in rise time to peak strain and slope of the curve after reaching peak strain. The general trend was an increase in rise time to peak strain and a decrease in magnitude of rebound with distance of propagation.

The same sample was subjected to increasing nominal overpressures of 50, 100, 200, and 300 psi. As a result, the magnitude of the strains that occurred after the first loading were less than would have occurred if a new specimen had been used for each load application. The effect of prior loadings on the measured strain is a function of initial density in the case of Ottawa sand, and initial density and moisture content in the case of EPK clay. Peak strain and strain rate data, for both the Ottawa sand and EPK clay are summarized in Appendix III.

a. Ottawa Sand

Data show that as density increases the magnitude of peak strain decreases for a given overpressure level. The data also indicate a general trend toward an increase in the magnitude of peak strain with an increase in overpressure. Variations in the trends noted are due to soil gage interaction phenomena

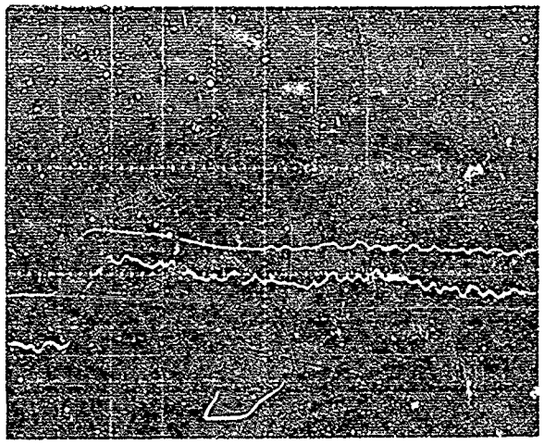

Upper

Distance: 8.5 in.
Peak Strain: 1.69 percent
Sweep Speed: 2 msec/cm

Lower

Distance: 13.5 in.
Peak Strain: 1.11 percent
Sweep Speed: 2 msec/cm

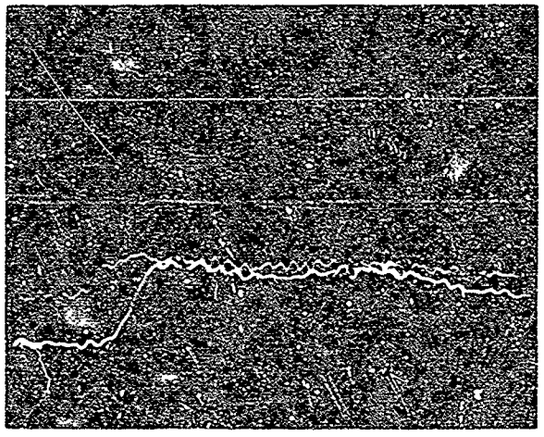

Upper

Distance: 21.0 in.
Peak Strain: 1.10 percent
Sweep Speed: 2 msec/cm

Lower

Distance: 28.5 in.
Peak Strain: 0.85 percent
Sweep Speed: 2 msec/cm

Figure 23 Typical Strain-Time Curves, Ottawa Sand
γ_m = 101.9, p_o = 166.0 psi

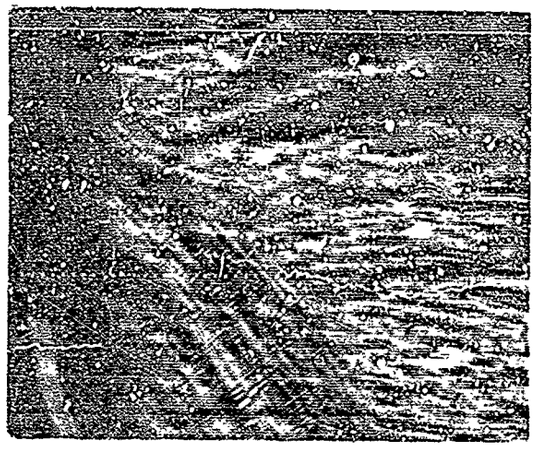

Upper

Distance: 8.5 in.
Peak Strain: 2.15 percent
Sweep Speed: 2 msec/cm

Lower

Distance: 13.5 in.
Peak Strain: 1.07 percent
Sweep Speed: 2 msec/cm

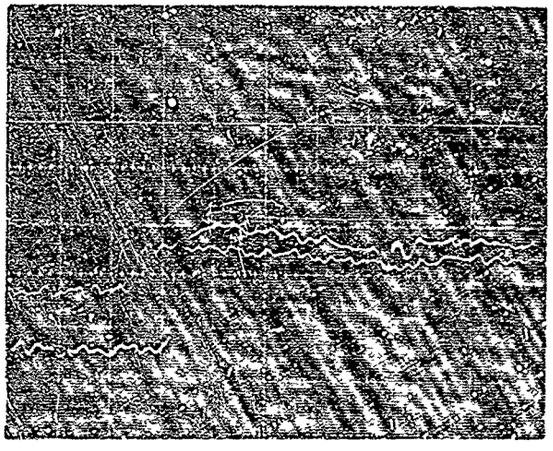

Upper

Distance: 21.0 in.
Peak Strain: 1.12 percent
Sweep Speed: 2 msec/cm

Lower

Distance: 28.5 in.
Peak Strain: 1.36 percent
Sweep Speed: 2 msec/cm

Figure 2. Typical Strain-Time Curves, EPK Clay, γ_m = 112 pcf, w = 33.2 percent, σ_o = 193 psi

related to the multiple loading of the specimens. For example, the sample of relatively dense soil, density 108.0 pcf, could upon repeated loading undergo a decrease in density which would cause a much greater strain than anticipated. The converse could also occur in loose or medium dense granular soils. It should be noted that the changes mentioned previously need not occur to the same extent at each strain gage location.

The strains in the loose sample, density of 96.6 pcf, and the strains in the medium dense specimen, 101.9 pcf, were generally less than two percent and the strain in the dense specimen, density of 108.0 pcf, was less than one percent. The values cited indicate the effect of density on the measured strain.

Rise time to peak strain tended to decrease with an increase in peak overpressure. This trend was evident in tests at all density levels tested. For a given overpressure, rise time to peak strain tended to increase the greater the distance of propagation. In addition, the rise time to peak strain decreased significantly with an increase in density.

Strain rate was determined by dividing peak strain by the time to peak strain, thus the calculated strain rates are average values. In general, the majority of the strain occurred at a faster rate; exactly how much depends upon the shape of the strain-time curve. This method of defining strain rate provides a uniform method of comparing the results from various tests.

The data show an increase in strain rate with an increase in overpressure. The magnitude of the increase appears to be a function of the magnitude of the overpressure and the distance of propagation. In this connection note that the magnitude of strain rate (percent per second) decreases with distance of propagation, for a given overpressure level.

Available data also tend to show that for a given overpressure and distance of propagation, strain rate decreases with an increase in density. The peak strains are smaller, the denser the specimen; therefore, for a given overpressure level one would

think that strain rate would increase with density. The fact that it does not is most probably related to inertia effects or the differences in mobility of the sand particles as a function of soil density, i.e., the greater the density the slower the particle velocity. It may also be due to the effect of taking an average strain rate. For larger strains, the rapid rise occurs during a greater percentage of the rise time.

Data were obtained from tests on specimens having approximately the same unit weight, 101.9 versus 102.4 pcf. The data from the former (101.9) were obtained by loading the specimen with an overpressure that had approximately a 1 msec dwell time of peak pressure. The data from the latter (102.4 pcf) were obtained by loading the specimen with an overpressure that had a zero dwell time of peak pressure.

The data on strain rate are not as consistent as are the peak strain and time to peak strain data. The data at a nominal overpressure of 50 psi show the strain rate for the dwell time of peak pressure of 1 msec, to be greater than that for a zero dwell time of peak pressure loading. However, the converse is generally true for all other nominal overpressure stress levels. The reason for this difference is not known.

b. EPK Clay

In addition to soil density, one also has to consider the effect of a change in moisture content on the parameters of interest for EPK clay. Since changes in moisture content and density occurred simultaneously, it was not possible to distinguish their effects.

Most of the data was obtained from samples subjected to an overpressure having approximately a 1 msec dwell time of peak pressure. These data show that as moisture content and wet density increases, the magnitude of peak strain at first tended to increase, for a given overpressure level, and then to decrease. The reason for this trend is related to the degree of saturation at the higher moisture content and density. At relatively low

degrees of saturation of the specimen, e.g., when water-filled voids are not interconnected, the quantity of air voids was relatively large and the sample could undergo comparatively large amounts of volume change before the stiffness of the confined water would have a measurable effect on the measured strain. Therefore, small increases in moisture content principally produce a decrease in stiffness of the soil and consequently an increase in strain, for a given overpressure.

At relatively high degrees of saturation when the water voids are interconnected and the quantity of air voids are small, the stiffness of the confined water has a significant effect on the stiffness of the soil-water system. The net result is a substantial decrease in the magnitude of the peak strain in relation to tests on specimens having lesser initial degrees of saturation. The degree of saturation (67.6 to 95.0 %) of the specimens span the range where the previously described effects occur. The effect of degree of saturation on the stiffness of confined soils was discussed by Wilson and Sibley (Reference 13).

For a given set of soil conditions the data indicate an increase in peak strain with an increase in overpressure. For a given overpressure level the data show a decrease in peak strain with distance of propagation. The data from specimens having densities of 101.9 and 103.8 pcf and moisture contents of 27.9 and 29.7 percent respectively, show peak strains generally less than six percent. The data for the specimen having a density of 113.2 pcf and moisture content of 33.2 percent, show peak strains less than three percent. Again, the effect of degree of saturation is illustrated.

For given soil parameters and distance of propagation, no definite trend could be discerned with respect to an increase in rise-time to peak strain with an increase or decrease in overpressure. However, for a given overpressure rise-time to peak strain increased with distance of propagation. The general trend

was toward a decrease in time to peak strain with an increase in moisture content and density. This trend was not consistent for all three specimens at a nominal overpressure of 50 psi.

The data show an increase in rate of strain, for a given distance of propagation, with an increase in overpressure. The magnitude of the increase, as in the tests on sand, depends on the magnitude of the overpressure and the distance of propagation. For a given overpressure the magnitude of the strain rate decreases with distance of propagation.

The data also show that strain rate initially increases with an increase in wet density and moisture content for a given overpressure level, and then decreases. This factor most probably reflects the effect of the large increase in degree of saturation.

A comparison was made of data obtained by subjecting a specimen to an overpressure that had a 1 msec dwell time of peak pressure to that obtained from a similar specimen subjected to an overpressure having a zero dwell time. It is apparent that for a given overpressure, peak strain, time to peak strain, and strain rate were greater the longer the dwell time of peak pressure.

3. Wave Velocity

In an effort to gain more accuracy in the determination of wave propagation and peak stress velocities, the oscilloscope traces were enlarged by use of a digital reader* and initial time of arrival and time of arrival of peak stress data picked off. These data, at a particular gage station, were then plotted against distance of propagation and the slope of the resulting plot was taken as the propagation velocity and the velocity of peak stress, respectively. The output from each gage was synchronized with the response of the other gages by a blanking pulse that appeared simultaneously on the polaroid pictures representing the output from each gage. This timing mark was used as the reference for determination of times of arrival.

* Gerber Digital X-Y Reader, Model GDDRS-3, The Gerber Scientific Instrument Co.

In certain cases, it was not possible to determine wave propagation velocity or peak stress velocity because either the timing marks were not sufficiently distinct, or the confining pressure on the sample (considering tests on sand) was temporarily lost. The latter sometimes occurred during tests at an overpressure of 200 psi, which rendered any subsequent test meaningless.

It should be noted that the weight of the confining chamber was approximately equal to the weight of the contained soil. The confining chamber moved with the soil and therefore its mass had an effect on wave propagation velocity and, correspondingly, velocity of peak stress. This effect of increased mass can be understood by considering the equation for wave propagation velocity during one-dimensional compression,

$$c = \sqrt{E/\rho}$$

where

- c is the propagation velocity,
- E is the modulus of the soil for the stress increment of interest, and
- ρ is the density of the soil.

It is apparent that as density is increased wave velocity decreases. Since the confining chamber moves with the soil, its mass effectively increases the mass of the soil and a decrease in propagation velocity should result. Thus, the wave velocities measured in these experiments should represent a lower bound.

The scatter in the data for the arrival time versus distance of propagation plots was found to be relatively small. However, in many cases the straight line representing the "best fit" to the data did not pass through the origin; there was a positive intercept on the distance axis. In such cases, no attempt was made to force the line to pass through the origin, the slope of the line was simply accepted as the velocity of propagation. The reason some of the arrival time versus distance plots did not go through the origin most probably resulted from a systematic error in taking the data from the polaroid pictures.

One of the major objectives in conducting test series 9 and 10 was to help determine if wave propagation velocity was a function of distance of propagation. Data from test series 1 and 2 suggest that this might be the relationship. The data from test series 9 were not adequate to aid in the resolution of this problem. Test series 10 provided some valuable information as did other test series. The net result of the information provided was that wave velocity proved independent of distance of propagation in these tests.

a. Ottawa Sand

Figure 25 is a plot of the data from five test series and shows the relationship between propagation velocity and peak overpressure. The general trend is for an increase in wave propagation velocity with an increase in peak overpressure. This may be due to the fact that for a given soil density, propagation velocity increases directly with modulus, and, for strain hardening materials, modulus increases with stress level. However, it could also be due to the effect of repeated loading of the same sample. Prior to tests at the higher overpressures the soil had been loaded previously with consequent volume change most probably volume decrease. If tests at each overpressure level had been performed on a virgin sample, it is possible that propagation velocity would have been found to be independent of stress level. Wave propagation velocity should be independent of stress level since, for a given soil density, it should be dependent on the initial tangent modulus only. In these tests, the initial tangent modulus should be a constant along the length of the specimen due to a constant geostatic stress.

The effect of a change in density, as indicated by a change in unit weight of the soil, and stiffness for a given overpressure is not as clear. For dry granular soils an increase in density produces an increase in stiffness and stiffness increases at a faster rate thus, an increase in density should produce a greater wave propagation velocity in these materials. This trend is present in the data but not strongly manifest, probably as a result of errors in taking the data off the polariod pictures.

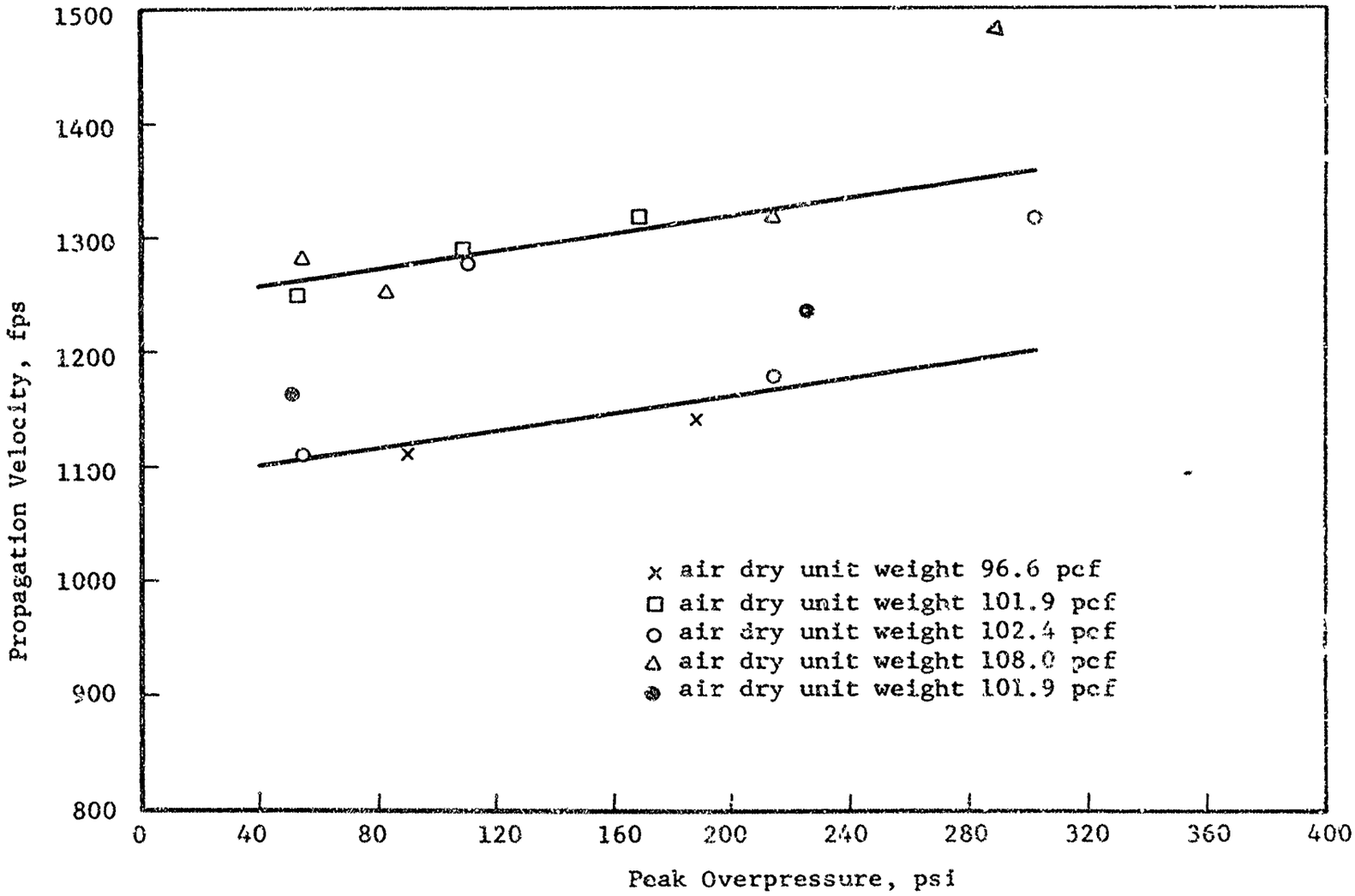

Figure 25 Peak Overpressure vs Propagation Velocity, Ottawa Sand

The lines in Figure 25 represent probable upper and lower bounds of wave propagation velocity for the specimens and stress levels used in this study. They also indicate that in changing the density of the soil from 96.6 to 108 pcf, wave propagation velocity in these tests, increased by approximately 15 percent.

Figure 26 is a plot of velocity of peak stress versus peak overpressure based on the data from five test series. The trend is toward an increase in velocity of peak stress with an increase in peak overpressure. A portion of this increase in velocity of peak stress is the result of densification of the specimens due to repeated loading. However, the magnitude of the increase in peak stress velocity is sufficiently large that a major portion of the velocity increase must be due to the increase in peak stress.

Strain hardening materials increase in stiffness with stress level. Ottawa sand has been shown to be a strain hardening material, e.g., see Appendix I. Therefore, it is to be expected that peak stress velocity would increase with an increase in overpressure.

Plots of arrival time of peak stress versus distance of propagation, from which velocity of peak stress was determined, could be represented by straight lines. This implies that the velocity of peak stress is independent of stress level since peak stress attenuates with distance of propagation. This apparent anomaly could possibly be the result of 1) the fact that stress measurements were made over a length of approximately two feet, 2) normal scatter in the data may have obscured a peak stress velocity decrease, and 3) the magnitude of the change in peak stress was not sufficient to produce an observable change in peak stress velocity.

The curves shown in Figure 26 represent approximate upper and lower bounds to the data. In general, it can be said that the trend is toward an increase in velocity of peak stress with an increase in density. Two points for a specimen at a density of 102.4 pcf lie on the upper boundary curve. The reason for this is

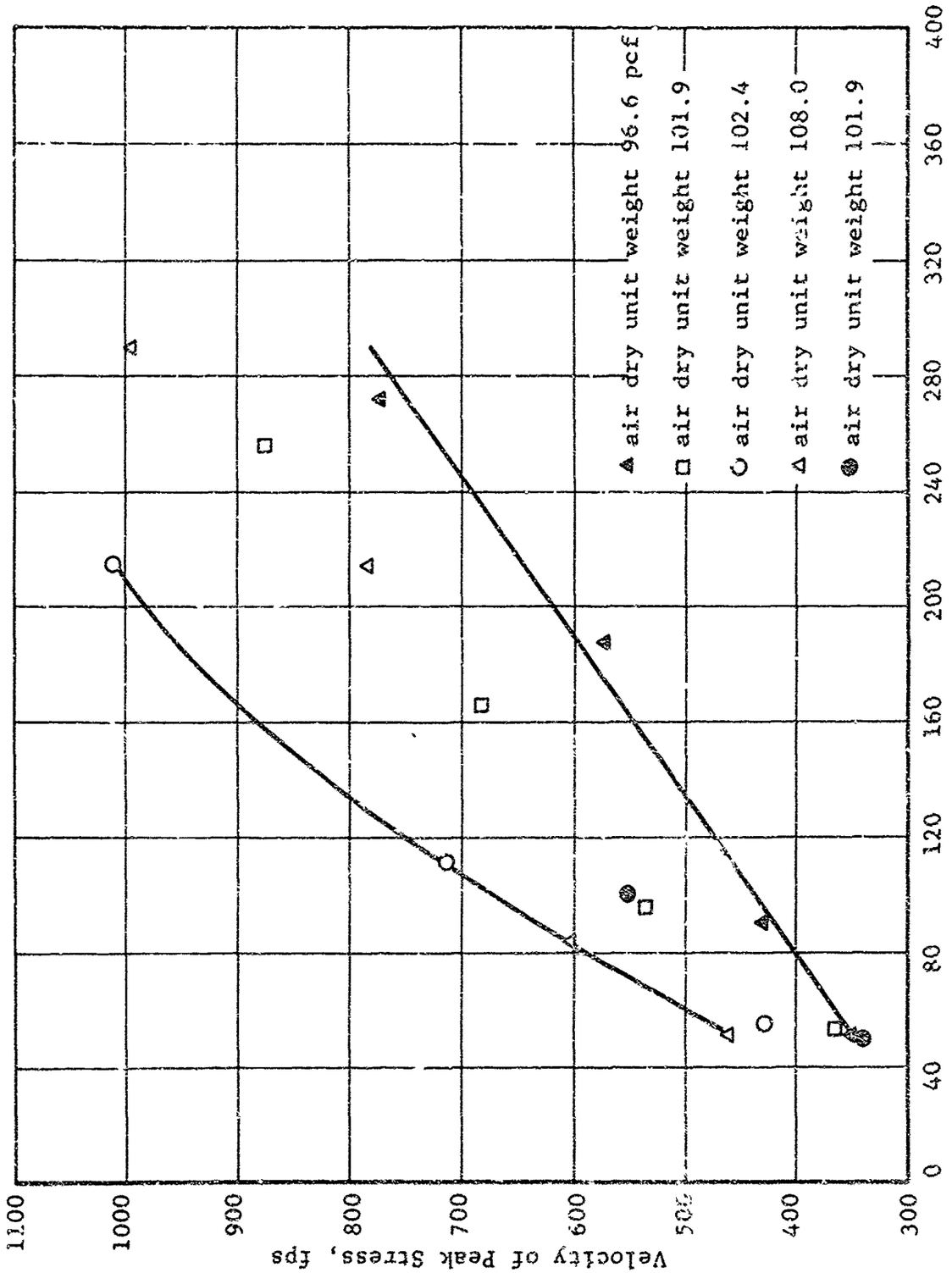

Figure 26 Peak Overpressure vs Velocity of Peak Stress, Ottawa Sand

not known. The specimen from which this data was obtained was subjected to a loading pulse having a zero dwell time of peak pressure while the other data was obtained from specimens loaded by a pulse having essentially a 1 msec dwell time of peak pressure. More data is needed to assess the effect of the shape of the loading pulse on the velocity of propagation of peak stress.

Comparing the data of Figure 25 with the data of Figure 26, it is apparent that the velocity of peak stress is very much less that the velocity of wave propagation, for a given overpressure and soil density. Available stress-strain data is not adequate to more fully evaluate wave propagation velocity and velocity of peak stress.

b. EPK Clay

Data showing the relationship between propagation velocity and overpressure for the EPK clay are shown in Figure 27. It is evident that the range of measured propagation velocities is much greater for clay than for sand and the wave propagation velocity for a given stress level is generally less for clay than for sand. In addition, the scatter in the clay data is relatively large and the effect of a change in stress level on propagation velocity appears to be significantly greater for clay than for sand. This increased significance of stress level on wave propagation velocity may be related to strain rate effects with regard to their effect on the stress-strain curves and consequently modulus. Available stress-strain data are not adequate to test this hypothesis.

In one of the tests there is shown a very strong tendency toward a decrease in propagation velocity with an increase in peak overpressure. The reason for this anomolous behavior is not known. The curves shown in Figure 27 represent approximate upper and lower bounds to the data.

The data presented in Figure 27 has been replotted as Figure 28 to illustrate the effect of degree of saturation on propagation velocity. It is evident that changes in degree of saturation produce very significant changes in propagation velocity.

○ γ_m = 104.9, w = 27.0 percent △ γ_m = 113.2, w = 33.2 percent
□ γ_m = 103.8, w = 29.7 percent ● γ_m = 101.9, w = 28.0 percent
× γ_m = 113.7, w = 33.1 percent ◇ γ_m = 105.8, w = 29.3 percent

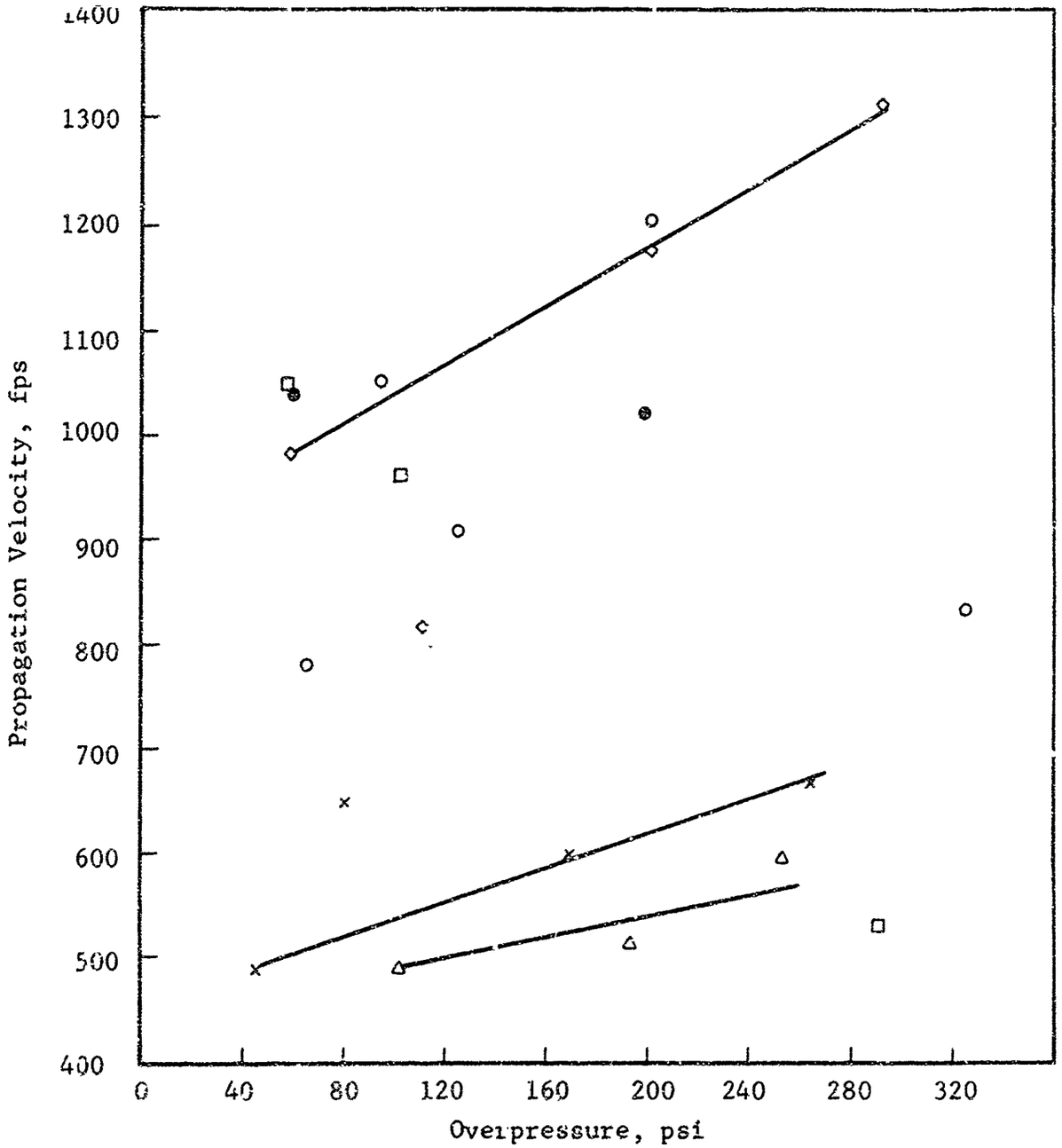

Figure 27 Peak Overpressure vs Propagation Velocity, EPK Clay

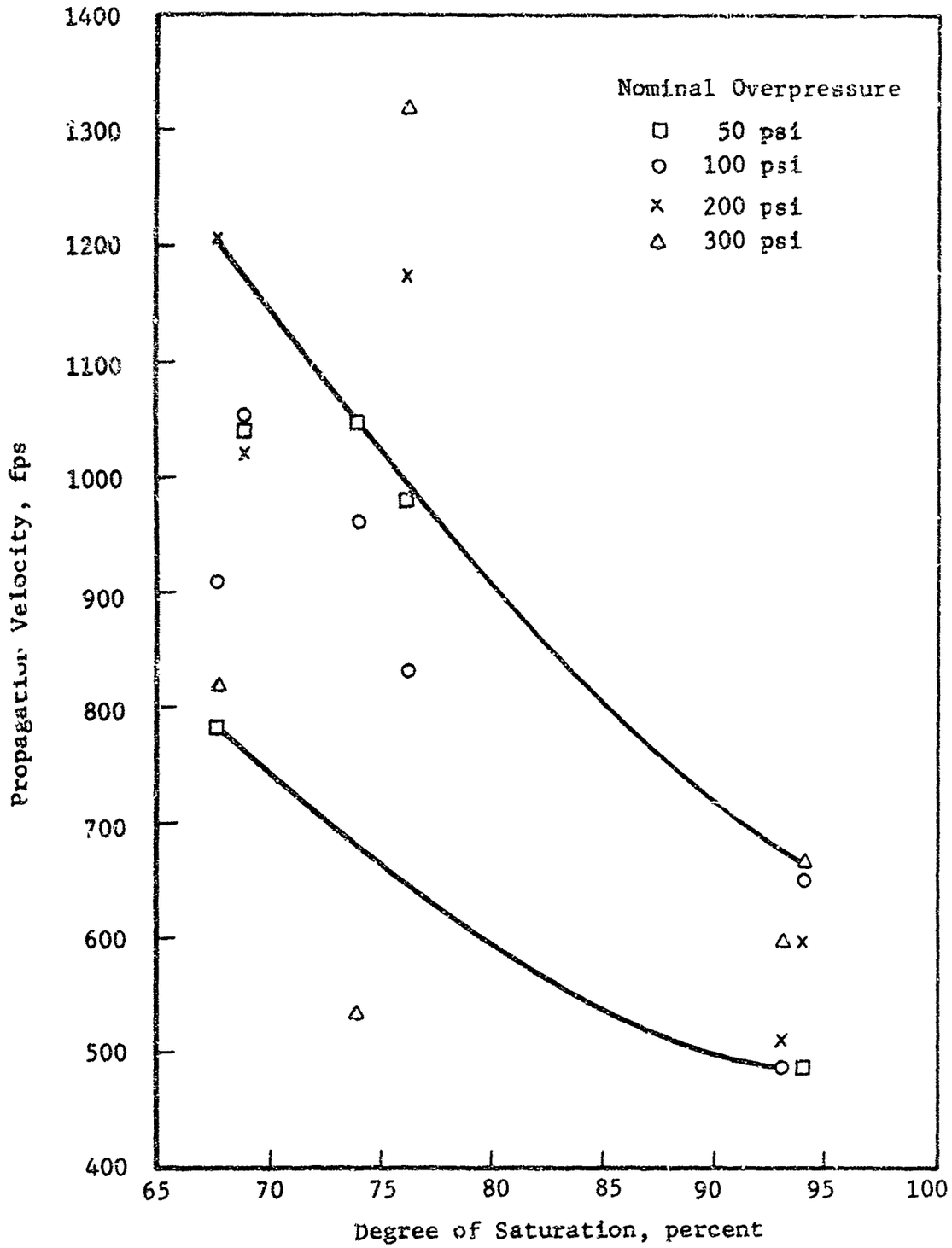

Figure 28 Degree of Saturation vs Propagation Velocity, EPK Clay

The trend is toward a decrease in propagation velocity with an increase in degree of saturation. This is the result of a decrease in initial tangent modulus and an increase in soil density with an increase in degree of saturation.

The curves shown in Figure 28 represent most probable upper and lower bounds to the data. The figure also shows that the greater the degree of saturation the less the probable range of propagation velocities for the range of overpressures used in this study.

Figure 29 is a plot of velocity of peak stress versus peak overpressure for four series of tests on EPK clay. With the exception of four data points, the data agrees quite well with the curve shown This implies that, for the conditions of test described, peak stress velocity is independent of soil properties. More data is needed to test this hypothesis.

Comparing Figure 27 and 29, it is apparent that the velocity of peak stress decreases with peak overpressure while the converse is true with respect to wave propagation. This is due to the fact that wave propagation velocity is dependent on initial tangent modulus, which will tend to increase with overpressure increase, due to densification under repeated loading, while peak stress velocity is dependent on the tangent modulus at the particular stress level under consideration, which will decrease with an increase in stress level due to plastic type stress strain characteristics of the clay (see Appendix I).

It should be noted that the range in velocity of peak stress, for a given overpressure level, is much less than for wave propagation velocity. This implies that, for clay soils, soil properties are much more important in determining the magnitude of wave propagation velocity than peak stress velocity.

Figure 30 is a plot of degree of saturation versus velocity of peak stress. It is apparent that the velocity of peak stress tends to decrease with an increase in degree of saturation but the magnitude of the decrease is relatively small. Also, it should be noted that, for a given degree of saturation, the range in velocity of peak stress is relatively small which indicates that it is not greatly affected by peak overpressure.

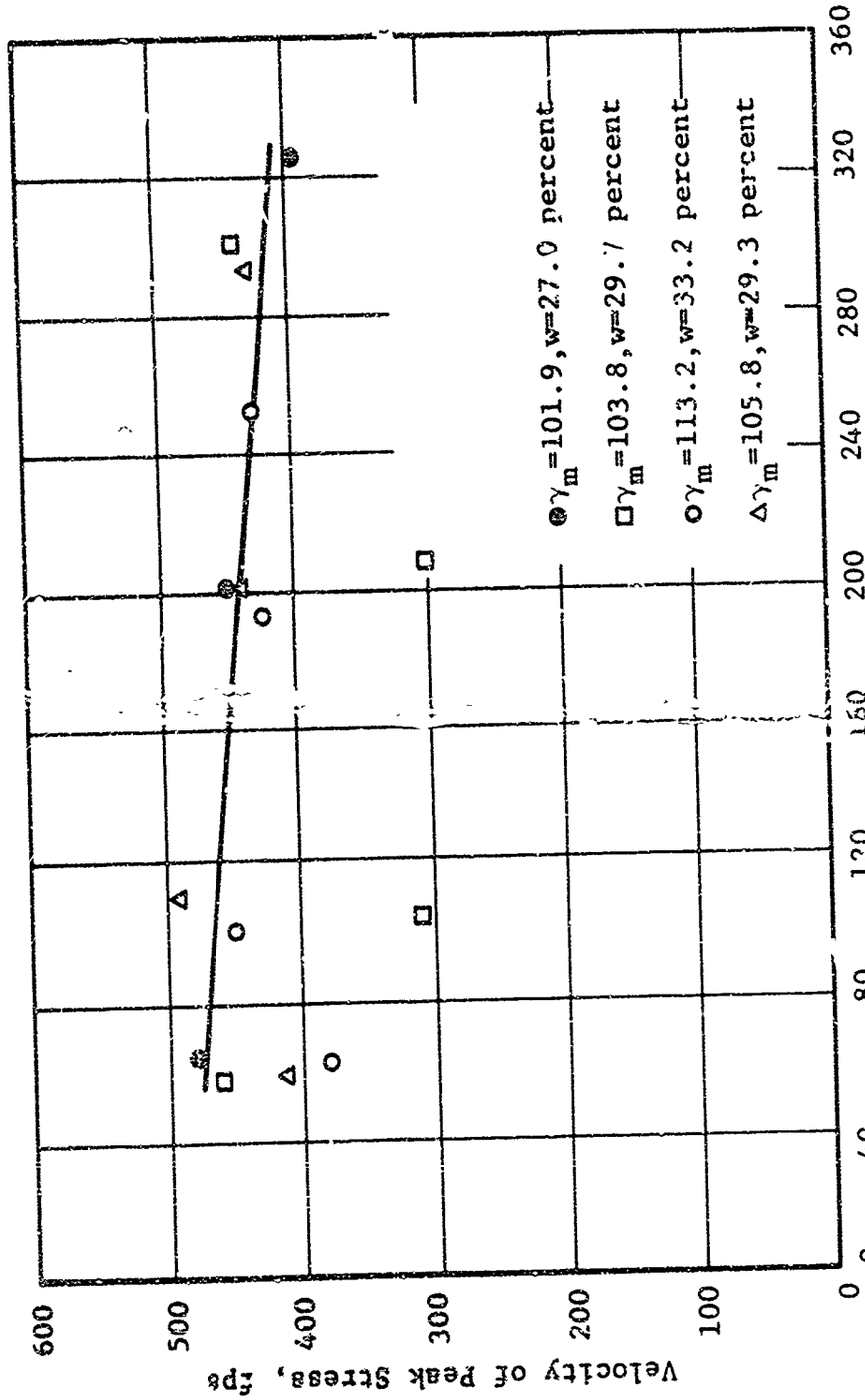

Figure 29 Peak Overpressure vs Velocity of Peak Stress EPK Clay

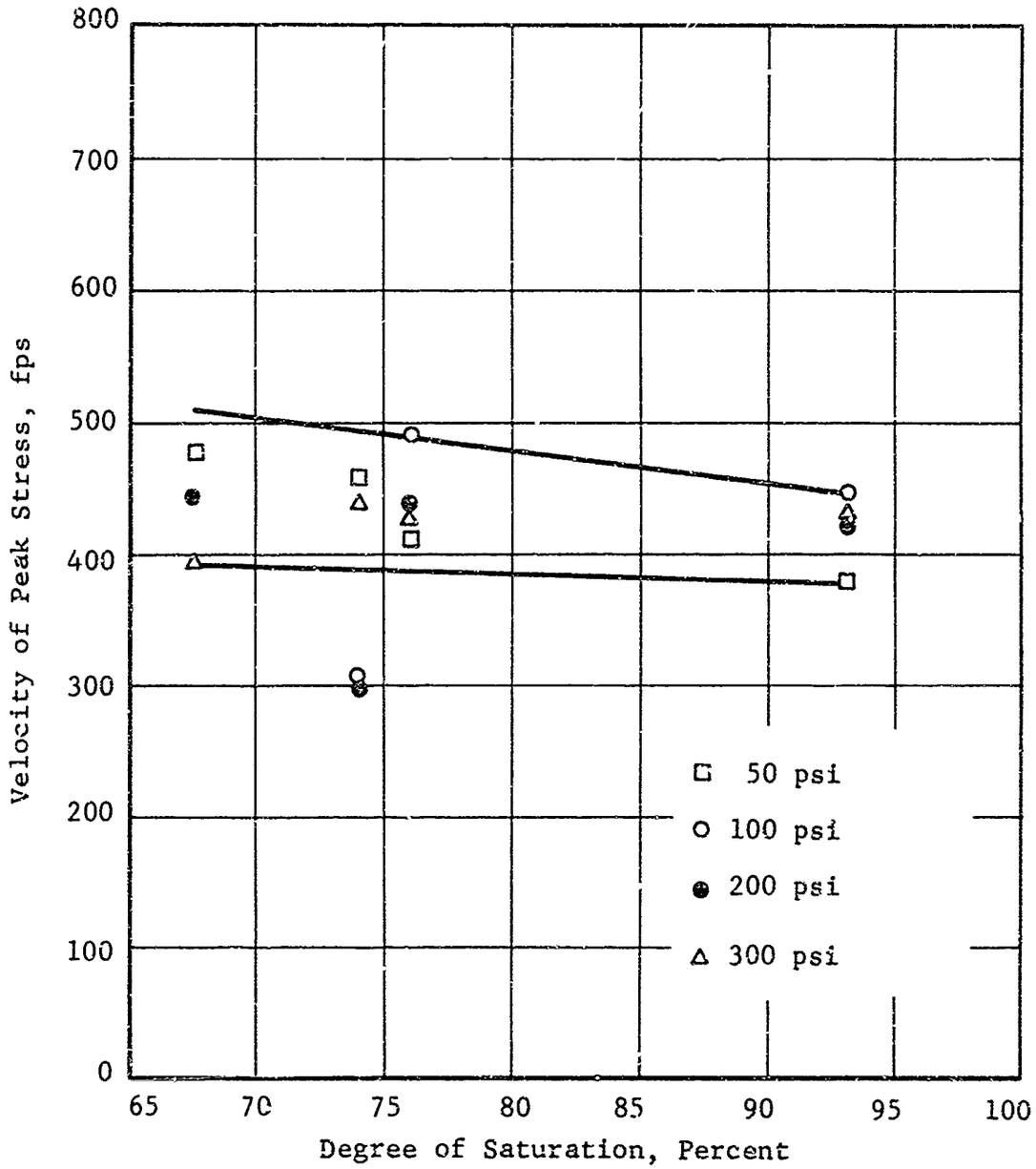

Figure 30 Degree of Saturation vs Velocity of Peak Stress, EPK Clay

Comparing Figure 28 and 30 it is evident that the degree of saturation has a much greater effect on propagation velocity than velocity of peak stress. Also, it should be noted that as degree of saturation increases wave propagation velocity and velocity of peak stress approach each other.

4. Stress Wave Front Development

The portion of the stress-time curve between the first appearance of a detectable signal and the main peak is termed the wave front. This portion of the report is concerned with the shape of the wave front and the rise time to peak stress associated with the front as well as to changes in these characteristics of the front as the front propagates through the soil.

When a soil is loaded by a pressure pulse the stress-time history of the wave propagating through the soil may behave basically in one of two ways. The rise time to peak stress may increase with distance of propagation, which is indicative of plastic type of wave propagation. The other alternative is represented by a decrease in rise time to peak pressure with distance of propagation resulting in the formation of a shock front at some depth below the surface. At some depth below the surface of loading, it is possible for the shock wave previously formed to degenerate into a plastic type wave.

Seaman and Whitman (Reference 3) have shown that both wave types are generated in sands and that the type existing at a particular depth is a function of stress increment at the wave front. In addition, they showed that formation and degeneration of shock waves could be explained by a rate-independent stress-strain model that incorporates an S-shaped stress-strain curve with the effects of geostatic stress. In their report they suggest, for sands, that when the ratio of the dynamic stress increment at the wave front to the initial geostatic stress exceeds 12, shock-wave formation can be anticipated. The aforementioned criterion is proposed as a crude estimate and it is recognized that the relationship may not be linear.

All 12 test series conducted in the study and reported herein provided information on wave front development. In particular, test series 9 and 10 provided a better understanding (one of their main goals) of wave front development. Test series 9 was performed on Ottawa sand while test series 10 was on EPK clay.

a. Ottawa Sand

Figure 31 is a set of pictures showing data obtained from a test on Ottawa sand at a nominal overpressure of 200 psi. These photos were obtained during test series 9 where the main purpose was to study wave front development. Seven stress gages were included in this test series but only four performed satisfactorily. It is quite apparent that plastic-type wave propagation behavior is evident, i.e., there is no tendency towards a decrease in rise time to peak stress with distance of propagation. Such was the case in all test series, for all overpressure levels, on Ottawa sand.

At a given overpressure and for a given soil density, rise time to peak stress always increased with distance of propagation. For the conditions previously specified, it can also be stated that rise time tended to decrease with an increase in soil density. The relationship becomes less distinct as stress level is increased, which is most probably due to changes in soil properties with each application of load. The same specimen was used for all stress levels in a given test series.

It was also clearly evident that rise time to peak stress decreased as peak overpressure increased. This was found to be true for all density states tested. Figure 32 shows typical gage traces for nominal overpressures of 50 and 200 psi and indicates the decrease in rise time with overpressure.

The discussion presented in previous paragraphs was found to be true for both loading conditions used in this study. That is for the condition where the dwell time of peak overpressure was essentially zero. The principal effect of a

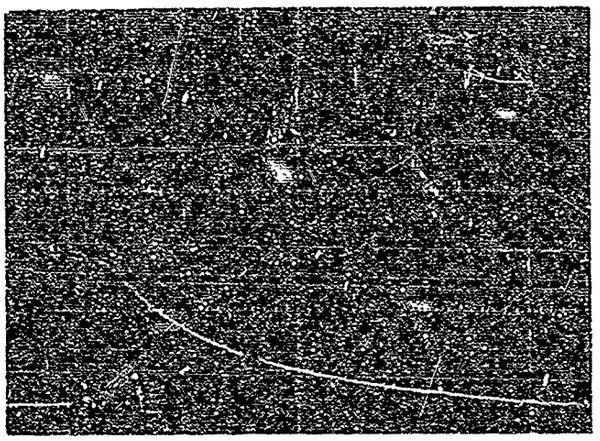

Upper
Trigger Cage

Lower
Overpressure Gage

Peak Overpressure: 225.4 psi
Distance: 0.0 in.

Sweep Speed: 1 msec/cm

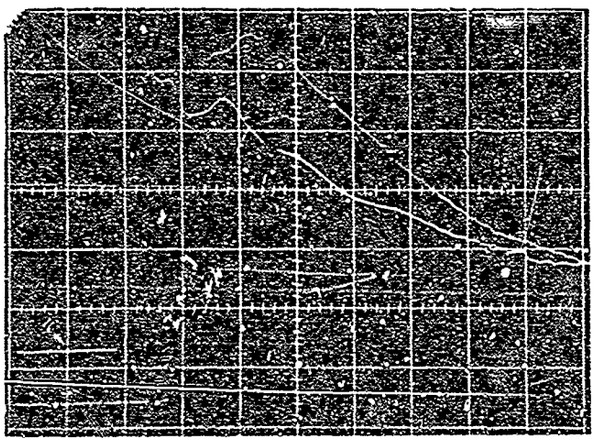

Upper
σ - Gage No. 2

Peak Stress: 296.0 psi
Rise Time: 0.600 msec
Distance: 7.6 in.

Lower
σ - Gage No. 3

Peak Stress: 264.0 psi
Rise Time: 1.757 msec
Distance: 15.3 in.

Sweep Speed: 1 msec/cm

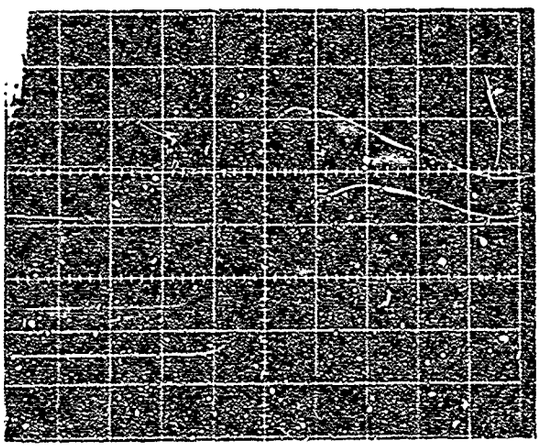

Upper
σ - Gage No. 11

Peak Stress: 203.0 psi
Rise Time: 2.239 msec
Distance: 30.6 in.

Lower
σ - Gage No. CS-2

Peak Stress: 138.0 psi
Rise Time: 3.066 msec
Distance: 38.2 in.

Sweep Speed: 1 msec/cm

Figure 31 Typical Overpressure and Stress Gage Records, Ottawa Sand γ_m = 101.9 pcf

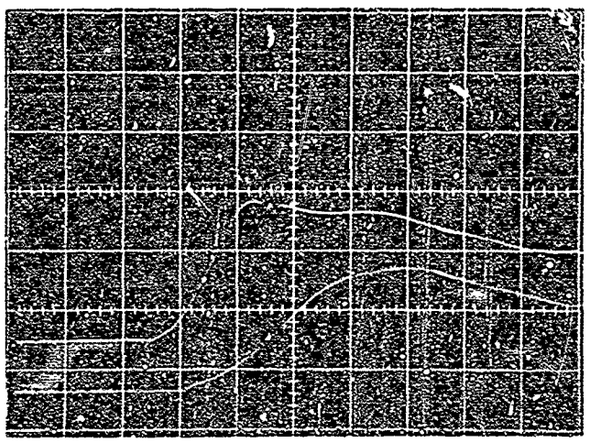

Upper
σ - Gage No. 2

Rise Time: 1.700 msec
Peak Stress: 81.0 psi
Distance: 7.6 in.

Lower
σ - Gage No. 3

Rise Time: 3.928 msec
Peak Stress: 59.0 psi
Distance: 15.3 in.

(a) Overpressure
Sweep Speed: 1 msec/cm

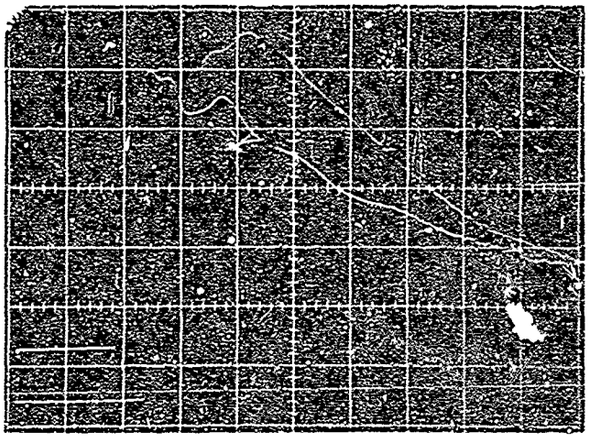

Upper
σ - Gage No. 2

Rise Time: 0.600 msec
Peak Stress: 296.0 psi
Distance: 7.6 in.

Lower
σ - Gage No. 3

Rise Time: 1.757 msec
Peak Stress: 264.0 psi
Distance: 15.3 in.

(b) Overpressure
Sweep Speed: 1 msec/cm

Figure 32 Typical Stress Gage Traces Indicating Change in Rise Time with an Increase in Overpressure, Ottawa Sand γ_m = 101.9 pcf

decrease in dwell time of peak pressure was to decrease the rise time to peak stress for a given peak overpressure and distance of propagation.

Based on previous discussion, it can be said that no evidence of shock-wave formation could be discerned in the data obtained in this experimental study. Only plastic-type wave propagation phenomena were observed. This manifested itself as an increase in time to peak stress with distance of propagation for all specimens and at all overpressure levels. The data upon which these conclusions are based is presented in tabulated form in Appendix IV.

b. EPK Clay

Figure 33 is a complete set of data obtained from a test on EPK clay at a nominal overpressure of 200 psi. These photos were obtained from test series 10 where the main purpose was to study wave front development. It is evident from these pictures that plastic type wave propagation is occurring throughout the entire length of the specimen. Such a tendency existed for tests on all specimens at all stress levels. However, these data did not appear as consistent as that for Ottawa sand. This is most probably due to the greater difficulty in pinpointing the time of arrival of the stress wave as well as the time of arrival of peak stress.

For a given stress level it was not possible to discern a definite relationship between rise time to peak stress and the properties of the specimens, i.e., moisture content (or degree of saturation) and density (or unit weight). However, the data shows that degree of saturation has a significant effect on rate of rise to peak stress (ratio of peak stress to risetime) and that its effect depends on stress level and distance of propagation. This relationship is complex and more data is needed to adequately determine it.

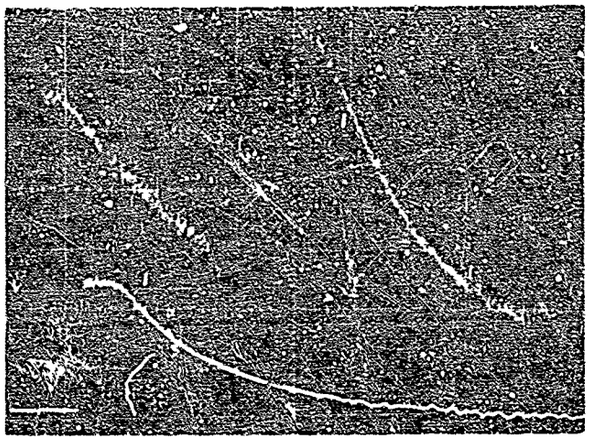

Upper
Trigger Gage

Lower
Overpressure Gage

Peak Overpressure: 198.4 psi
Distance: 0.0 in.

Sweep Speed: 1 msec/cm

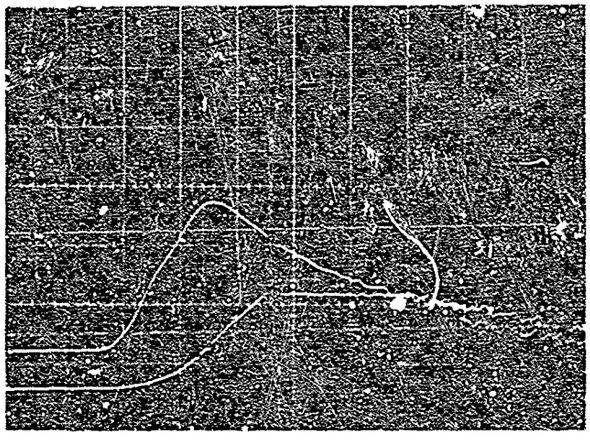

Upper
σ - Gage No. 3

Peak Stress: 153.0 psi
Rise Time: 1.810 msec
Distance: 7.6 in.

Lower
σ - Gage No. 1

Peak Stress: 95.0 psi
Rise Time: 2.555 msec
Distance: 15.2 in.

Sweep Speed: 1 msec/cm

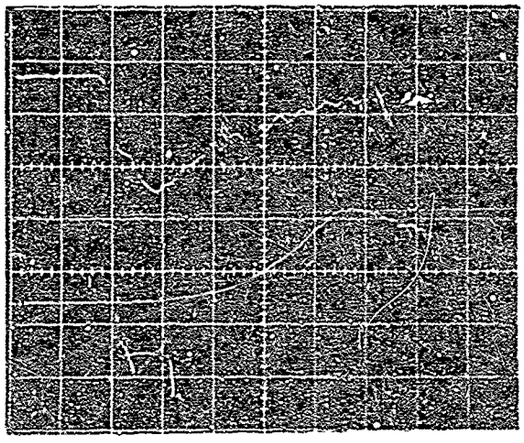

Upper
Circum. Strain at 3.9 in.

Peak Strain: 43.2 με
Rise Time: 1.177 msec
Distance: 3.9 in.

Lower
σ - Gage No. 2

Peak Stress: 51.0 psi
Rise Time: 3.710 msec
Distance: 22.8 in.

Sweep Speed: 1 msec/cm

Figure 33a Typical Overpressure, Stress, Circumferential Strain, and Reaction End Gage Records, EPK Clay
γ_m= 101.9 pcf, w = 28.0 percent

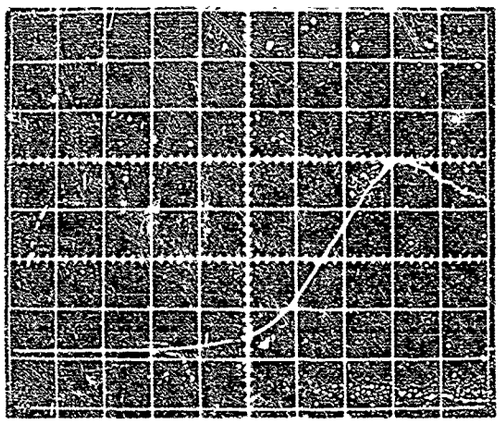

Lower
σ - Gage No. 4

Peak Stress: 118.0 psi
Rise Time: 4.631 msec
Distance: 30.5 in.

Sweep Speed: 1 msec/cm

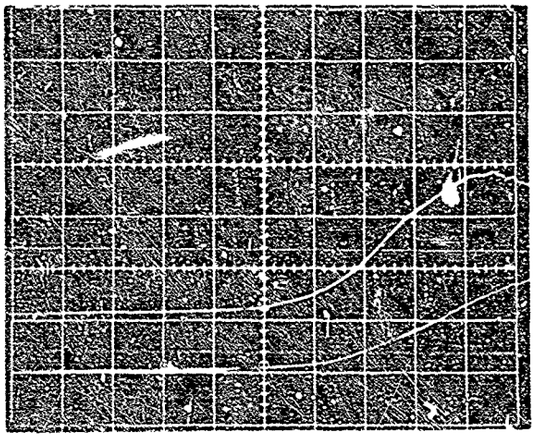

Upper
σ - Gage No. CS-2

Peak Stress: 59.0 psi
Rise Time: 5.110 msec
Distance: 38.1 in.

Lower
σ - Gage No. 11

Peak Stress: 32.0 psi
Rise Time: 5.800 msec
Distance: 45.7 in.

Sweep Speed: 1 msec/cm

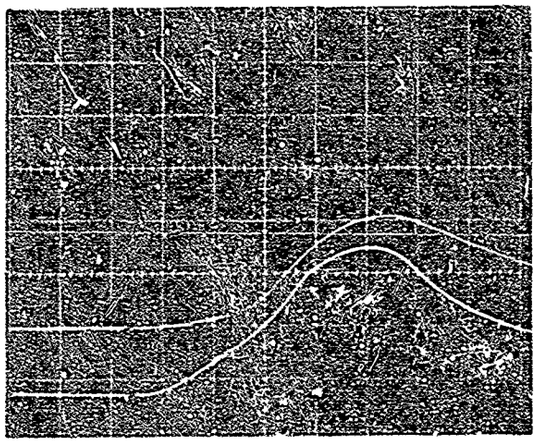

Upper
σ - Gage No. 6

Peak Stress: 54.0 psi
Rise Time: 8.427 msec
Distance: 53.3 in.

Lower
Soil Reaction Load Cell

Peak Load: 408.1 lbs
Rise Time: 9.410 msec
Distance: 60.3 in.

Sweep Speed: 2 msec/cm

Figure 33b Typical Overpressure, Stress, Circumferential Strain, and Reaction End Gage Records, EPK Clay
γ_m = 101.9 pcf, w = 28.0 percent

Data were not adequate to establish a definite trend regarding the effect of a change in overpressure on rise time to peak stress. However, data shows that the rate of rise to peak stress, for a given set of soil conditions, increases with an increase in peak stress.

Comparing the data from test series 3 with that of test series 12 one can ascertain the effect of dwell time of peak pressure on rise time to peak stress.

Properties of Specimens Used

Test Series	γ_m(pcf)	w(%)
3	105.8	29.3
12	103.8	27.9

Test series 3 was performed using an overpressure-time curve having a dwell time of peak pressure of approximately 1 msec while that of test series 12 had a dwell time of peak pressure of essentially zero. The data show that for a given overpressure, rise time to peak stress increases with an increase in dwell time of peak overpressure.

In summary, it can be said that plastic type wave propagation was evidenced in all tests on EPK clay at all overpressure levels. Simultaneous changes in moisture content and wet unit weight did not permit establishment of trends on the effect of changes in these parameters on wave front development, but the rate of rise to peak stress increased with overpressure. The data considered here is presented in tabular form in Appendix IV.

5. Wave Shape

An effort was made to evaluate the change in wave shape as the stress waves propagated through the samples. This was done by plotting nondimensional depth, $\tau_p = t_p/T_a$ (ratio of time to peak stress to the time required for peak overpressure to attenuate to 50 percent of its maximum value), versus T/T_a (ratio of the time required for peak stress to attenuate to 50 percent of its maximum value to time required for the overpressure to attenuate, relatively, the same amount). It was found that 50 percent attenuation was the

maximum that could be used to get a value of the time constant T from most of the gage responses. This was due principally to superposition of the reflected and incident waves.

The data indicated a trend toward an increase in T/T_a with nondimensional depth, τ_p. This indicates a broadening of the stress wave as it propagates through the soil, i.e., an increase in positive phase duration with nondimensional depth. The magnitude of the increase in the ratio T/T_a with nondimensional depth is dependent on density, in the case of Ottawa sand, and density and moisture content, in the case of EPK clay. Figure 34a is a plot of the data from a specimen of sand having an air dry unit weight of 96.6 pcf. Figure 34b is a plot of data obtained experimentally from a specimen of EPK clay having a wet density of 101.9 pcf and a moisture content of 27 percent. The plots indicate the possibility that at high values of nondimensional depth a constant value of T/T_a would be reached. This implies that the time required for 50 percent attenuation is a constant after some limiting distance of propagation.

6. Stress-Strain Relations

In the wave propagation experiments soil stress gages and soil strain gages were alternately positioned in the specimens approximately 3 in. apart. The responses of these stress and strain gages were combined to construct the stress-strain relationship of the soil as the wave propagated along the specimen. The curves were constructed in the following manner.

(a) The strain-time relation for a given soil strain gage was plotted (Figure 35a) with the timing reference shown.

(b) The stress-time relations for the stress gages directly upstream and downstream from the given soil strain gage were plotted (Figure 35b).

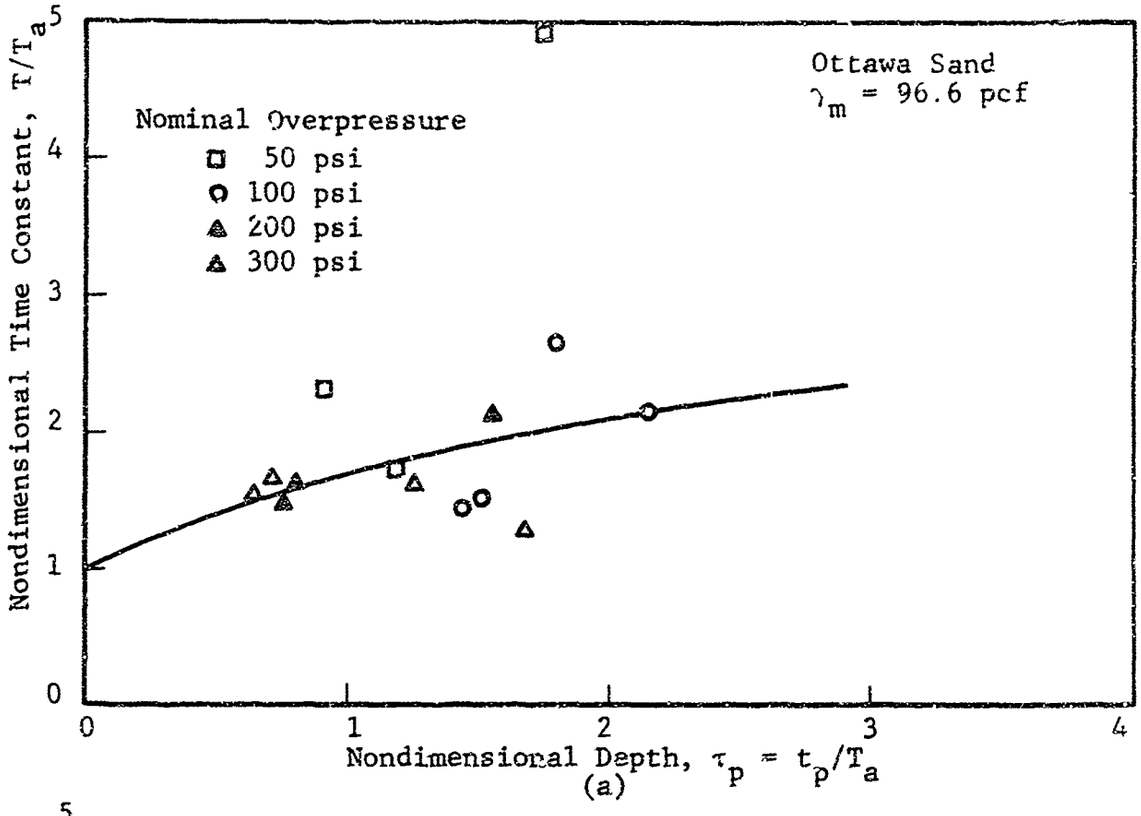

(a)

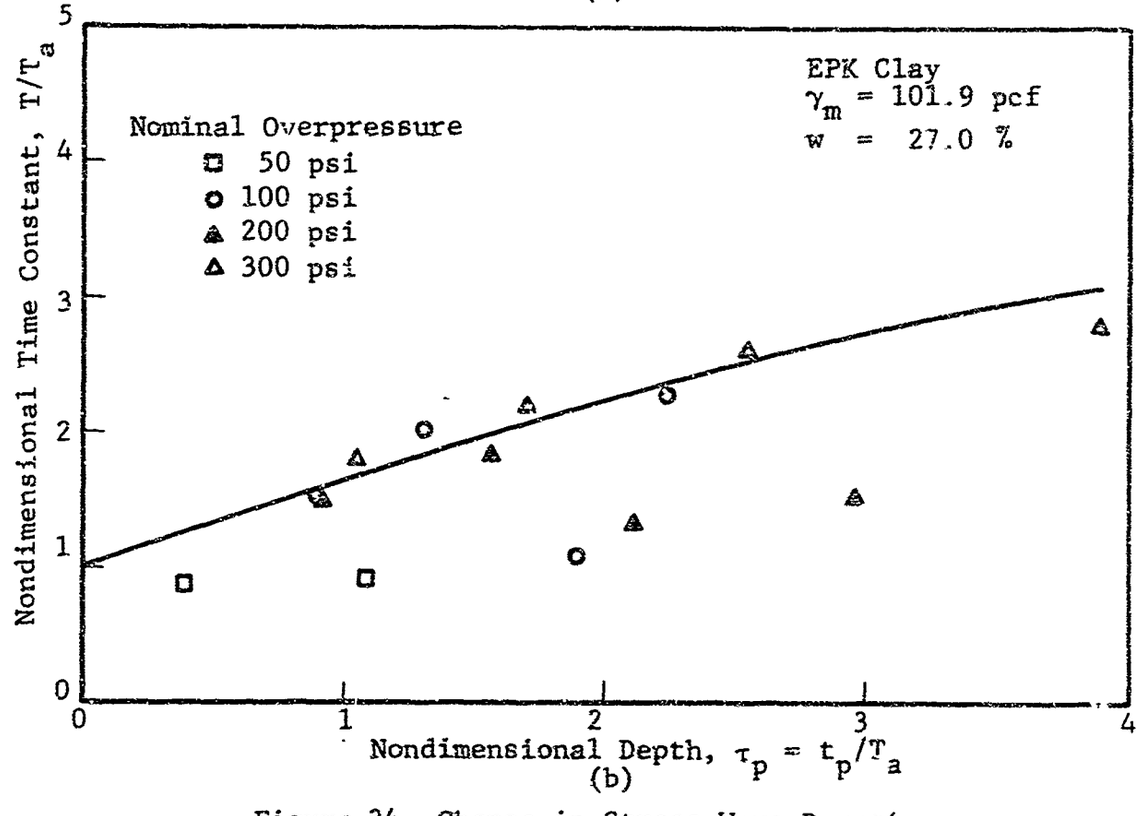

(b)

Figure 34 Change in Stress Wave Duration

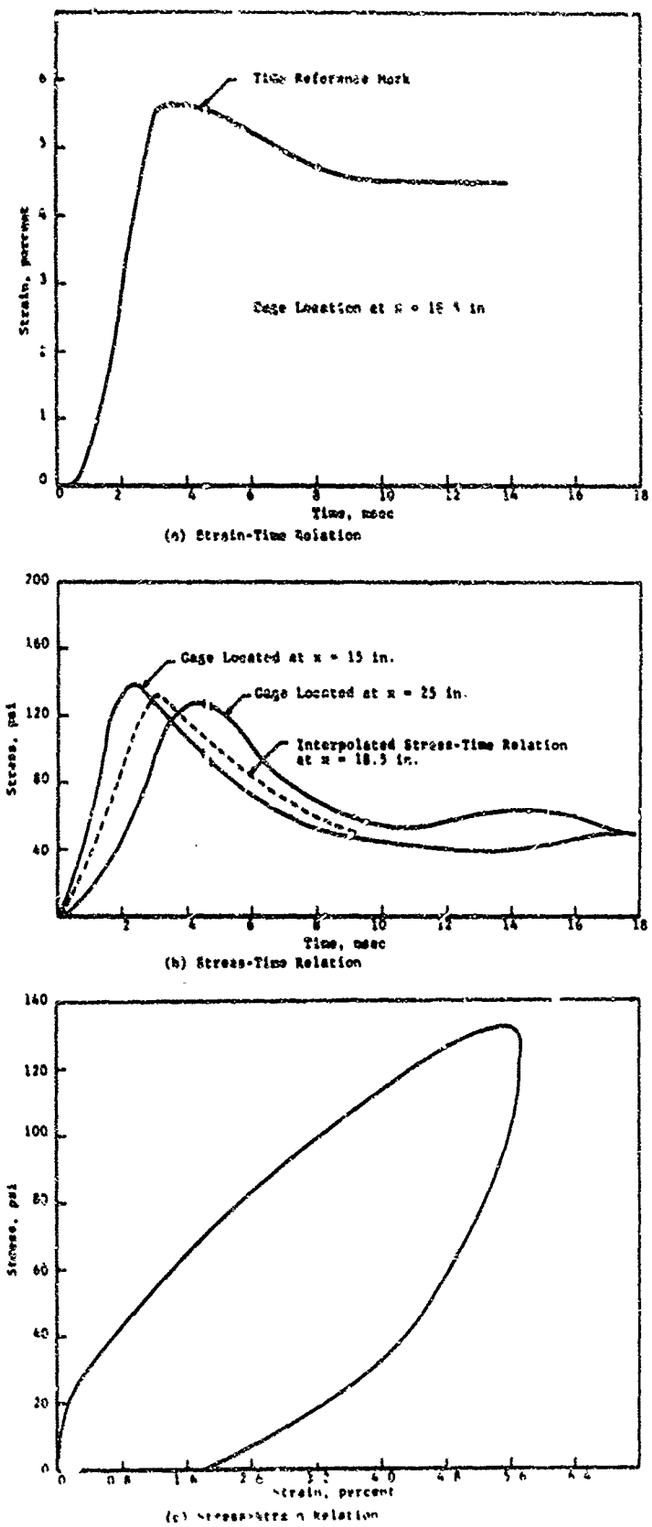

Figure 35 Method of Constructing Stress-Strain Curves

(c) The curves were synchronized by adjusting their position on the time axis such that the time reference mark appeared at the same instant.

(d) An interpolation between the two stress-time histories was made to approximate the stress-time relation at the location of the soil strain gage (Figure 35b).

(e) Stress and strain values corresponding to the same time instants were picked off to construct the stress-strain relation (Figure 35c).

Stress-strain curves constructed for Ottawa sand specimens are presented in Figures 36 and 37. Figure 36 shows curves from a test at an initial density of 96.6 pcf while the curves in Figure 37 are from a test at an initial density of 101.9 pcf. Strains are plotted as total strain to indicate the complete stress history of the specimen. The curves are generally S-shaped with a yielding nature below approximately 40 psi and a stiffening behavior above that level.

In summary, it can be said that the data indicate an S-shaped stress-strain relationship for the sand, with stiffening occurring at stress levels above approximately the 40 psi stress level. The data also show that soil modulus tends to increase with stress level at a given point in the soil.

Stress-strain curves constructed for two EPK clay specimens at moisture contents of 27 percent and 29.7 percent are presented in Figures 38 and 39 ,respectively. The curves are nominally linear on loading and do not strongly exhibit the S-shaped characteristics indicative of sand. It is possible that such behavior would become manifest at higher stress levels. More research is needed to study the stress-strain characteristics of clay in one-dimensional compression.

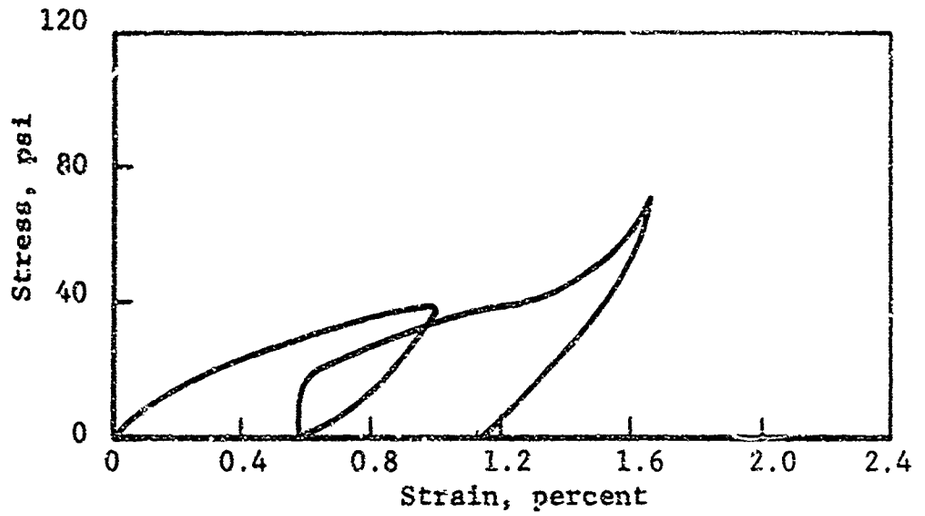

(b) Gage Located at x = 21.0 in.

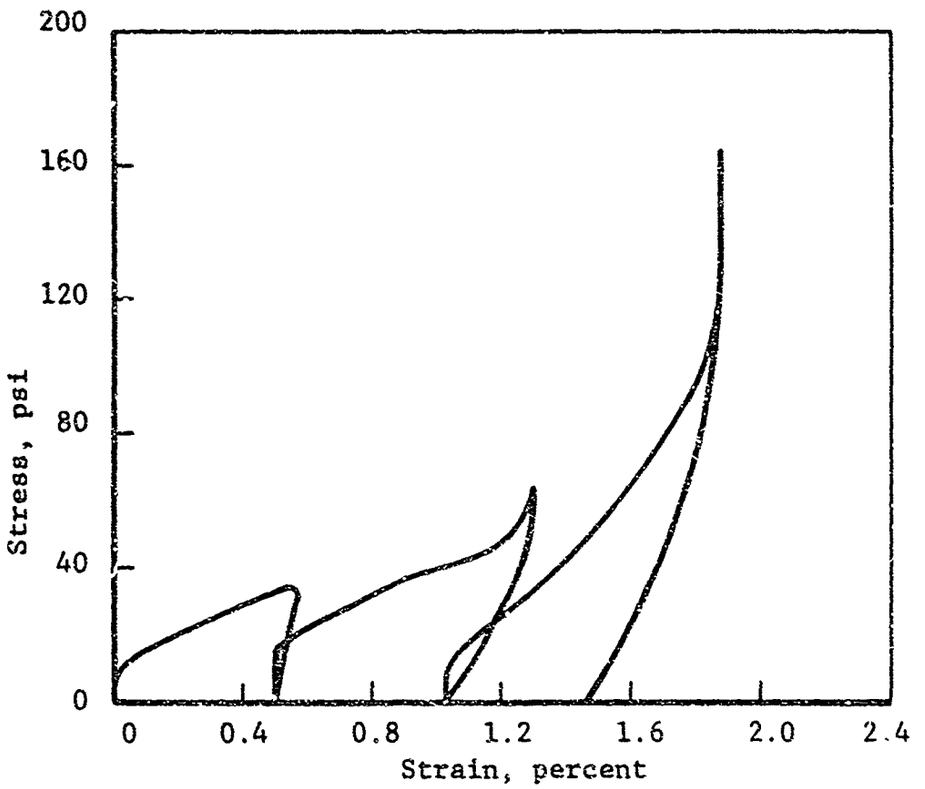

(a) Gage Located at x = 13.5 in.

Figure 36 Stress Strain Curves from Embedded Gages, Ottawa Sand γ_m = 96.6 pcf

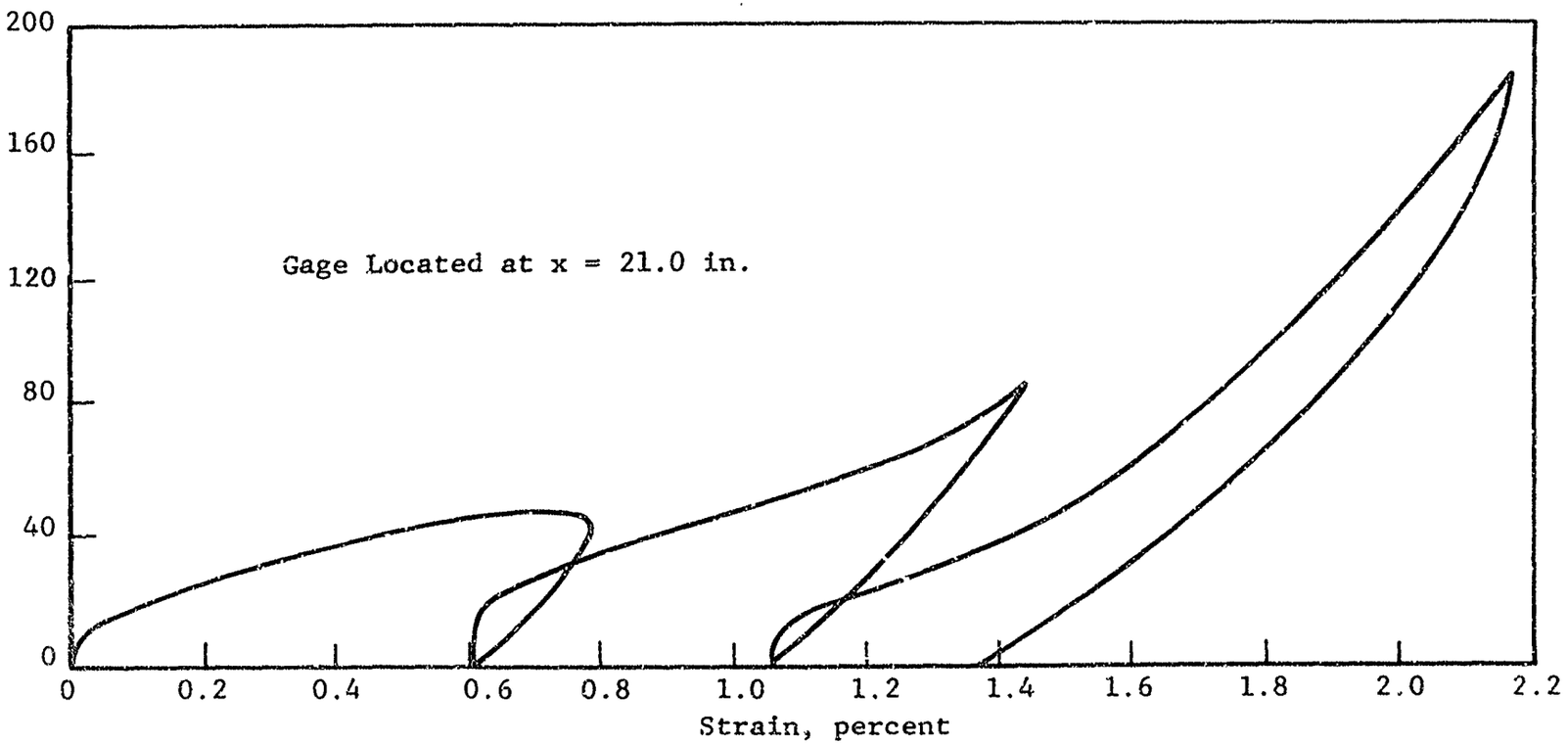

Figure 37 Stress-Strain Curves from Embedded Gages, Ottawa Sand γ_m = 101.9 pcf,

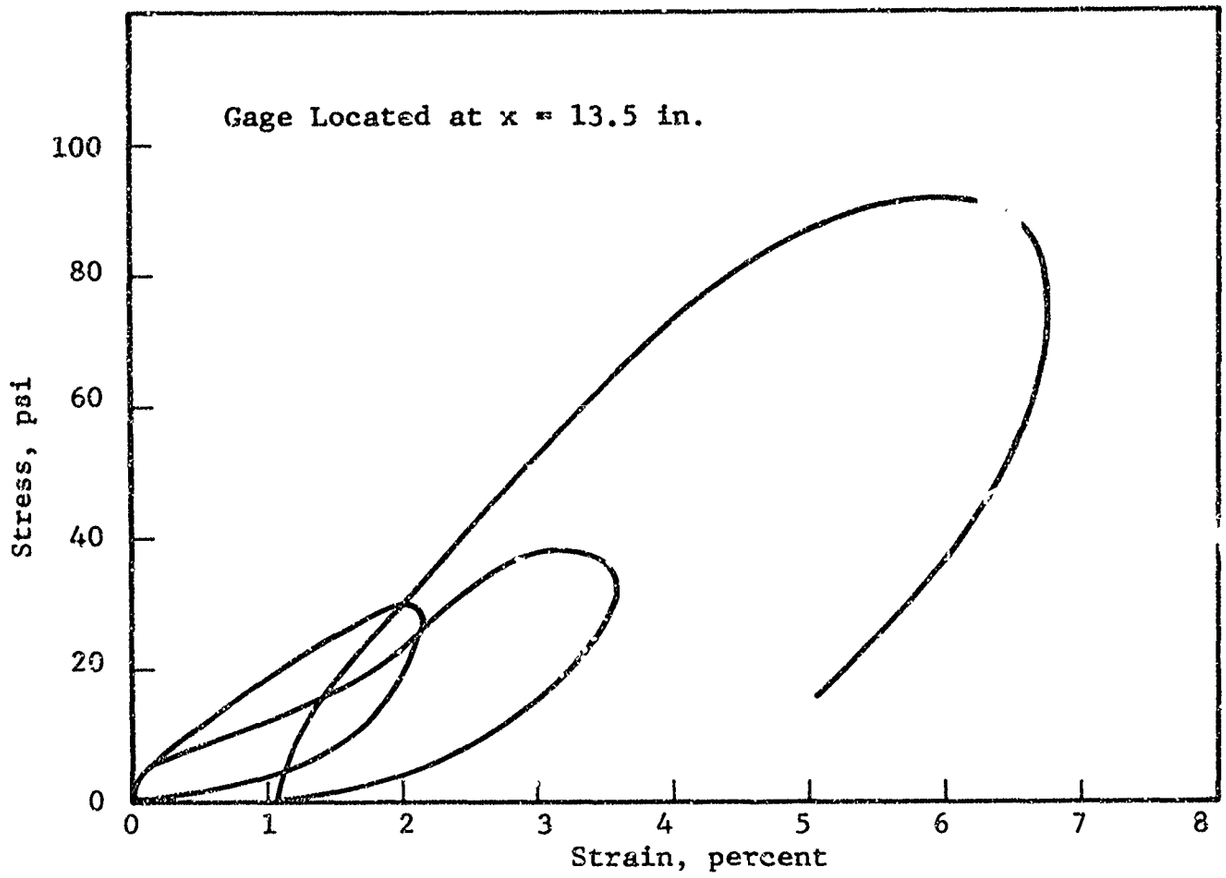

Figure 38 Stress-Strain Curves from Embedded Gages, EPK Clay
γ_m = 103.8 pcf, w = 29.7 percent

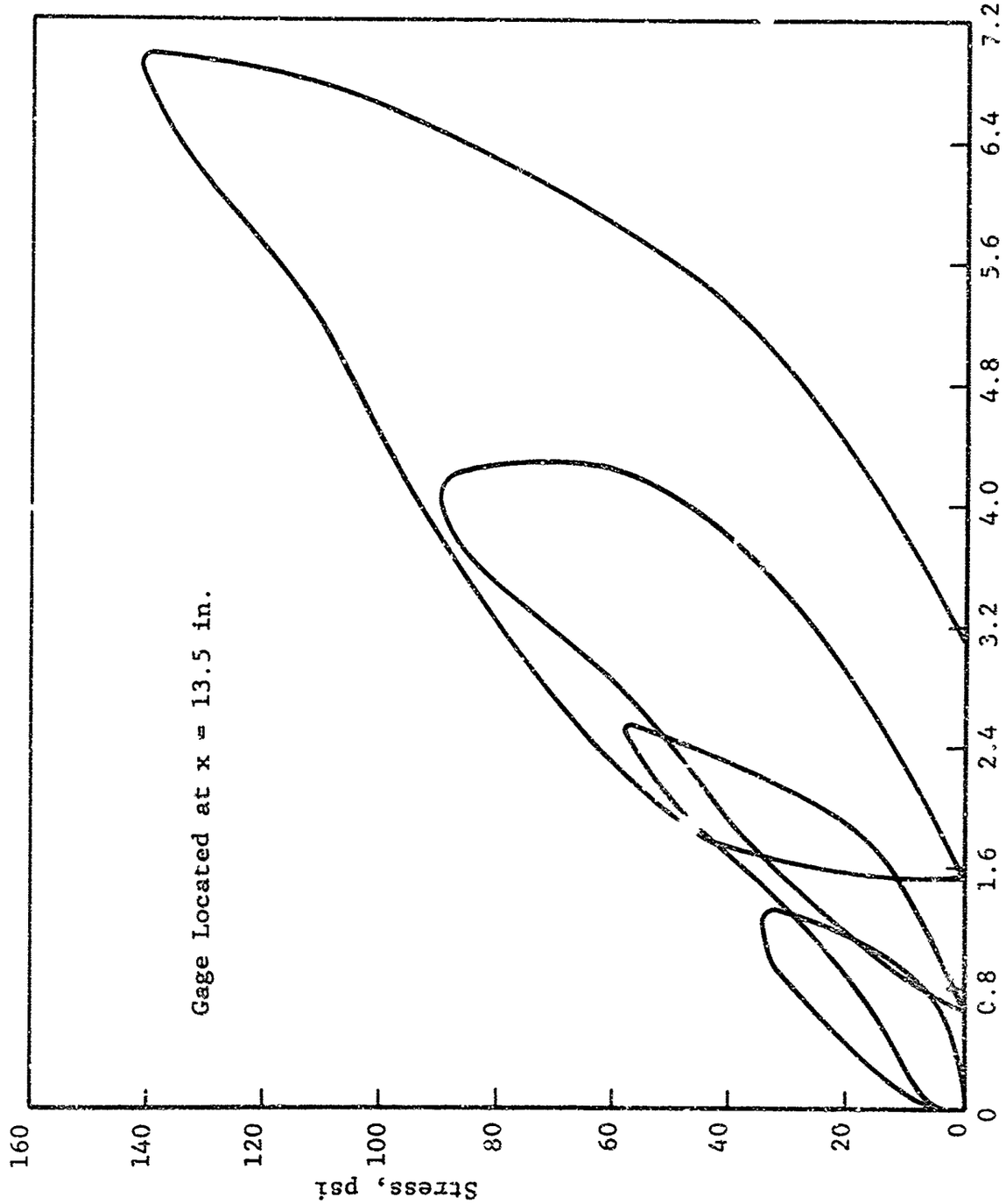

Figure 39 Stress-Strain Curves from Embedded Gages, EPK Clay
γ_m = 101.9 pcf, w = 27.0 percent

Peak strain lagged peak stress, which is indicative of a viscoelastic material. Clay is known to have viscoelastic properties and this property has been used extensively as the basis for models used to describe the stress-strain and wave propagation characteristics of these types of soils.

The stress-strain curves presented were for test conditions in which the rise time to peak stress at the strain gage location was 3 msec or greater, representing only a small part of the test data obtained. The major portion of the data for which the rise time was less than 3 msec were not considered due to the limitation in the response time of the strain gage units (0.3 msec from 10 to 90 percent of full scale output). A definite time lag between stress and strain was observed for the test conditions with a rise time to peak less than 3 msec, however, this lag was at least partially due to instrumentation and therefore was not considered reliable.

The stress-strain curves obtained indicate the feasibility of the method used to obtain the data. The big problem remaining is to improve the response of the strain gages so as to be able to more accurately ascertain the stress-strain relationship for the soil.

7. Strain of the Confining Chamber

During conduction of the experiments reported, measurements were made of the strain in the walls of the confining chamber. These measurements were made for the purpose of ascertaining the magnitude of the radial strain and its possible effect on wave propagation phenomena. The measurements were made in the range from 3.5 to 4 in. from the upstream end of the sample since closer to the upstream end the radial strain should be greater.

It was observed that peak radial strain increased approximately linearly with an increase in peak overpressure. The peak radial strain was approximately 70 microinches per in. at a peak

overpressure of 300 psi. This magnitude of strain can be considered negligible and therefore should have no significant effect on the wave propagation phenomena.

Section V

COMPARISONS WITH THEORETICAL MODELS

One of the principal purposes of this investigation was to compare the experimental results obtained with available theory to gain insight into the suitability of these theories for predicting wave propagation phenomena. Due to limitations on time and funding, it was not possible to make comparisons of the data with a variety of theoretical solutions to the problem of one-dimensional wave propagation. Therefore, it was decided to choose a single theoretical approach applicable to wave propagation through granular soils, and another, applicable to cohesive soils, and compare the experimental results obtained in this study with them. Past experience indicates that it is not possible to use a single model for both soil types.

In previous wave propagation research performed at IITRI (References 1 and 2) a theoretical solution employing a nonlinear inelastic model for one-dimensional wave propagation was used. A special case of this is the linear hysteretic model proposed by Seaman and Whitman (Reference 3) which will be compared with the results obtained from tests on Ottawa sand.

The theoretical solution based on the constant tan δ model will be compared with the results obtained on the clay (References 3 and 4). Based on extensive experimental and theoretical work it is felt that these two models are adequate for a good approximation of peak stress attenuation. This will be the major purpose for which they are used. Limitations in the data did not permit comparisons of experimental and theoretical results on changes in stress wave shape and attenuation of peak particle velocity. Stress decay was not sufficient prior to the return of the reflected wave to allow a comparison of changes in wave shape and no particle velocity measurements were made.

Comparison of experimental results with theory was hampered by the lack of one-dimensional stress-strain data. This information was not available in time for inclusion in this report. It was felt that a reasonable prediction of model parameters could not be made without these data. Therefore, there was a resort to a curve fitting procedure in order to determine the most reasonable theoretical curve for the experimental data. This was accomplished by plotting the data according to the dictates of the particular theory and finding which theoretical curve would best fit the experimental results. Whether or not the same curve would have been used, had the model parameters been known, is a moot question.

1. Peak Stress Attenuation

a. Ottawa Sand

The linear hysteretic model is characterized by a stress-strain relationship where loading and unloading occur along different straight line paths in such a manner that a loading cycle causes a certain amount of permanent set and energy loss. The principal features of the model (Reference 3) are as follows:

(a) The model is independent of the rate of load application. It is characterized by the attenuation parameter α and the modulus E_o both of which can be determined from static or dynamic tests.

(b) Loading and unloading wave velocities are constants: there is no shocking up or other change in the general shape of the wave front.

(c) Attenuations of peak stress and particle velocity are entirely dependent on α which is a function of the loading and unloading velocities.

(d) The duration of a stress wave propagating through the medium tends to lengthen with depth. This lengthening is a function of α and depth.

The attenuation parameter α may be defined in the following ways.

$$\alpha = \frac{1 - \sqrt{\frac{E_o}{E_1}}}{1 + \sqrt{\frac{E_o}{E_1}}} \qquad \text{(a)}$$

$$\alpha = \frac{1 - \frac{c_o}{c_1}}{1 + \frac{c_o}{c_1}} \qquad \text{(b)}$$

$$\alpha = \frac{1 - \sqrt{r}}{1 + \sqrt{r}} \qquad \text{(c)}$$

and

$$\alpha = \frac{1 - \sqrt{1 - \frac{2H}{\sigma_m \varepsilon_m}}}{1 + \sqrt{1 - \frac{2H}{\sigma_m \varepsilon_m}}} \qquad \text{(d)}$$

where

E_o is the loading modulus,
E_1 is the unloading modulus,
c_o is the wave velocity on loading,
c_1 is the wave velocity on unloading,
r is the ratio of recovered strain to maximum strain,
H is the area within the hysteresis loop,
σ_m is the maximum stress obtained, and
ε_m is the maximum strain attained.

The value of α should be the same regardless of which of the four methods is used to determine it. Actually, due to the fact that soil stress-strain curves are sufficiently nonlinear, the method used to determine α may significantly affect its magnitude. Definition of α on the basis of the loading and unloading wave

velocities appears to be the correct interpretation (Reference 3). These velocities can be obtained from the tangent moduli of the stress-strain curve since

$$c = \sqrt{\frac{E}{\rho}}$$

where

E is the tangent modulus and

ρ is the density.

For a nonlinear stress-strain relationship, the tangent modulus should be determined at the peak stress attained.

Shock type loadings, i.e., where peak stress occurs at the shock front, require that as the wave propagates through the soil the peak stress always occurs at the shock front and therefore at the arrival time

$$t_p = \frac{z}{c_o}$$

where

z is the depth in question, and

c_o is the loading wave velocity.

The data collected in this study indicated plastic type wave propagation phenomena, in which time of arrival of peak stress occurred later than the initial arrival of stress. Therefore, in the comparisons which follow, t_p is the actual time to peak stress, i.e., arrival time plus rise time. This is in accordance with References 3 and 4.

Figure 40 shows plots of nondimensional peak stress

$$\left(\frac{\sigma_m}{p_o}\right) \text{ versus nondimensional depth } \left(\tau_p = \frac{t_p}{T_o}\right)$$

In this discussion σ_m is the peak measured stress at a particular point, p_o is the peak overpressure, t_p is arrival time of peak stress, T_o is the time constant and τ_p is nondimensional depth.

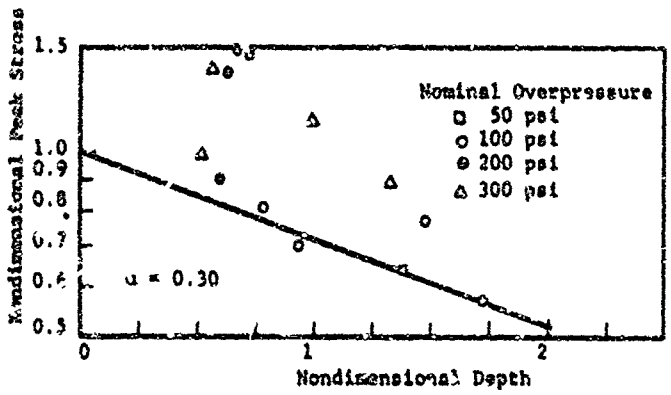

(a) Test Series 6, γ_m = 96.6 pcf

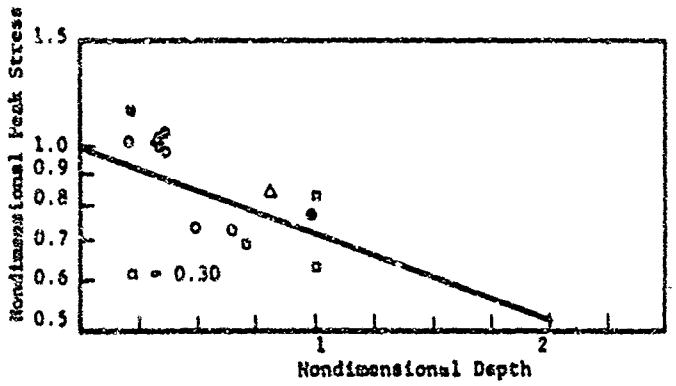

(b) Test Series 8, γ_m = 108.0 pcf

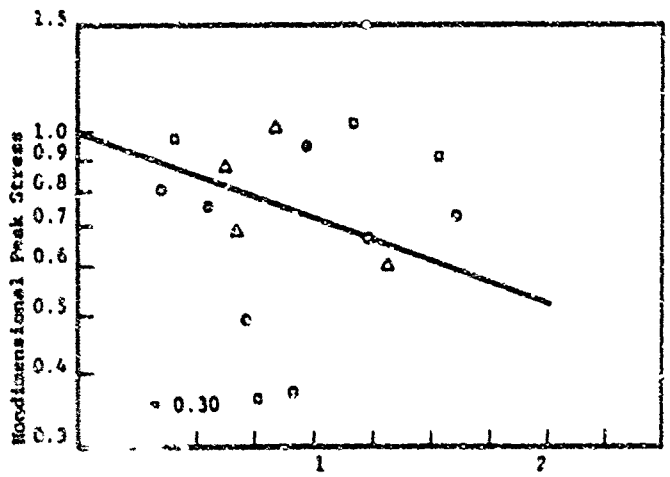

(c) Test Series 11, γ_m = 102.4 pcf

Figure 40 Attenuation of Peak Stress, Ottawa Sand

Figure 41 indicates how the aforementioned parameters are obtained. Determination of the time constant, T_o, on the basis of the time required to attenuate the peak stress to 0.368 of its peak value is due to the fact that, for a spiked wave with an exponential decay, T_o becomes the exponential time constant.

The results of only three of the six test series conducted on sand are presented in Figure 40. This is due principally to the fact that for two test series the nondimensional depth data were incomplete to the extent that sufficient data points were not available for plotting, and a third test series was omitted because only four of a possible 16 data points indicated any attenuation of peak stress.

Figure 40a and 40b indicate data obtained by loading specimens of the Ottawa sand with a shock wave having a dwell time of peak stress of 1 msec. The initial soil densities were 96.6 and 108 pcf, respectively. Figure 40c shows data from a specimen at a density of 102.4 pcf, which was subjected to a shock wave having essentially a zero dwell time of peak stress. Superimposed upon each plot is a theoretical curve based on the linear hysteretic model (the theoretical curve is for an overpressure having a zero dwell time of peak pressure). The theoretical curve was chosen so as to produce a best possible fit of the experimental data. The curve representing an attenuation factor $\alpha = 0.30$ appeared to be the most appropriate in each case.

It appears that the greater the initial density of the soil the better the fit of the theoretical curve to the data. This is probably due to a decrease in the magnitude of overregistration of the gage, with an increase in density, because of the closer proximity of the moduli of the gage and soil the greater the density. In comparing Figures 40a with 40b the effect of soil density on soil-gage interaction phenomena is apparent from the higher degree of overregistration for the loose sand than for the dense sand. Values of nondimensional peak stress greater than unity are caused by gage overregistration.

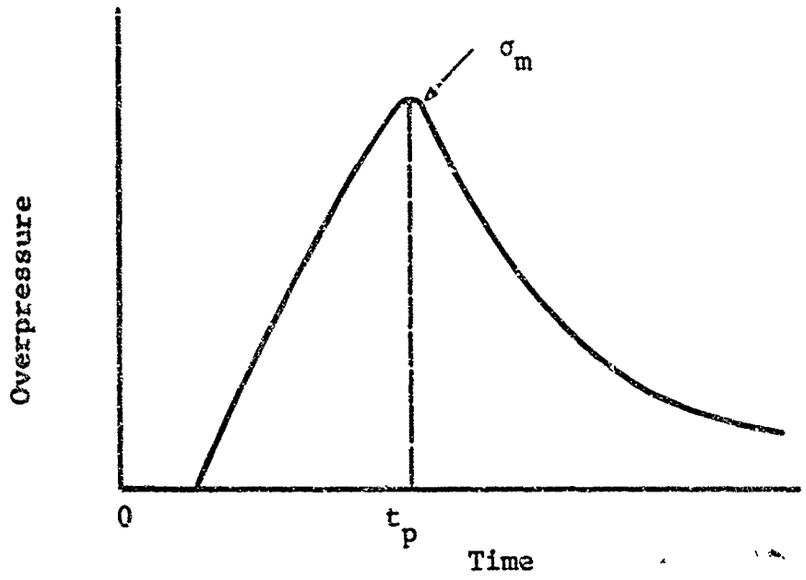

(a) Schematic Response of Soil Stress Gage

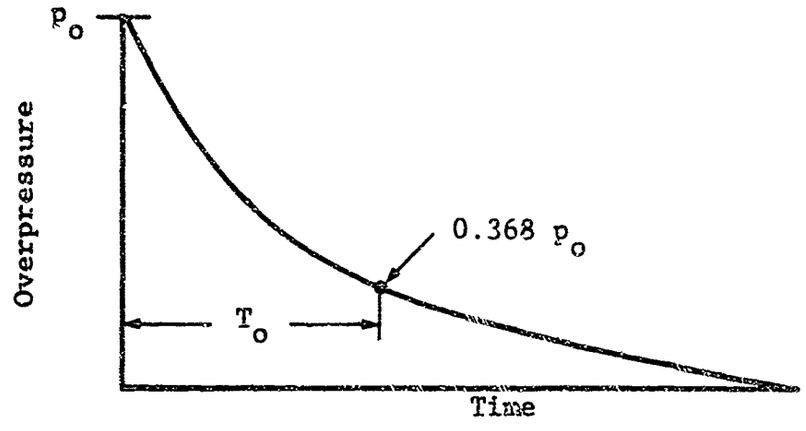

(b) Determination of T_o

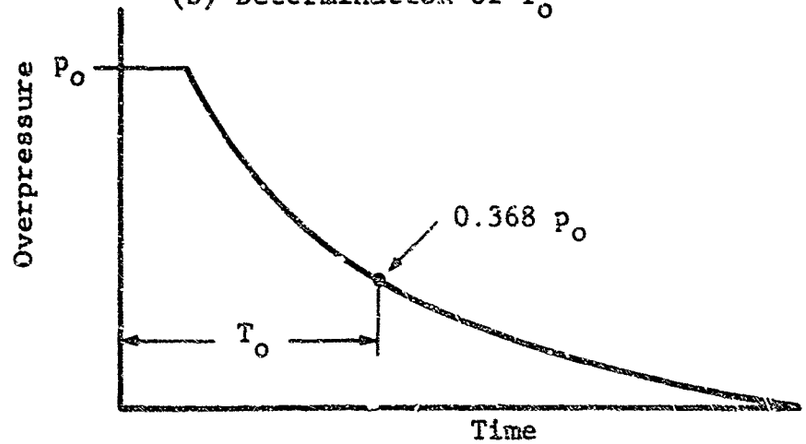

(c) Determination of T_o

Figure 41 Methods of Determination of Critical Parameters

The data shown in Figure 40a correlate least with the theoretical curve. This results from the increased significance of variations introduced by soil-gage interaction phenomena as related to the larger modulus mismatch between the gage and the soil, and the greater difficulty of uniform sample fabrication and gage placement. However, the trend in the data is such that for values of nondimensional depth greater than approximately 1.5 the data points may be randomly distributed about the theoretical curve for $\alpha = 0.30$. One must also allow for the possibility that α might be greater than 0.30. The data for the dense sand fits the theoretical curve for $\alpha = 0.30$ fairly well and α should decrease with an increase in soil stiffness. More data are needed to resolve this question.

The data in Figure 40c show scatter but generally fit the theoretical attenuation curve relatively close. The data in this figure were obtained by subjecting a specimen with an initial unit weight of 102.4 pcf to overpressures having essentially a zero dwell time of peak stress.

Attempts were made to evaluate the parameter α based on stress-strain data from the wave propagation tests. This was done by using Equation (d) because the shape of the stress-strain curves were such that this was felt to be the most reasonable approach. The calculated values of α decreased with each loading of the specimen. This same trend was found by others (Reference 4). Based on the calculated values of the attenuation parameter, $\alpha = 0.30$ seems reasonable.

In summary, the linear hysteretic model, using an attenuation parameter $\alpha = 0.30$ provided a reasonable approximation to the attenuation which occurred in the dense sand ($\gamma_m = 108.0$ pcf) subjected to overpressures having approximately 1 msec dwell time of peak stress, but the data from the loose sand ($\gamma_m = 96.6$ pcf) did not fit the model as well, probably because of soil-gage interaction phenomena. The data from the sample of medium dense sand ($\gamma_m = 102.4$ pcf) subjected to overpressures having essentially a

zero dwell time of peak pressure generally followed the prediction of the linear hysteretic model ($\alpha = 0.30$) but showed large scatter.

The effect of the approximately 1 msec dwell time of peak stress was evident. The net result was to decrease the rate of attenuation in the near surface region over that which would occur for an essentially zero dwell time of peak pressure. However, the effect of the dwell time of peak stress diminishes with distance of propagation and as nondimensional depth increases the data approaches the theoretical curve established on the basis of a zero dwell time of peak stress. The significant depth of influence of dwell time to peak stress appears to increase with a decrease in density.

b. EPK Clay

Indications are that a theoretical analysis based on the constant tan δ model can be used to predict peak stress attenuation in cohesive soils (Reference 4). This model is a linear viscoelastic model which has the same phase lag between stress and strain at all frequencies. The lag is due to viscous energy loss and causes a hysteresis loop to appear on a plot of stress versus strain. The principal features of the constant tan δ model (Reference 3) are as follows:

(a) The model is characterized by a modulus which is a function of frequency and a phase angle δ.

(b) At all frequencies (including static) there is a lag between stress and strain so that a hysteresis loop is formed on a stress-strain diagram.

(c) The phase lag between stress and strain is the same at all frequencies.

(d) The average modulus for the model is a function of both tan δ (the phase lag) and the frequency of load application.

(e) Different frequency components of a stress pulse travel at different velocities so that stress waves are spread out as they propagate. Both the rise time of stress and the decay time are lengthened.

(f) The attenuation of peak stress in the range of interest on the project is a function of $[(z/T_o)\tan \delta]^{1/2}$, where z is depth and T_o is the exponential time constant of the applied pressure.

Figures 42, 43 and 44 are plots of nondimensional peak stress versus nondimensional depth for three tests on EPK clay. The data for three other tests were omitted from presentation. One because of the scatter in the data was too great to offer a meaningful trend, another due to the fact that it was not possible to estimate time of arrival to a sufficient degree for determination of meaningful values of nondimensional depth, and the third because a departure from the normal method of sample preparation appeared to have a significant effect on the results.

Superimposed on the three figures are theoretical predictions of peak stress attenuation (based on a zero dwell time of peak overpressure) based on the constant tan δ model of Seaman-Whitman (Reference 3 and 4). It is quite apparent that this model provides a reasonable approximation to the experimental data. The scatter in the data of Figures 43 and 44, in general, is relatively small. The scatter in the data of Figure 42 is much larger,which may be partially due to the fact that this was the first test on clay.

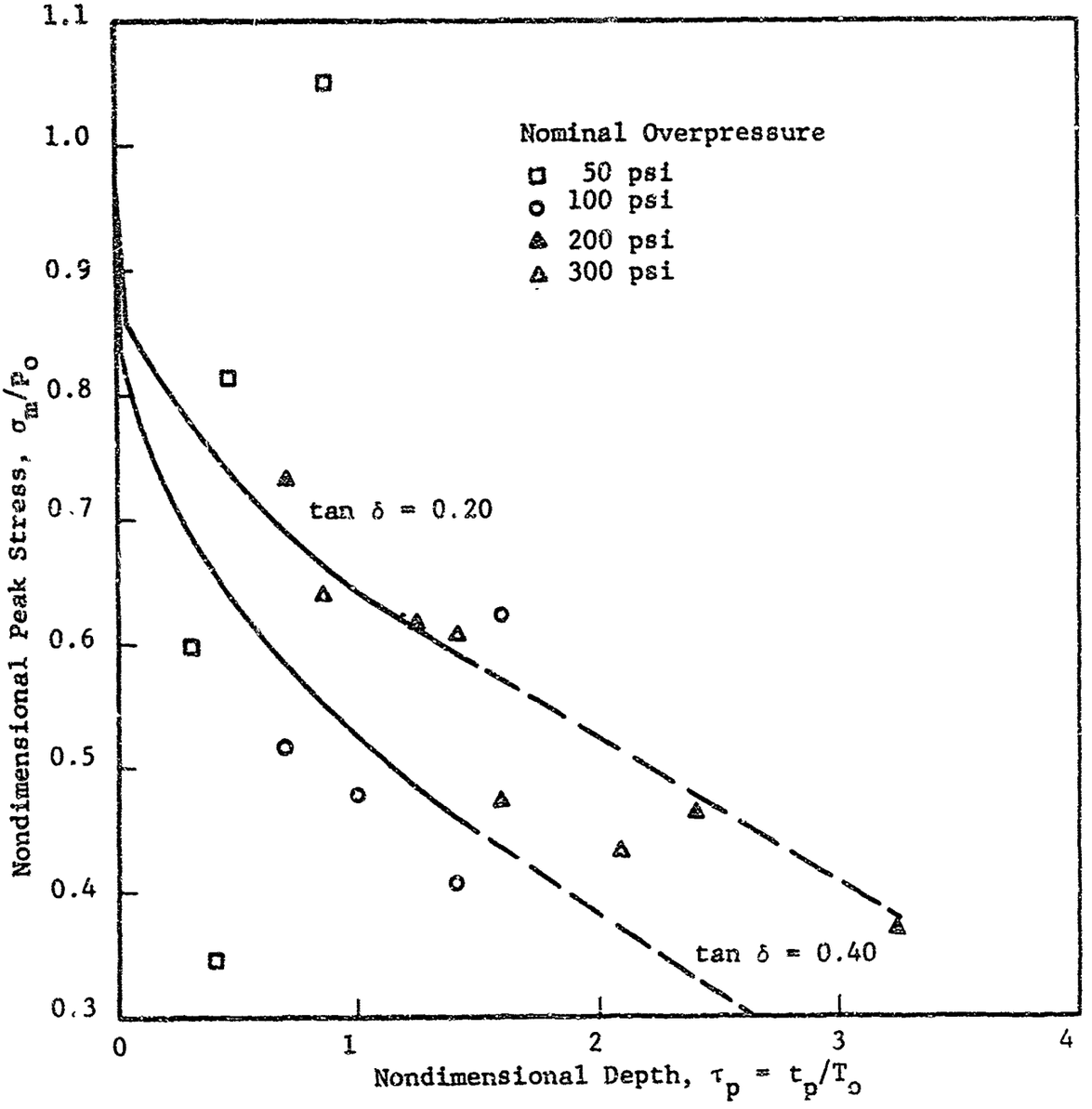

Figure 42 Attenuation of Peak Stress, EPK Clay
γ_m = 101.9 pcf, w = 27.0 percent

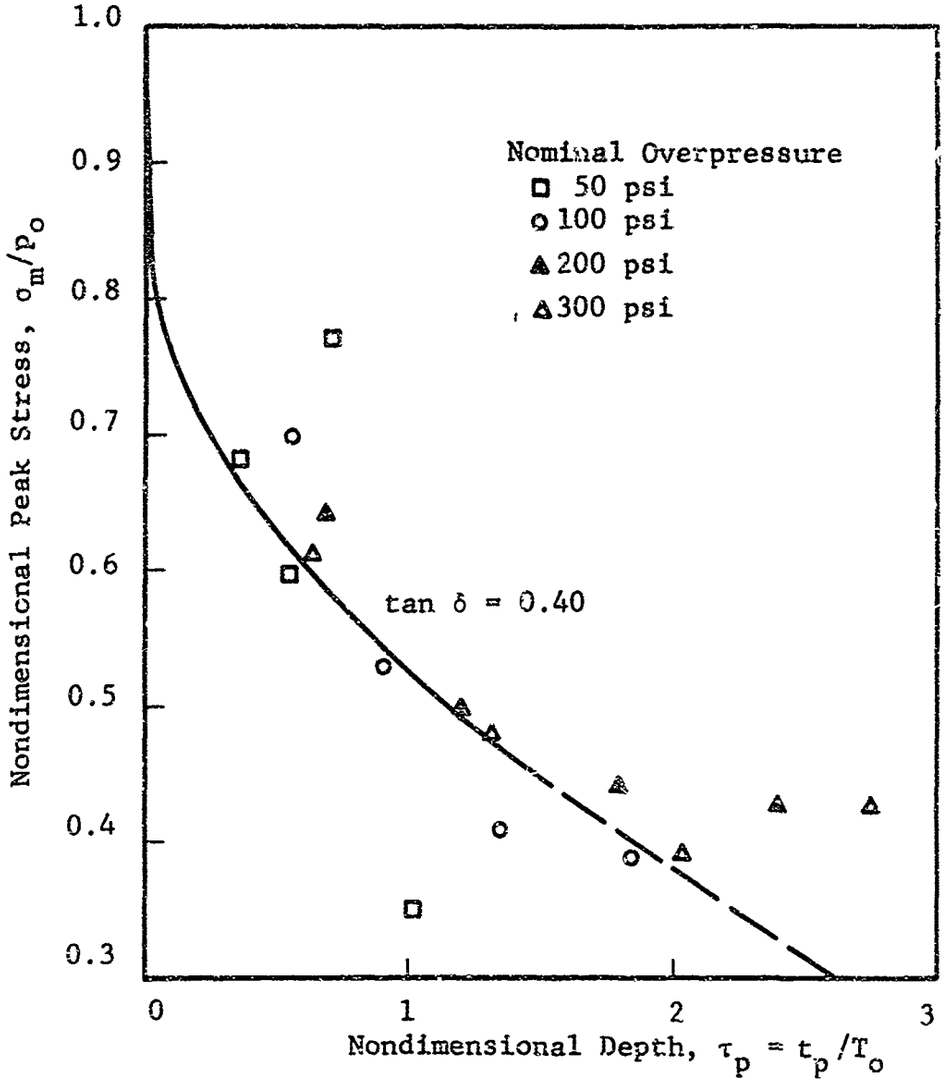

Figure 43 Attenuation of Peak Stress, EPK Clay
γ_m = 103.8 pcf, w = 29.7 percent

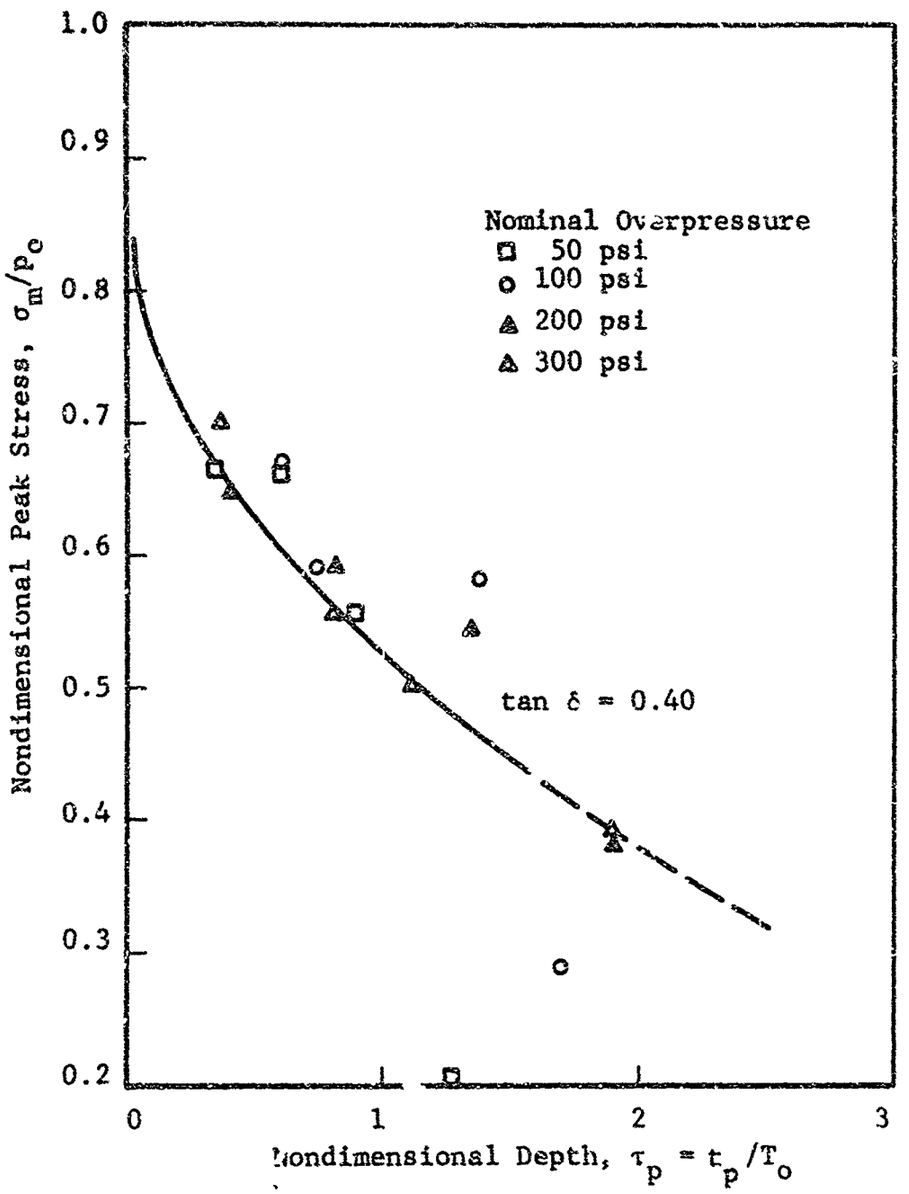

Figure 44 Attenuation of Peak Stress, EPK Clay
γ_m = 113.2 pcf, w = 33.2 percent

The scatter in the data of Figure 42 is such that it was felt necessary to include the theoretical predictions for two values of tan δ; 0.20 and 0.40. It is not certain which of the two values is more correct and more data are required before a conclusion can be reached. However, since most of the data at the lower stress levels correspond to the theoretical curve for tan δ = 0.40 and data for the two highest stress levels tend to correspond to the theoretical curve for δ = 0.20, it is possible that densification of the specimen under the two lower stress levels was sufficient to change the viscoelastic character of the soil to an extent sufficient to change tan δ from 0.40 to 0.20. The data under consideration were obtained on a specimen having an initial wet unit weight of 101.9 pcf and a moisture content of 27 percent.

The data obtained in test series 3 on a specimen having an initial wet unit weight of 103.8 pcf and a moisture content of 29.7 percent is shown in Figure 43. In this case the theoretical predictions for tan δ = 0.40 provide a good representation of the experimental data. The data of Figure 44, for a specimen having a wet unit weight of 113.2 pcf and a moisture content of 33.2 percent, also agree well with the theoretical curve for tan δ = 0.40.

In summary, it can be said that the constant tan δ model appeared to be able to reasonably approximate peak stress attenuation characteristics of EPK clay if tans δ were properly evaluated. Therefore, the major problem is arriving at the appropriate value of tan δ.

Chapter VI

CONCLUSIONS AND RECOMMENDATIONS

1. Summary of Conclusions

Data obtained in this study illustrate the feasibility of determining the stress-strain characteristics of soils during wave propagation tests. Having stress-strain data on wave propagation test specimens permits a much better understanding of phenomena which occurs as stress waves propagate through soils.

The testing equipment; soil column, loading system, and instrumentation, are suitable for one-dimensional wave propagation experiments.

2. Discussion of Conclusions

a. Peak Stress Attenuation

The data indicate that the linear hysteretic model could be used to evaluate peak stress attenuation with a relatively good degree of accuracy if the appropriate value of the attenuation parameter α were chosen. Unfortunately, it is not presently possible to ascertain if the appropriate value of α could have been chosen were standard laboratory one-dimensional stress-strain data available. An exact value of α was not obtainable from the stress-strain curves generated as a result of the wave propagation experiments. However, the values of α obtained in this manner, using the ratio of the hysteretic energy loss to the total area under the loading curve, was relatively close to the values obtained by curve fitting.

The clay data indicate that the constant tan δ model could be used to evaluate peak stress attenuation in the EPK clay if the appropriate value of tan δ was chosen. The selection of tan δ is a difficult process, as was shown in Reference 4. The only stress-strain data available for the prediction of this parameter

was that obtained from the wave propagation experiments and it was felt that this was inadequate. Therefore, evaluation of this parameter for the EPK clay must await future research.

By plotting the data in the form of nondimensional peak stress versus nondimensional depth it was found that attenuation was independent of overpressure. However, in plotting nondimensional peak stress versus distance of propagation, attenuation appears to be affected by peak overpressure, most probably the result of repeated loading of the same specimen.

b. Strain Rate

In both the sand and clay tests, rate of strain varied substantially with overpressure and distance of propagation. This indicates that in conducting tests to evaluate parameters as input to theoretical models it may, in certain cases, be feasible to conduct a series of tests over a range of rates of strain. As far as peak stress attenuation is concerned it appears that the mechanism can be considered strain rate insensitive. However, this may not be true of other aspects of stress wave propagation phenomena in soils which are significantly strain-rate sensitive.

c. Wave Front Development

Both the sand and clay indicated plastic type wave propagation behavior. It was thought that shocking up might be observed, at least in the sand tests at the higher overpressures, on the basis of the criterion established in Reference 3. It was not observed, and this may be due to the confining pressure on the sand in combination with the attenuation of peak stress.

d. Stress-Strain Relations

A limited number of stress-strain curves were constructed by combining the responses of the embedded stress and strain gages. The curves for Ottawa sand were S-shaped with stiffening behavior indicated at the higher stress levels. For EPK clay the stress-strain relation was nominally linear over the loading portion with a relatively large hysteresis loop on unloading. A time lag between peak stress and peak strain was observed for the clay tests.

3. Recommendations for Further Research

(a) Perform additional one-dimensional wave propagation tests on clay soils, sand soils, and sand-clay mixtures to measure the stress and particle velocity attenuation, change of wave form and velocity. Use this data to evaluate models which seem feasible.

(b) Where necessary, for example in the prediction of change of waveform, modify these theories to permit reasonable predictions.

(c) Perform a series of experiments in which each specimen is subjected to only one loading to more fully assess effects of density and degree of saturation on stress wave propagation phenomena.

(d) Conduct dynamic one-dimensional compression tests to determine the loading characteristics of soils and how to apply these characteristics to best obtain parameters needed as input to appropriate theoretical models.

(e) Conduct additional tests with embedded stress and strain gages to more fully evaluate the stress-strain characteristics of soil as a stress wave propagates through it.

(f) Continue refinement of stress and strain gages for use in wave propagation experiments. This includes techniques for in-place calibration of the stress gages.

(g) Development of a gage that will produce a complete particle velocity-time record during wave propagation.

APPENDIX I

EVALUATION OF CONFINING CHAMBER

One of the most important phases of this research program was to construct a confining chamber that had essentially zero axial stiffness and infinite radial rigidity. These boundary conditions are necessary for the study of one-dimensional stress wave propagation.

1. Basic Apparatus

A composite ring type confining chamber was used in this study. Figure 1, in the main body of this report, shows a schematic diagram of the system. At the start of the program, each section was 4 in. long and consisted of an aluminum cylinder 3-13/16 in. in length plus two neoprene rubber spacers, each 3/32 in. thick. The inside diameter of the composite sections 2- 51/64 in. and the outside diameter was 3-1/4 in. A rubber membrane was placed inside each section and separated from the chamber walls by a thin lubricating layer.

Using three sections of the confining chamber (total length of 12 in.), the static axial modulus of the composite chamber was determined experimentally to be 11.4×10^3 psi. As will be seen subsequently, this stiffness proved to be too great.

Two static tests on Ottawa sand were run to aid in the evaluation of the confining chamber previously described.

	Test 1	Test 2
Density (pcf)	101.3	105.0
Specimen length (in.)	47.1	47.1
Confining pressure (psi)	13.0	13.0
Sample area (sq in.)	6.1	6.1

The basic differences between these tests and the wave propagation tests were that the specimen was shorter and the load was applied statically through a screw-type loading mechanism.

In Test 1, vaseline was used to lubricate the chamber walls. Instrumentation consisted of a proving ring to measure the load on the upstream end of the sample and a force washer* for measuring the load transmitted through the soil, a strain gage to measure hoop strain in the confining chamber and a dial gage to measure the total deflection of the soil specimen. Figure 2 shows the technique of measuring the load transmitted through the soil and through the confining chamber.

The results of Test 1 are shown in Figure 45. It is apparent that only approximately one-third of the load was transmitted through the soil. The hoop strain measured at a point 16 in. from the upstream end was found to be 80 micro-inches per in. at an axial load of 265 psi.

During the latter stage of the test, it was observed that the specimen began to buckle, i.e., at midlength its centerline rose to a height of approximately 1/4 in. above its original position. This may have been, at least partially, the cause of the low degree of stress transmission through the soil.

Static Test 2 was essentially the same as Test 1. The differences between the two were that two load cells were added to measure the load through the walls of the confining chamber, a soil strain gage was placed 13 in. from the upstream end, silicon grease (instead of vaseline) was used as the lubricant, and the confining chamber was supported at the third points to prevent buckling. Approximately 40 percent of the load was transmitted through the soil in Test 2. The load-displacement data from Test 2 were similar to that from Test 1 and, consequently, will not be presented. Soil strain gage

* Force Washer, Model No. 1050, Lockheed Electronics Co.

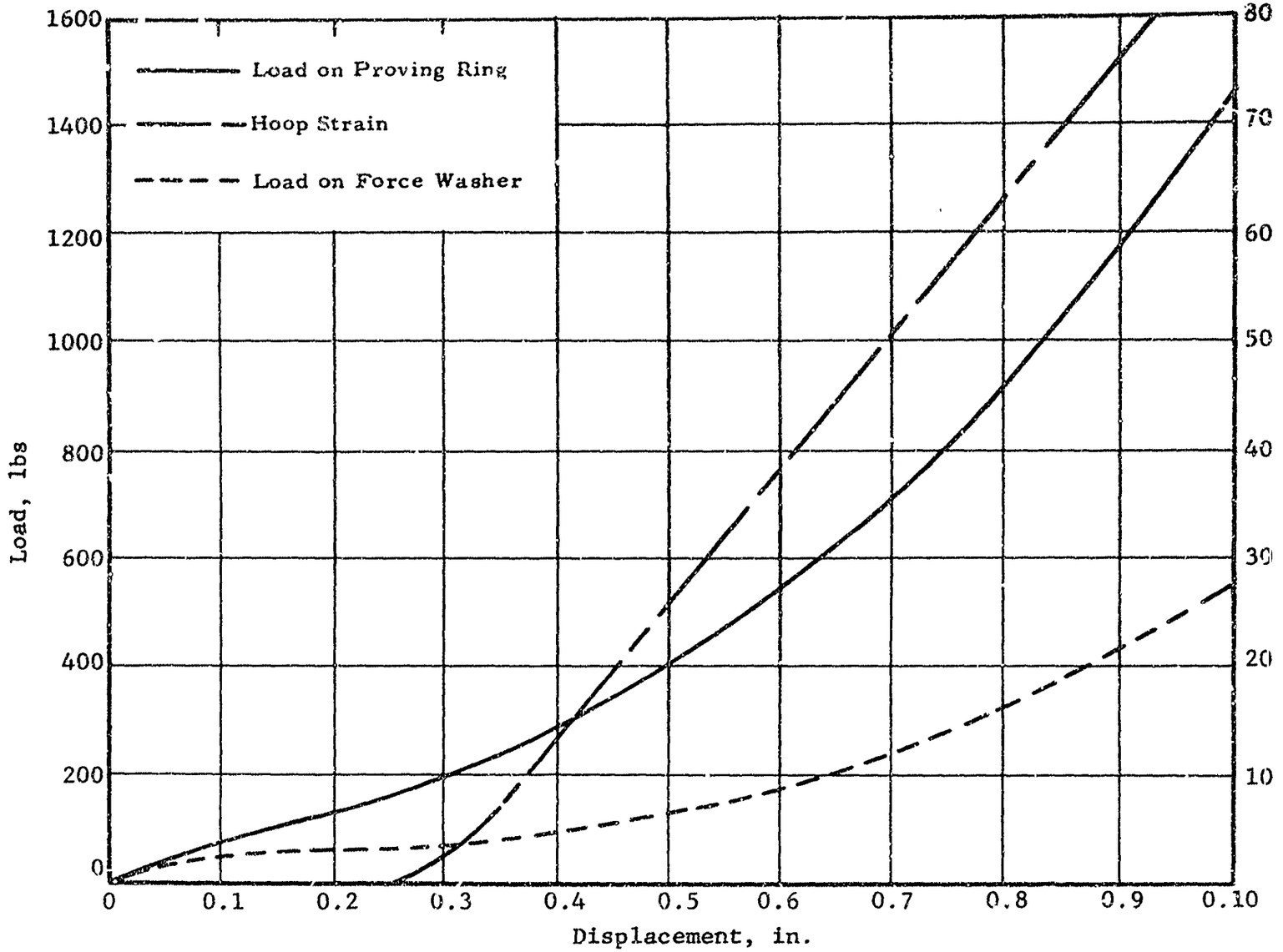

Figure 45 Load and Hoop Strain vs End Displacement, Static Test No. 1, Ottawa Sand γ_m = 101.3 pcf

data for the static tests under consideration will not be considered in this section.

a. Modification 1

Load transmission of 40 percent is insufficient. In an effort to increase the load transmission through the soil the axial modulus of the confining chamber was decreased by increasing the number of rubber spacers at each joint from one to four. To ascertain the effectiveness of this modification static tests were conducted on both Ottawa sand and EPK clay.

	Ottawa Sand	EPK Clay
Density (pcf)	104.0	80.7*
Specimen length (in.)	44.9	44.9
Confining pressure (psi)	14.0	0.0
Sample area (sq in.)	6.1	6.1
Moisture content	Air Dry	27.5

*Dry Density

With the exception of doubling the number of rubber spacers, all test conditions were the same as previously noted for static Test 2. The data from the test on Ottawa sand, shown in Figure 46, indicate that the load transmission through the soil was between 75 and 85 percent of the applied load. Thus, doubling the number of spacers between metal sections essentially doubled the percent of load transmitted through the Ottawa sand.

The data for the clay test are shown in Figure 47. The sample was compacted by kneading compaction using a Harvard Miniature Compactor. The data show an average load transmission through the soil of approximately 65 percent. The shape of the load-deflection curve is significantly different for the sand than the clay. This curve is concave to the load axis for the Ottawa sand and concave to the deflection axis for the EPK clay over the pressure range tested.

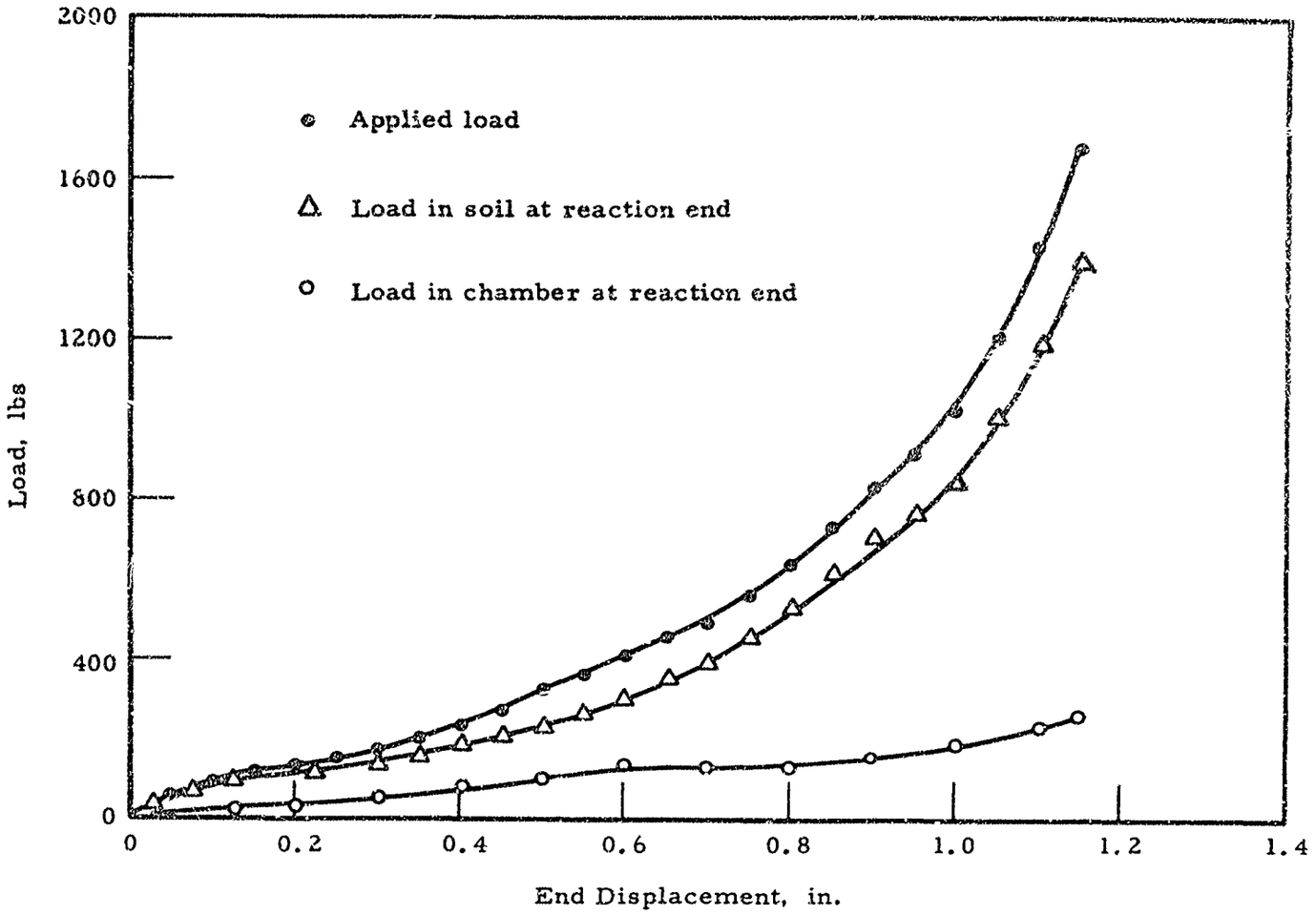

Figure 46 Load vs End Displacement, Static Test No. 3, Ottawa Sand
γ_m = 104.0 pcf

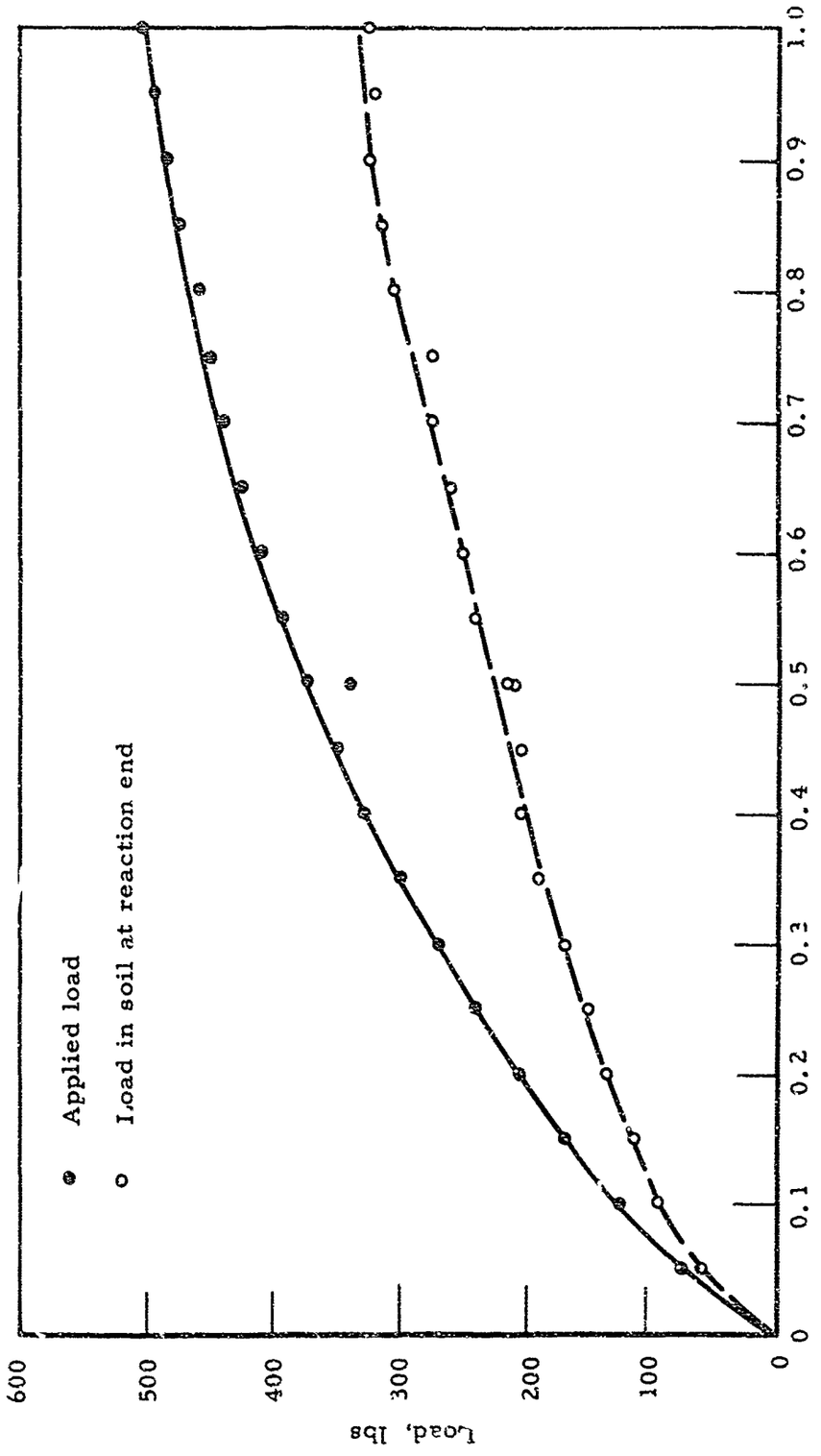

Figure 47 Load vs End Displacement, Static Test No. 4, EPK Clay
γ_m = 102.9 pcf, w = 27.5 percent

As the clay sample was loaded the rubber spacers began bulging. At an axial load of 485 lb (79.5 psi) the soil began to squeeze out at the rubber spacers. As a result, the test was terminated at this point. Hoop strain in the confining chamber, measured 23 in. from the loading end, reached a maximum of 27 microinches per in. at an axial stress of 79.5 psi. The deflection at the time the test was halted was 1 in.

b. Modification 2

In an attempt to increase the percent load transmission the segmented confining chamber was modified such that each unit was 2-12 in. in length including four neoprene rubber spacers. The only other difference between the tests conducted to evaluate the chamber as first modified and the ones now under consideration is that the load transmitted through the soil was measured by load cell* rather than a force washer.

	Sand	Clay
Density (pcf)	103.6	108.0**
Specimen length (in.)	49.3	43.9
Confining pressure (psi)	13.0	0.0
Sample area (sq in.)	6.1	6.1
Moisture content (%)	Air Dry	29.2

** Wet Density

For the test on the clay, the average percent load transmission was above 70 percent which represents a significant increase over the data reported for Modification 1. As previously noted for the clay, the load deflection curve was concave to the deflection axis. At an axial stress of 135 psi, the hoop strain, measured 7-12 in. from the loaded end, was 49 microinches per in., and the hoop strain measured 35 in. from the loaded end, was 39 microinches per in.

*Load Cell, Model No. 211., Kistler Instrument Corp.

The Ottawa sand data showed an S-shaped load-deflection curve that, as deflection increased, became concave to the load axis. Stress transmission through the soil initially decreased slightly and then increased slightly as average specimen strain increased. The average percent stress transmission through the sand was less (approximately 70 percent), with the confining chamber now under consideration, than the one considered under modification 1. This could possibly be the result of the tendency of the chamber of shorter segments to buckle and thus increase the friction loss to the support system as well as to cause eccentric loading of the column. In addition, the proportionate area of soft material was significantly increased which produced more local bulging of the sample and possibly an increase in load on the confining chamber.

The fact that the sand and clay produced approximately the same percent stress transmission for both the sand and clay is gratifying. This indicates that the confining system treats both soils essentially the same.

The load deflection curves obtained with modification 2 of the confining chamber are very similar to those obtained with modification 1 and consequently, will not be presented.

c. Modification 3

In an attempt to further increase the percent load transmission it was decided to replace the neoprene rubber spacers with foam rubber spacers having one-tenth the stiffness. To evaluate the efficiency of the new system a test was conducted on 20-30 Ottawa sand.

Density (pcf)	105.0
Specimen length (in.)	45.7
Confining pressure (psi)	14.0
Sample area (sq in.)	6.1
Moisture content (%)	Air Dry

Figure 48 shows the data obtained from the test under consideration and indicates that modification 3 of the confining chamber was more effective than anything used thus far. The load transmission was not significantly affected by displacement (strain) and the average transmission was above 90 percent.

It was anticipated that there possibly would be a problem with bulging of the soft foam spacers and possible extrusion of the soil with this system especially for the clay tests. However, it was decided that the high degree of load transmission through the soil outweighed the disadvantage of the spacer bulging. Therefore, it was decided to use the confining chamber as represented by modification 3 for the wave propagation experiments.

2. Summary

The confining chamber went through three modifications before one was determined to be adequate for the conduct of stress wave propagation tests. In the process of the evaluation of the confining chamber, a total of 9 static tests were conducted on Ottawa sand and EPK clay. As a result, modification 3 of the confining chamber was chosen for the stress wave propagation tests. This chamber was composed of hollow cylindrical sections 2-5/8 in. long with an inside diameter of 2-51/64 in. and an outside diameter of 3-1/4 in. The individual sections consisted of an aluminum cylinder 2-1/8 in. long with a 1/4-in. thick foam rubber ring glued to both ends. The

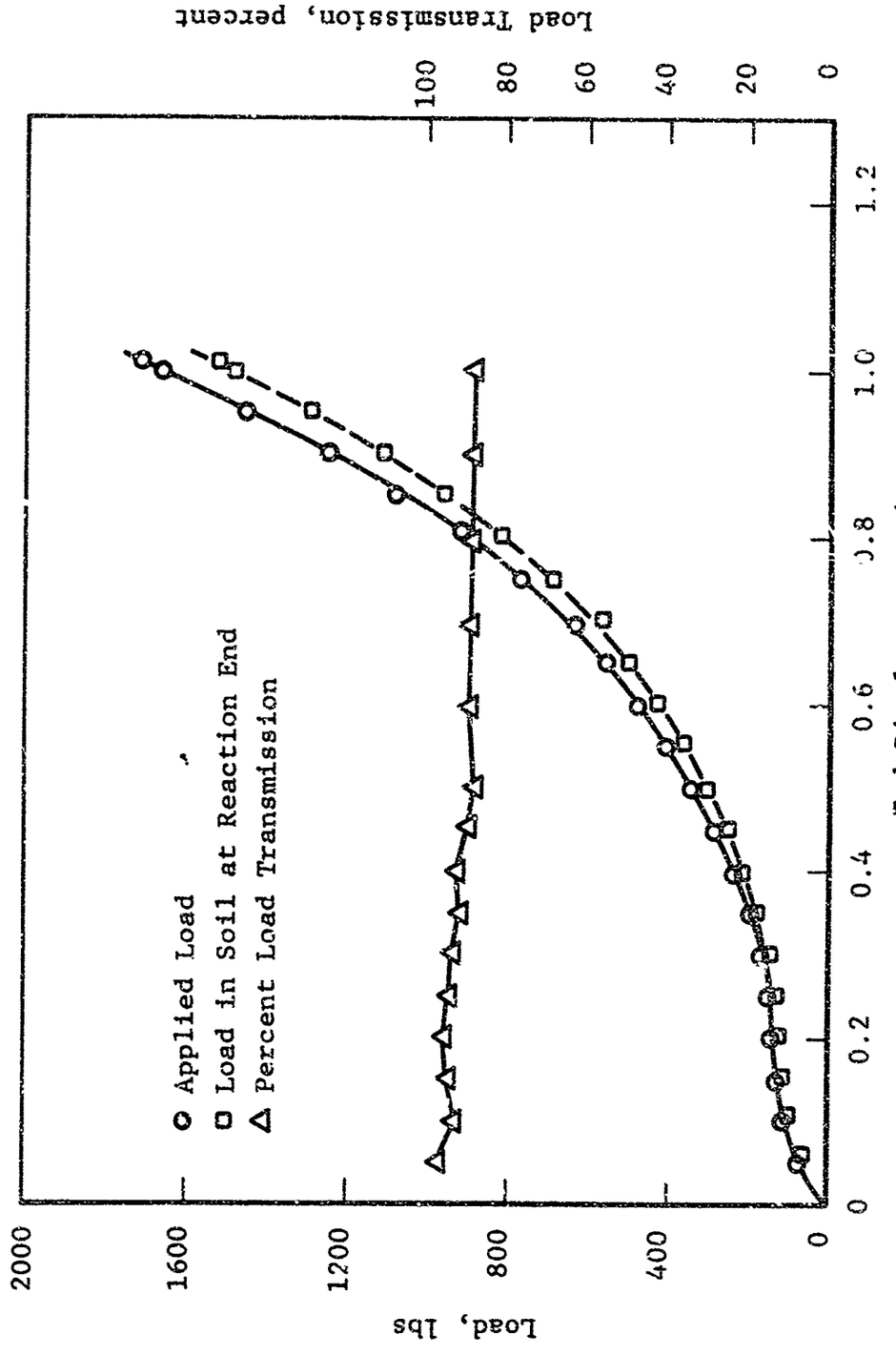

Figure 48 Static Load and Load Transmission vs End Displacement, Ottawa Sand
γ_m = 105.0 pcf

system produced load transmission above 90 percent for stresses up to 300 psi and appeared to be independent of soil type.

Three problems were noted with respect to the use of the confining chamber.

(1) Bulging of the soil at the location of the compressible spacers.

(2) The relatively large mass of the confining chamber.

(3) The tendency toward buckling of the column composed of the soil and the confining chamber.

In the static evaluation tests of the chamber some bulging of the soil occurred at the location of the compressible spacers. This bulging was more prominent in the clay tests than in the sand tests. A possible result of this bulging is to increase the load carried through the walls of the confining chamber. To ascertain quantitatively the effectiveness of this bulging on decreasing the percent stress transmission is not possible. However, based on the data obtained with modification 3 of the confining chamber it cannot be significant. In addition, for stress wave propagation tests the magnitude of the bulging should be much less because of the lateral inertia effect.

The thickness of the walls of the confining chamber does present certain problems. The mass of the confining chamber is approximately equal to the mass of the soil contained therein. Since the confining chamber moves with the soil, its mass will have an effect on shock wave propagation phenomena. An attempt will be made to take the effect of this increase in mass into consideration in the analysis of the data.

In certain instances there was a tendency for the chamber to buckle, which increases the friction loss to the support system and causes eccentric loading of the column. The loading time of the soil specimen in the wave propagation

experiments will be much less than for the static tests, and the sample will not be loaded simultaneously throughout its length. Therefore, it was anticipated that the friction loss produced by the tendency toward local buckling of the column would not be a problem in the dynamic tests. This conclusion was justified by observation during the wave propagation experiments.

In addition, it should be noted that the ball-bearing support system for the confining chamber worked well. The friction loss due to the confining chamber moving on the ball bearings appeared to be negligible.

In conclusion, the data collected on the performance of the confining chamber justifies its suitability for use in stress wave propagation experiments.

APPENDIX II

SOIL PROPERTIES

1. General

The two soils used in this study are standard 20-40 Ottawa sand and EPK clay. The properties and characteristics of these soils are described herein to aid in a better understanding of phenomena which occur when these soils are subjected to air shock loading. In addition, the particular properties which pertain to each specimen used in the wave propagation experiments are tabulated.

Ottawa sand comes from the region around Ottawa, Illinois and consists of subrounded particles of relatively uniform size. The grain-size distribution curve for this soil is shown in Figure 49. The specific gravity of solids for Ottawa sand is 2.66.

Edgar Plastic Kaolin (EPK) clay, a naturally occurring kaolinite, is hydraulically mined and water processed from a 1-million ton deposit in North Central Florida. The clay is available in both disintegrated pellet and airfloated grades; the airfloated grade was used in this study.

The grain-size distribution curve for this soil is shown in Figure 49. It is apparent that the EPK clay is much finer and more well graded than the Ottawa sand, i.e., its range in particle size is much larger. The difference in particle size and grain-size distribution produce significant differences in wave propagation phenomena. The specific gravity of solids of this soil is 2.65, the liquid limit 56.2 and the plasticity index is 19.6.

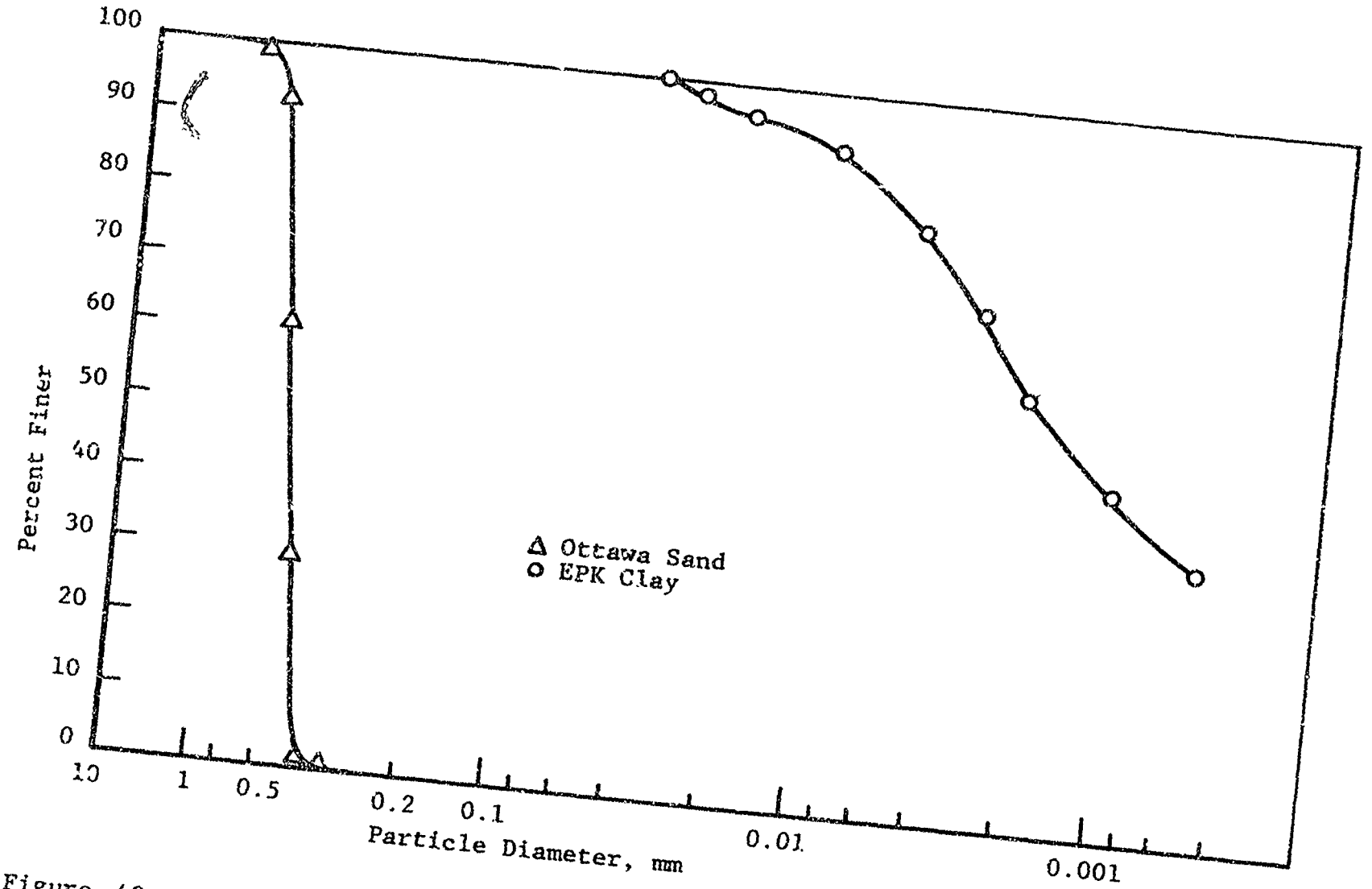

Figure 49 Grain Size Distribution Curves, Ottawa Sand and EPK Clay

One of the principal reasons for choosing the EPK clay was that it is practically pure kaolin — greater than 99 percent. Kaolin clays are not thixotropic, i.e., their properties do not change with time at constant moisture content (References 14 and 15). This characteristic is extremely important due to the fact that sample preparation, test setup, and testing required a minimum of approximately 2 days for tests on clay.

2. Wave Propagation Specimens

Specimens used in the wave propagation tests were made up of either Ottawa sand or EPK clay. The properties and characteristics of these specimens are given in Table 1, for the Ottawa sand specimens, and Table 2, for the EPK clay specimens. These tabulated data provide information on the range of soil properties considered.

3. Strain-Rate Effects

It is generally conceded that strain-rate effects are of no consequence in air-dry Ottawa sand. Therefore, no attempt was made to evaluate strain-rate phenomena for this soil.

Strain-rate phenomenon is known to be of great significance with respect to the stress-strain characteristics of fine grained soils. Accordingly, in choosing the clay to be used in this study, a necessary requirement was that the soil be significantly strain-rate sensitive. Upon receiving samples of the EPK clay, one of the first tasks was to ascertain whether it was sufficiently strain-rate sensitive.

To check the degree of strain-rate sensitivity of the soil a special series of dynamic unconfined compression tests were run. Specimens of the clay were prepared at various moisture contents and compacted at a given compactive effort with the Harvard Miniature Compaction apparatus. The compactive effort was 5 layers, 25 blows per layer, with a 20 pound spring. The specimens obtained were 1-5/16 in. diameter and 2-13/16 in. long.

Table 1

PROPERTIES OF WAVE PROPAGATION TEST SPECIMENS, OTTAWA SAND

Test Series No.	*Mass Density (pcf)	+Void Ratio	Confining Pressure (psi)	Specimen Length (in.)	Specimen Area (sq in.)
1	103.8	0.60	**13.0	61.9	6.1
5	108.0	0.54	13.0	61.1	6.1
6	96.6	0.72	13.0	61.4	6.1
7	101.9	0.63	13.0	61.3	6.1
9	101.9	0.63	13.0	60.5	6.1
11	102.4	0.62	14.0	60.3	6.1

* All specimens were tested in the air dry state.

** Nominal confining pressure, actual confining pressure less due to line losses.

\+ Specific gravity of soils 2.66.

Table 2

PROPERTIES OF WAVE PROPAGATION TEST SPECIMENS, EPK CLAY

Test Series No.	Mass Density (pcf)	Moisture Content (%)	*Degree of Saturation (%)	Void Ratio	Specimen Length (in.)	Specimen Area (sq in.)
2	101.9	27.0	67.6	1.06	61.7	6.1
3	103.8	29.7	73.9	1.07	61.1	6.1
4	113.7	33.1	94.0	0.94	59.9	6.1
8	113.2	33.2	93.1	0.95	61.6	6.1
10	101.9	28.0	68.8	1.08	60.3	6.1
12	105.8	29.3	76.2	1.02	60.6	6.1

* Specific gravity of solids 2.65.

The rate of strain in the dynamic tests was 64-1/2 in per second and was constant throughout the time of loading. The static tests were conducted at a rate of compression of 0.049 in. per minute. The difference in rate of strain for the static and dynamic tests was sufficient to determine if the soil was strain-rate sensitive.

The results of this study are shown in Figure 50. It is quite evident, from the data, that the soil is strain-rate sensitive. For the range of moisture contents tested, the dynamic strength at failure was always greater than the static strength by at least a factor of two. Thus, it was established that the soil was strain-rate sensitive to a significant degree and suitable for inclusion in the wave propagation experiments.

It is recognized that the strain-rate effect may not be the same for confined as for unconfined compression. Nevertheless, this effect is sufficiently large in unconfined compression, and it is certain to be significant in one-dimensional compression. Strain-rate sensitivity is a soil property and boundary effects can alter but not eliminate it.

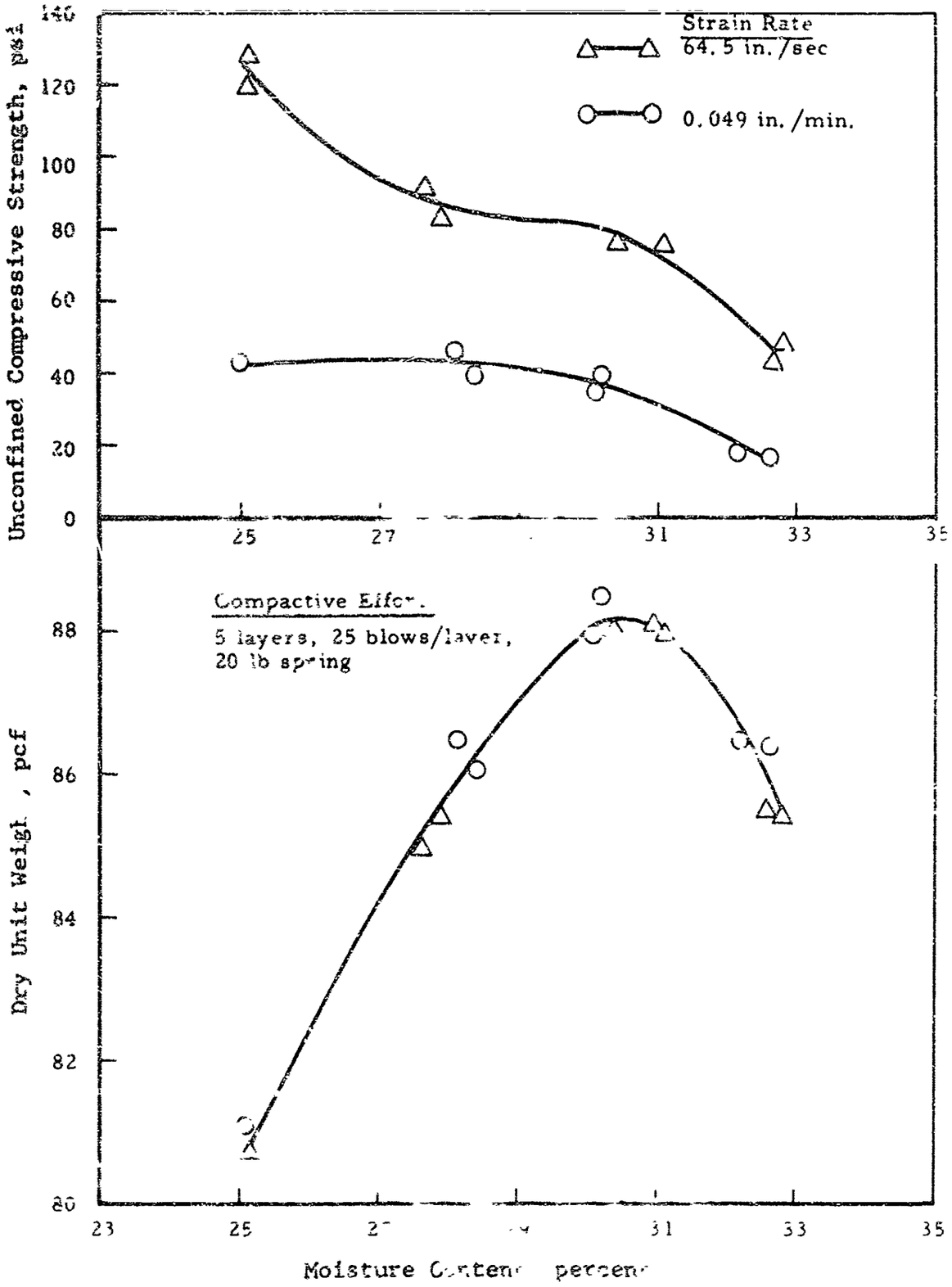

Figure 50 Moisture Content, Density, Strength Relationships, EPK Clay

APPENDIX III

SUMMARY OF STRAIN AND STRAIN RATE DATA

Strain and strain rate data from wave propagation tests are summarized in this Appendix. The data include that obtained from tests on Ottawa sand and EPK clay. The data include information on peak strain, rise time to peak strain and strain rate and indicates variation in these measured values with soil properties, peak overpressure, distance of propagation and peak overpressure duration.

Tables 3 to 5 and 7 to 9 contain data obtained by loading specimens of Ottawa sand and EPK clay, respectively, with an overpressure having approximately a 1 msec duration of peak pressure. Tables 6 and 10 contain data obtained by loading samples of Ottawa sand and EPK clay, respectively, with an overpressure having essentially a zero dwell time of peak overpressure.

Table 3

SUMMARY OF STRAIN-TIME DATA
Ottawa Sand, γ_m = 96.6 pcf

Test No.	Gage No.	Gage Location (in.)	Peak Over-pressure (psi)	Peak Strain (%)	Rise Time to Peak Strain (msec)	Strain Rate (%/sec)
6-1	εF	8.5	51.0	1.37	4.49	305
	ε1	13.5		1.00	5.14	194
	ε2	21.0		0.55	3.18	173
	ε3	28.5				
6-2	εF	8.5	90.2	1.32	2.26	584
	ε1	13.5		1.07	1.90	563
	ε2	21.0		0.81	2.20	368
	ε3	28.5		1.06	4.07	260
6-3	εF	8.5	188.0	1.87	1.54	1214
	ε1	13.5		1.72	2.10	819
	ε2	21.0		0.85	2.39	357
	ε3	28.5		1.61	2.69	599
6-4	εF	8.5	272.0	1.88	1.97	954
	ε1	13.5		1.97	1.44	1368
	ε2	21.0		1.01	1.34	754
	ε3	28.5		1.60	1.11	1441

Table 4

SUMMARY OF STRAIN-TIME DATA
Ottawa Sand, γ_m = 101.9 pcf

Test No.	Gage No.	Gage Location (in.)	Peak Over-pressure (psi)	Peak Strain (%)	Rise Time to Peak Strain (msec)	Strain Rate (%/sec)
7-1	εF	8.5	53.4	1.03	2.41	427
	ε1	13.5		0.93	2.58	360
	ε2	21.0		0.76	3.35	227
	ε3	28.5		0.52	5.39	96
7-2	εF	8.5	95.8	1.21	2.34	517
	ε1	13.5		0.86	2.08	413
	ε2	21.0		0.61	2.84	215
	ε3	28.5		0.68	3.60	189
7-3	εF	8.5	166.0	1.69	1.72	983
	ε1	13.5		1.11	1.53	725
	ε2	21.0		1.10	2.74	401
	ε3	28.5		0.85	2.12	401
7-4	εF	8.5	255.9	1.81	1.11	1631
	ε1	13.5		1.27	1.19	1067
	ε2	21.0		1.06	1.39	763
	ε3	28.5		0.95	1.42	669

Table 5

SUMMARY OF STRAIN-TIME DATA
Ottawa Sand, γ_m = 108.6 pcf

Test No.	Gage No.	Gage Location (in.)	Peak Over-pressure (psi)	Peak Strain (%)	Rise Time to Peak Strain (msec)	Strain Rate (%/sec)
5-1	εF	8.5	50.7	0.42	1.92	219
	ε1	13.5		0.36	3.05	118
	ε2	21.0		0.33	2.11	156
	ε3	28.5				
5-2	εF	8.5	82.7	0.24	1.21	281
	ε1	13.5		0.32	0.63	506
	ε2	21.0		0.49	2.16	227
	ε3	28.5		0.19	1.17	162
5-3	εF	8.5	214.0	0.68	1.21	562
	ε1	13.5		0.57	0.56	1018
	ε2	21.0		0.97	1.80	539
	ε3	28.5		0.80	2.30	348
5-4	εF	8.5	290.0	0.60	0.62	968
	ε1	13.5		0.69	0.95	726
	ε2	21.0		0.93	0.83	1120
	ε3	28.5		1.77	1.47	1204

Table 6

SUMMARY OF STRAIN-TIME DATA
Ottawa Sand, γ_m = 102.4 pcf

Test No.	Gage No.	Gage Location (in.)	Peak Over-pressure (psi)	Peak Strain (%)	Rise Time to Peak Strain (msec)	Strain Rate (%/sec)
11-1	εF	8.6	55.3	0.59	2.10	281
	ε1	13.7		1.13	3.64	310
	ε2	21.3		0.42	1.67	251
	ε3	28.9		0.28	3.20	87
11-2	εF	8.6	110.6	0.80	1.54	5.9
	ε1	13.7		1.24	1.80	689
	ε2	21.3		0.51	2.33	218
	ε3	28.9		0.55	2.73	201
11-3	εF	8.6	214.6	1.01	1.05	962
	ε1	13.7		1.51	1.34	1127
	ε2	21.3		0.77	1.30	592
	ε3	28.9		0.64	1.97	325
11-4	εF	8.6	302.8	1.37	1.21	1132
	ε1	13.7		1.68	1.08	1555
	ε2	21.3		0.96	0.73	1315
	ε3	28.9		0.70	1.40	500

Table 7

SUMMARY OF STRAIN-TIME DATA
EPK Clay, γ_m = 101.9 pcf, w = 27.0 Percent

Test No.	Gage No.	Gage Location (in.)	Peak Over-pressure (psi)	Peak Strain (%)	Rise Time to Peak Strain (msec)	Strain Rate (%/sec)
2-1	εF	5.0	65.0	1.11	2.18	509
	ε1	13.5		1.53	2.34	653
	ε2	18.5				
	ε3	28.5				
2-2	εF	5.0	125.0	2.35	2.02	1163
	ε1	13.5		2.60	2.50	1040
	ε2	18.5				
	ε3	28.5				
2-3	εF	5.0	201.0	4.40	2.24	1964
	ε1	13.5		3.85	3.23	1192
	ε2	18.5		3.79	3.70	1024
	ε3	28.5		2.38	4.68	508
2-4	εF	5.0	325.0	6.60	1.92	3428
	ε1	13.5		5.61	2.31	2429
	ε2	18.5		5.72	2.64	2166
	ε3	28.5		2.88	4.37	659

Table 8

SUMMARY OF STRAIN-TIME DATA
EPK Clay, γ_m = 103.8 pcf, w = 29.7 Percent

Test No.	Gage No.	Gage Location (in.)	Peak Over-pressure (psi)	Peak Strain (%)	Rise Time to Peak Strain (msec)	Strain Rate (%/sec)
3-1	εF	8.5	58.2	1.10	2.95	373
	ε1	13.5		2.20	2.80	786
	ε2	21.0				
	ε3	28.5		2.62	3.61	726
3-2	εF	8.5	105.2	2.45	2.03	1207
	ε1	13.5		3.53	3.03	1165
	ε2	21.0		1.25	3.27	527
	ε3	28.5		2.62	3.18	824
3-3	εF	8.5	208.3	5.35	2.52	2123
	ε1	13.5		5.78	3.10	1864
	ε2	21.0		2.76	2.63	1049
	ε3	28.5		3.67	4.33	848
3-4	εF	8.5	300.5	5.60	1.28	4375
	ε1	13.5		11.13		
	ε2	21.0		3.48	2.00	1740
	ε3	28.5		5.16	3.25	1588

Table 9

SUMMARY OF STRAIN-TIME DATA
EPK Clay, γ_m = 113.2 pcf, w = 33.2 Percent

Test No.	Gage No.	Gage Location (in.)	Peak Over-pressure (psi)	Peak Strain (%)	Rise Time to Peak Strain (msec)	Strain Rate (%/sec)
8-1	εF	8.5	62.6	1.32	1.90	695
	ε1	13.5		0.60	1.97	305
	ε2	21.0		0.56	1.41	397
	ε3	28.5		0.56	3.54	159
8-2	εF	8.5	100.9	1.84	1.77	1040
	ε1	13.5		0.81	0.90	896
	ε2	21.0		1.02	1.87	545
	ε3	28.5		0.62	1.28	481
8-3	εF	8.5	193.1	2.15	0.80	2687
	ε1	13.5		1.07	0.77	1390
	ε2	21.0		1.12	0.75	1493
	ε3	28.5		1.36	2.23	610
8-4	εF	8.5	252.2	2.82	1.87	1508
	ε1	13.5		1.17	1.22	959
	ε2	21.0		1.10	0.37	2973
	ε3	28.5		1.36	0.62	2193

Table 10

SUMMARY OF STRAIN-TIME DATA
EPK Clay, γ_m = 10..8 pcf, w = 29.3 Percent

Test No.	Gage No.	Gage Location (in.)	Peak Over-pressure (psi)	Peak Strain (%)	Rise Time to Peak Strain (msec)	Strain Rate (%/sec)
12-1	εF	8.7	58.5	0.48	1.70	282
	ε1	13.8		0.80	2.46	325
	ε2					
	ε3	21.4		0.42	2.07	203
12-2	εF	8.7	110.5	1.50	1.93	777
	ε1	13.8		1.79	2.52	710
	ε2					
	ε3	21.4		0.77	3.18	242
12-3	εF	8.7	201.2	3.60	1.90	1900
	ε1	13.8		3.20	2.92	1096
	ε2					
	ε3	21.4		0.92	3.70	249
12-4	εF	8.7	292.4	3.60	1.73	2081
	ε1	13.8		4.14	2.39	1732
	ε2					
	ε3	21.4		1.64	3.08	532

APPENDIX IV

SUMMARY OF STRESS ARRIVAL AND RISE TIME DATA

Time of arrival and rise time to peak stress data are summarized in this Appendix. The data includes that obtained from tests on Ottawa sand and EPK clay. The data are presented in tabular form and gives arrival time and rise time to peak stress as functions of air dry unit weight, for Ottawa sand, moisture content and wet unit weight, for EPK clay, overpressure and distance of propagation.

The sum of arrival time and rise time to peak stress, t_p, was divided by the exponential time constant, T_o, of the overpressure to produce a nondimensional depth, τ_p. Values of nondimensional depth are also shown in each table.

In every instance it was not possible to show a complete set of arrival time and rise time data for each test. The reason for such absences is either a malfunction of a particular gage or gages and/or the blanking pulse, which acted as a time reference, was not distinguishable.

The test numbers give an indication of the nominal peak overpressure for each test. For example, tests 6.1, 6.2, 6.3 and 6.4 would indicate nominal peak overpressures of 50, 100, 200 and 300 psi. For actual values of peak overpressure for a given test, refer to the tables of Appendix III.

Table 11

SUMMARY OF STRESS ARRIVAL AND RISE TIME DATA
Ottawa Sand, γ_m = 96.6 pcf

Test No.	Gage No.	Position (in.)	Blanking Pulse (msec)	Arrival Time (msec)	Rise Time (msec)	Time To Peak Stress t_p (msec)	T_o (msec)	$\tau_p = \frac{t_p}{T_o}$
6-1	p_o	0	4.649				4.620	
	σ#6	5	4.382	0.267	3.033	3.300		0.714
	σ#3	10	4.029	0.620	3.676	4.296		0.930
	σ#5	17.5	3.633	1.016	5.333	6.349		1.374
	σ#11	25	2.633	2.016	6.033	8.049		1.742
6-2	p_o	0	5.380				3.699	
	σ#6	5	5.088	0.292	2.176	2.468		0.667
	σ#3	10	4.765	0.615	2.235	2.850		0.770
	σ#5	17.5	4.133	1.247	4.133	5.380		1.454
	σ#11	25	3.600	1.780	4.600	6.380		1.725
6-3	p_o	0	5.526				3.187	
	σ#6	5	5.206	0.320	1.676	1.996		0.626
	σ#3	10	4.912	0.614	1.265	1.879		0.589
	σ#5	17.5	4.166	1.360	2.466	3.826		1.200
6-4	p_o	0	5.614				2.836	
	σ#6	5	5.235	0.379	1.206	1.585		0.559
	σ#3	10	4.970	0.644	0.794	1.438		0.507
	σ#5	17.5	4.133	1.481	1.300	2.781		0.981
	σ#11	25	3.467	2.147	1.600	3.747		1.321

Table 12

SUMMARY OF STRESS ARRIVAL AND RISE TIME DATA
Ottawa Sand, γ_m = 101.9 pcf

Test No.	Gage No.	Position (in.)	Blanking Pulse (msec)	Arrival Time (msec)	Rise Time (msec)	Time To Peak Stress t_p (msec)	T_o (msec)	$\tau_p = \frac{t_p}{T_o}$
7-1	p_o	0	4.609				4.783	
	σ#6	5	4.464	0.145	1.942	2.087		0.436
	σ#5	10	4.029	0.580	2.485	3.065		0.641
	σ#11	17.5	3.627	0.982	3.864	4.846		1.013
	σ#3	25	2.949	1.660	5.661	7.321		1.531
7-2	p_o	0	5.275				3.942	
	σ#6	5	4.985	0.290	1.188	1.478		0.375
	σ#5	10	4.608	0.667	2.289	2.956		0.750
	σ#11	17.5	4.237	1.038	3.050	4.088		1.037
	σ#3	25	3.559	1.716	3.559	5.275		1.788
7-3	p_o	0	5.536				3.420	
	σ#6	5	5.333	0.203	1.710	1.913		0.559
	σ#5	10	4.840	0.696	1.652	2.348		0.686
	σ#11	17.5	4.372	1.164	2.237	3.401		0.994
	σ#3	25	4.000	1.536	4.338	5.874		1.717
7-4	p_o	0	5.594				2.913	
	σ#6	5	5.362	0.232	1.304	1.536		0.527
	σ#5	10	4.956	0.638	1.130	1.768		0.607
	σ#11	17.5	4.407	1.187	1.491	2.678		0.913
	σ#3	25	3.864	1.730	1.593	3.323		1.140

Table 13

SUMMARY OF STRESS ARRIVAL AND RISE TIME DATA
Ottawa Sand, γ_m = 108.0 pcf

Test No.	Gage No.	Position (in.)	Blanking Pulse (msec)	Arrival Time (msec)	Rise Time (msec)	Time To Peak Stress t_p (msec)	T_o (msec)	$\tau_p = \frac{t_p}{T_o}$
5-1	p_o	0	4.628				5.357	
	σ#3	5	4.470	0.158	1.617	1.775		0.331
	σ#6	10	1.268	0.336	2.000	2.336		1.000
	σ#11	17.5	3.661	0.967	2.779	3.746		0.699
	σ#5	25	3.050	1.578	3.796	5.374		1.003
5-2	p_o	0	5.057				6.429	
	σ#3	5	4.911	0.146	1.176	1.322		0.206
	σ#6	10	4.558	0.499	1.764	2.263		0.352
	σ#11	17.5	4.067	0.990	2.135	3.125		0.486
	σ#5	25	3.627	1.430	2.678	4.108		0.639
5-3	p_o	0	5.200				3.257	
	σ#3	5	5.088	0.112	0.911	1.023		0.314
	σ#6	10	4.823	0.377	1.205	1.582		0.486
	σ#11	17.5						
	σ#5	25	3.830	1.370	1.762	3.132		0.962
5-4	p_o	0	5.342				2.957	
	σ#3	5	5.264	0.078	0.647	0.725		0.245
	σ#6	10	4.970	0.372	0.705	1.077		0.364
	σ#11	17.5						
	σ#5	25	4.135	1.207	1.186	2.393		0.809

Table 14

SUMMARY OF STRESS ARRIVAL AND RISE TIME DATA
Ottawa Sand, γ_m = 101.9 pcf

Test No.	Gage No.	Position (in.)	Blanking Pulse (msec)	Arrival Time (msec)	Rise Time (msec)	Time To Peak Stress t_p (msec)	T_o (msec)	$\tau_p = \frac{t_p}{T_o}$
9-1	p_o	0	2.449				4.667	
	σ#2	7.6	1.886	0.563	1.700	2.263		0.485
	σ#3	15.3	1.328	1.121	3.928	5.049		1.082
	σ#11	30.4	0.245	2.203	5.770	7.973		1.708
9-3	p_o	0	3.029				2.739	
	σ#2	7.5	2.528	0.501	0.600	1.101		0.402
	σ#3	15.1	1.986	1.043	1.757	2.800		1.022
	σ#11	30.2	0.967	2.062	3.393	4.455		1.626
	σ#CS-2	37.7	0.410	2.619	3.066	5.685		2.076

Table 15

SUMMARY OF STRESS ARRIVAL AND RISE TIME DATA
Ottawa Sand, γ_m = 102.4 pcf

Test No.	Gage No.	Position (in.)	Blanking Pulse (msec)	Arrival Time (msec)	Rise Time (msec)	Time To Peak Stress t_p (msec)	T_o (msec)	$\tau_p = \frac{t_p}{T_o}$
11-1	p_o	0	4.985				3.420	
	σ#3	5.1	4.795	0.190	1.228	1.518		0.415
	σ#2	10.1	4.444	0.541	2.047	2.588		0.757
	σ#4	17.8	3.833	1.152	2.833	3.985		1.165
	σ#11	25.4	3.400	1.585	3.666	5.251		1.535
11-2	p_o	0	5.536				2.609	
	σ#3	5.1	5.234	0.302	0.614	0.916		0.351
	σ#2	10.1	4.854	0.682	1.696	2.378		0.911
	σ#4	17.8	4.367	1.169	2.033	3.302		1.227
	σ#11	25.4	3.967	1.569	2.633	4.202		1.610
11-3	p_o	0	5.623				2.319	
	σ#3	5.1	5.526	0.097	1.169	1.266		0.546
	σ#2	10.1	5.234	0.379	1.169	1.558		0.672
	σ#4	17.8	4.566	1.057	1.233	2.290		0.987
11-4	p_o	0	5.739				2.120	
	σ#3	5.1	5.449	0.290	1.023	1.313		0.620
	σ#2	10.1	5.188	0.551	0.878	1.429		0.674
	σ#4	17.8	4.633	1.106	0.667	1.773		0.836
	σ#11	25.4	4.000	1.739	1.033	2.772		1.308

Table 16

SUMMARY OF STRESS ARRIVAL AND RISE TIME DATA
EPK Clay, γ_m = 101.9 pcf, w = 27.0 Percent

Test No.	Gage No.	Position (in.)	Blanking Pulse (msec)	Arrival Time (msec)	Rise Time (msec)	Time to Peak Stress t_p (msec)	T_o (msec)	$\tau_p = \frac{t_p}{T_o}$
2-1	p_o	0	5.475				6.200	
	σ#CS-2	5	4.918	0.539	1.443	1.982		0.320
	σ#3	10	4.833	0.624	2.361	2.985		0.481
	σ#6	15	3.972	1.485	1.027	2.512		0.405
	σ#1	25	3.377	2.080	3.377	5.457		0.880
2-2	p_o	0	5.886				2.971	
	σ#CS-2	5	5.311	0.575	1.443	2.018		0.679
	σ#3	10	5.111	0.775	2.136	2.911		0.980
	σ#6	15	4.639	1.247	2.944	4.191		1.411
	σ#1	25	3.672	2.214	2.787	5.001		1.683
2-3	p_o	0	6.000				2.543	
	σ#CS-2	5	5.705	0.295	1.574	1.869		0.735
	σ#3	10	5.306	0.694	2.472	3.166		1.245
	σ#6	15	4.889	1.111	3.167	4.278		1.682
	σ#1	25	4.393	1.607	4.393	6.000		2.359
2-4	p_o	0	6.086				1.800	
	σ#CS-2	5	5.967	0.119	1.443	1.562		0.868
	σ#3	10	5.528	0.558	2.000	2.558		1.421
	σ#6	15	4.500	1.586	2.222	3.808		2.116
	σ#1	25	4.328	1.758	4.066	5.824		3.236

Table 17

SUMMARY OF STRESS ARRIVAL AND RISE TIME DATA
EPK Clay, γ_m = 103.8 pcf, w = 29.7 Percent

Test No.	Gage No.	Position (in.)	Blanking Pulse (msec)	Arrival Time (msec)	Rise Time (msec)	Time to Peak Stress t_p (msec)	T_o (msec)	$\tau_p = \frac{t_p}{T_o}$
3-1	p_o	0	6.857				5.442	
	σ#3	5	6.750	0.107	1.806	1.913		0.352
	σ#CS-2	10	6.512	0.345	2.644	2.989		0.549
	σ#11	17.5	5.667	1.190	2.750	3.940		0.724
	σ#6	25	5.124	1.733	3.802	5.535		1.017
3-2	p_o	0	7.343				3.057	
	σ#3	5	7.222	0.111	1.583	1.694		0.554
	σ#CS-2	10	6.777	0.566	2.215	2.781		0.910
	σ#11	17.5	5.417	1.926	2.139	4.065		1.330
	σ#6	25	4.595	2.748	2.843	5.591		1.829
3-3	p_o	0	7.486				2.371	
	σ#3	5	7.333	0.153	1.444	1.597		0.674
	σ#CS-2	10	7.008	0.478	2.248	2.726		1.150
	σ#11	17.5	6.167	1.319	2.944	4.263		1.798
	σ#6	25	4.727	2.759	2.975	5.734		2.418
3-4	p_o	0	7.686				1.971	
	σ#3	5	7.555	0.131	1.094	1.225		0.622
	σ#CS-2	10	6.909	0.777	1.818	2.595		1.317
	σ#11	17.5	5.194	2.492	1.500	3.992		2.025
	σ#6	25	4.463	3.233	2.182	5.405		2.742

Table 18

SUMMARY OF STRESS ARRIVAL AND RISE TIME DATA
EPK Clay, γ_m = 113.2 pcf, w = 33.2 Percent

Test No.	Gage No.	Position (in.)	Blanking Pulse (msec)	Arrival Time (msec)	Rise Time (msec)	Time to Peak Stress t_p (msec)	T_o (msec)	$\tau_p = \frac{t_p}{T_o}$
8-1	p_o	0	4.724				4.783	
	σ#3	5	3.826	0.898	1.797	1.695		0.354
	σ#11	10	3.362	1.362	1.681	3.043		0.636
	σ#6	17.5	3.311	1.413	3.311	4.724		0.988
	σ#5	25	2.736	1.988	4.121	6.109		1.277
8-2	p_o	0	5.275				3.420	
	σ#3	5	4.522	0.723	1.362	2.085		0.610
	σ#11	10	3.681	1.594	0.956	2.550		0.745
	σ#6	17.5	3.593	1.682	3.007	4.689		1.371
	σ#5	25	1.081	4.194	1.622	5.816		1.700
8-3	p_o	0	5.333				2.696	
	σ#3	5	4.725	0.608	0.522	1.130		0.419
	σ#11	10	4.029	1.304	0.898	2.202		0.817
	σ#6	17.5	2.804	2.529	1.115	3.644		1.352
	σ#5	25	1.486	3.847	1.268	5.115		1.897
8-4	p_o	0	5.623				2.580	
	σ#3	5	4.927	0.696	0.261	0.957		0.371
	σ#11	10	4.290	1.333	0.783	2.116		0.820
	σ#6	17.5	3.176	2.447	0.507	2.954		1.145
	σ#5	25	1.926	3.697	1.149	4.846		1.878

Table 19

SUMMARY OF STRESS ARRIVAL AND RISE TIME DATA
EPK Clay, γ_m = 101.9 pcf, w = 28.0 Percent

Test No.	Gage No.	Position (in.)	Blanking Pulse (msec)	Arrival Time (msec)	Rise Time (msec)	Time to Peak Stress t_p (msec)	T_o (msec)	$\tau_p = \frac{t_p}{T_o}$
10-1	p_o	0	2.638				5.072	
	σ#3	7.6	2.277	0.361	1.869	2.230		0.440
	σ#1	15.2	1.810	0.828	1.766	2.594		0.511
	σ#2	22.8	0.629	2.009	2.387	4.396		0.867
	σ#4	30.5	0.403	2.235	3.596	5.831		1.150
10-2	p_o	0	3.217				4.304	
	σ#3	7.6	2.920	0.297	2.233	2.530		0.588
	σ#1	15.2	2.511	0.706	3.200	3.906		0.907
	σ#2	22.8	1.419	1.798	3.532	5.330		1.238
	σ#4	30.5	1.070	2.147	4.333	6.480		1.506
	σ#CS-2	38.1	0.483	2.734	5.050	7.784		1.808
10-3	p_o	0	3.333				2.391	
	σ#3	7.6	2.832	0.501	1.810	2.311		0.966
	σ#1	15.2	2.555	0.778	2.555	3.333		1.394
	σ#2	22.8	1.468	1.865	3.710	5.575		2.332
	σ#4	30.5	1.228	2.105	4.631	6.736		2.817
	σ#CS-2	38.1	0.400	2.933	5.117	8.050		3.367

Table 20

SUMMARY OF STRESS ARRIVAL AND RISE TIME DATA
EPK Clay, γ_m = 105.8 pcf, w = 29.3 Percent

Test No.	Gage No.	Position (in.)	Blanking Pulse (msec)	Arrival Time (msec)	Rise Time (msec)	Time to Peak Stress t_p (msec)	T_o (msec)	$\tau_p = \frac{t_p}{T_o}$
12-1	p_o	0	5.043				4.347	
	σ#3	5.1	4.812	0.231	0.928	1.159		0.267
	σ#2	10.2	4.232	0.811	1.420	2.231		0.513
	σ#11	17.9	3.765	1.278	2.487	3.765		0.866
	σ#4	23.0	3.294	1.749	2.655	4.404		1.013
	σ#6	30.6	2.656	2.387	2.656	5.043		1.160
12-2	p_o	0	5.420				3.275	
	σ#3	5.1	5.275	0.145	1.420	1.565		0.479
	σ#2	10.2	4.754	0.666	2.029	2.695		0.823
	σ#11	17.9	4.000	1.420	2.487	3.907		1.193
	σ#4	23.0	3.798	1.622	3.193	4.815		1.470
	σ#6	30.6						
12-3	p_o	.0	5.739				2.174	
	σ#3	5.1	5.594	0.145	1.449	1.594		0.733
	σ#2	10.2	5.188	0.551	2.174	2.725		1.253
	σ#11	17.9	4.672	1.067	3.092	4.159		1.913
	σ#4	23.0	4.336	1.403	3.764	5.167		2.377
	σ#6	30.6	3.738	2.001	4.525	6.526		3.002
12-4	p_o	0	5.710				1.638	
	σ#3	5.1	5.594	0.116	1.188	1.304		0.796
	σ#2	10.2	5.043	0.667	1.681	2.348		1.433
	σ#11	17.9	4.605	1.105	2.723	3.828		2.337
	σ#4	23.0	4.067	1.643	3.193	4.836		2.952
	σ#6	30.6	3.770	1.940	4.328	6.268		3.827

REFERENCES

1. Wetzel, R. A., Shock Induced Stress Wave Propagation in a Cohesive Soil, Master's Thesis, Illinois Institute of Technology, Chicago, Illinois, January 1965.

2. Selig, E. T. and Vey, E., "Shock Induced Stress Wave Propagation in Sand", Journal Soil Mech. and Founds. Div., ASCE, V. 91, No. SM3, May 1965, pp. 19-50.

3. Seaman, L. and Whitman, R. V., Stress Propagation in Soils, Final Report, Part IV, SRI for DASA (Contract DA-49-146-XZ-018), Washington, D. C., DASA 1266-4, June 1964.

4. Seaman, L., One-Dimensional Stress Wave Propagation in Soils, Final Report, SRI for DASA (Contract DA-49-146-XZ-343), Washington, D. C., DASA 1757, February 1966.

5. Stoll, R. D. and Ebeido, I. A., Dynamic Response of Granular Soils, Columbia University for United States Naval Civil Engineering Laboratory, (Contract NBy 32198) Port Hueneme, California, Tech. Rpt. No. 2, May 1964.

6. Durbin, W. L., Study of the Dynamic Stress-Strain and Wave Characteristics of Soils, URS for U.S.A. Engr. Waterways Experiment Station (Contract DA-22-079-eng-373) Rpt. 2, Contract Rpt. 3-91, November 1964.

7. Alekseenko, V. D., "Experimental Investigation of the Dynamic Stress Field in Soft Ground During a Contact Explosion", Zh. Prikl. Mekh. Tekh. Fiz., No. 5, Sept. to Oct. 1963, pp. 99-106.

8. McNeill, R. L., A Study of the Propagation of Stress Waves in Sand, Doctoral Disertation (draft copy), University of New Mexico, Albuquerque, New Mexico, 1965.

REFERENCES (Cont.)

9. Selig, E. T. and Wetzel, R. A., A Miniature Piezoelectric Gage for Static and Dynamic Soil Stress Measurement, Contract Report No. 1-105, for U.S. Army Engineer Waterways Experiment Station, Vicksburg, Mississippi, Nov. 1964.

10. Truesdale, W. B., Development of a Small Soil Strain Gage, AFSWC TDR-63-3, Armour Research Foundation, March 1963.

11. Keller, R. W., Development of a Soil Strain Gage for Laboratory Dynamic Tests, AFWL TDR 64-7, IIT Research Institute, April 1964.

12. Truesdale, W. B. and Schwab, R. B., Soil Strain Gage Instrumentation, IITRI for AFWL, to be released.

13. Wilson, S. D. and Sibley, E. A., "Ground Displacements from Air-Blast Loading", J. Soil Mech. and Founds. Div., ASCE, V. 88, No. SM6, Dec. 1962, pp. 1-32.

14. Seed, H. B. and Chan, C. K., "Thixotropic Characteristics of Compacted Clays", J. Soil Mech. and Founds. Div., ASCE, V. 83, No. SM4, Nov. 1957.

15. Mitchell, J. K., "Fundamental Aspects of Thixotropy in Soils", J. Soil Mech. and Founds. Div., ASCE, V. 86, No. 3, June 1960.

UNCLASSIFIED
Security Classification

DOCUMENT CONTROL DATA - R&D

(Security classification of title, body of abstract and indexing annotation must be entered when the overall report is classified)

1 ORIGINATING ACTIVITY (Corporate author) IIT Research Institute Technology Center Chicago, Illinois 60616	2a REPORT SECURITY CLASSIFICATION UNCLASSIFIED 2b GROUP

3 REPORT TITLE

STRESS WAVE PROPAGATION IN CONFINED SOILS

4 DESCRIPTIVE NOTES (Type of report and inclusive dates)

15 January 1965-15 August 1966

5 AUTHOR(S) (Last name, first name, initial)

Hampton, Delon; Wetzel, R. A.

6 REPORT DATE	7a TOTAL NO. OF PAGES	7b NO OF REFS
October 1966	154	15

8a CONTRACT OR GRANT NO AF 29(601)-6717	9a ORIGINATOR'S REPORT NUMBER(S)
b PROJECT NO 5710	AFWL-TR-66-56
c Subtask No. 13.144	9b OTHER REPORT NO(S) (Any other numbers that may be assigned this report)
d	

10 AVAILABILITY/LIMITATION NOTICES This document is subject to special export controls and each transmittal to foreign governments or foreign governments or foreign nationals may be made only with prior approval of AFWL (WLDC), Kirtland AFB, NM, 87117. Distribution is limited because of the technology discussed in the report.

11 SUPPLEMENTARY NOTES	12. SPONSORING MILITARY ACTIVITY
	AFWL (WLDC) Kirtland AFB, NM 87117

13 ABSTRACT

Phenomena involved with the propagation of air-induced stress waves in soil were investigated in experiments on Edgar Plastic Kaolin (EPK) clay and Ottawa sand. The principal soil variables were moisture content and density in the case of clay, and density in the case of sand. The soil specimens were loaded with overpressures in the range of from approximately 50 to 300 psi. Two overpressure wave shapes were used, one where peak overpressure had a dwell time of approximately 1 msec and the other having essentially a zero dwell time of peak pressure. Stress-time and strain-time relationships were measured at various points along the length of the specimens. Peak stress attenuation, strain and strain-rate relationships, propagation velocity, changes in wave shape, and stress-strain relationships are discussed in the light of the data obtained. Experimental data are compared with theoretical predictions of a linear hysteretic model in the case of Ottawa sand, and a constant tan δ viscoelastic model, in the case of the EPK clay. It was found that in both cases the theories could be used to predict the experimental results with proper evaluation of critical attenuation parameters to be input with the theories.

DD FORM 1 JAN 64 1473

UNCLASSIFIED
Security Classification

UNCLASSIFIED

Security Classification

14. KEY WORDS	LINK A		LINK B		LINK C	
	ROLE	WT	ROLE	WT	ROLE	WT
Wave propagation Dynamic properties of soils One dimensional soil testing						

INSTRUCTIONS

1. ORIGINATING ACTIVITY: Enter the name and address of the contractor, subcontractor, grantee, Department of Defense activity or other organization *(corporate author)* issuing the report.

2a. REPORT SECURITY CLASSIFICATION: Enter the overall security classification of the report. Indicate whether "Restricted Data" is included. Marking is to be in accordance with appropriate security regulations.

2b. GROUP: Automatic downgrading is specified in DoD Directive 5200.10 and Armed Forces Industrial Manual. Enter the group number. Also, when applicable, show that optional markings have been used for Group 3 and Group 4 as authorized.

3. REPORT TITLE: Enter the complete report title in all capital letters. Titles in all cases should be unclassified. If a meaningful title cannot be selected without classification, show title classification in all capitals in parenthesis immediately following the title.

4. DESCRIPTIVE NOTES: If appropriate, enter the type of report, e.g., interim, progress, summary, annual, or final. Give the inclusive dates when a specific reporting period is covered.

5. AUTHOR(S): Enter the name(s) of author(s) as shown on or in the report. Enter last name, first name, middle initial. If military, show rank and branch of service. The name of the principal author is an absolute minimum requirement.

6. REPORT DATE: Enter the date of the report as day, month, year, or month, year. If more than one date appears on the report, use date of publication.

7a. TOTAL NUMBER OF PAGES: The total page count should follow normal pagination procedures, i.e., enter the number of pages containing information.

7b. NUMBER OF REFERENCES: Enter the total number of references cited in the report.

8a. CONTRACT OR GRANT NUMBER: If appropriate, enter the applicable number of the contract or grant under which the report was written.

8b, 8c, & 8d. PROJECT NUMBER: Enter the appropriate military department identification, such as project number, subproject number, system numbers, task number, etc.

9a. ORIGINATOR'S REPORT NUMBER(S): Enter the official report number by which the document will be identified and controlled by the originating activity. This number must be unique to this report.

9b. OTHER REPORT NUMBER(S): If the report has been assigned any other report numbers *(either by the originator or by the sponsor)*, also enter this number(s).

10. AVAILABILITY/LIMITATION NOTICES: Enter any limitations on further dissemination of the report, other than those imposed by security classification, using standard statements such as:

(1) "Qualified requesters may obtain copies of this report from DDC."

(2) "Foreign announcement and dissemination of this report by DDC is not authorized."

(3) "U. S. Government agencies may obtain copies of this report directly from DDC. Other qualified DDC users shall request through

_____."

(4) "U. S. military agencies may obtain copies of this report directly from DDC. Other qualified users shall request through

_____."

(5) "All distribution of this report is controlled. Qualified DDC users shall request through

_____."

If the report has been furnished to the Office of Technical Services, Department of Commerce, for sale to the public, indicate this fact and enter the price, if known.

11. SUPPLEMENTARY NOTES: Use for additional explanatory notes.

12. SPONSORING MILITARY ACTIVITY: Enter the name of the departmental project office or laboratory sponsoring *(paying for)* the research and development. Include address.

13. ABSTRACT: Enter an abstract giving a brief and factual summary of the document indicative of the report, even though it may also appear elsewhere in the body of the technical report. If additional space is required, a continuation sheet shall be attached.

It is highly desirable that the abstract of classified reports be unclassified. Each paragraph of the abstract shall end with an indication of the military security classification of the information in the paragraph, represented as *(TS)*, *(S)*, *(C)*, or *(U)*.

There is no limitation on the length of the abstract. However, the suggested length is from 150 to 225 words.

14. KEY WORDS: Key words are technically meaningful terms or short phrases that characterize a report and may be used as index entries for cataloging the report. Key words must be selected so that no security classification is required. Identifiers, such as equipment model designation, trade name, military project code name, geographic location, may be used as key words but will be followed by an indication of technical context. The assignment of links, rules, and weights is optional.